Horizontal and Vertical Profiles of Mouse Barrel Cortex Activity Revealed by *in vivo* Imaging of Genetically Encoded Calcium Indicators

Dissertation

zur

Erlangung der naturwissenschaftlichen Doktorwürde (Dr. sc. nat.)

vorgelegt der

Mathematisch-naturwissenschaftlichen Fakultät

der

Universität Zürich

von

WENRUI LIU

aus

China

Promotionskomitee

Prof. Dr. Fritjof Helmchen (Vorsitz)

Prof. Dr. Bruno Weber

Prof. Dr. Sebastian Jessberger

Zürich, 2016

Table of Contents

Summary

Scientists have always been intrigued, generation after generation, by the most mysterious organ in the world – the brain. Among the main components of the mammalian brain, the neocortex is particularly intriguing due to its involvement in cognition and its prominence in the human brain. The mammalian neocortex forms the surface of most of the cerebral hemispheres with different primary cortical areas processing different modalities (e.g., visual, auditory, somatosensory and motor). The large number of neurons in the neocortex, which are of heterogeneous type, are organized in six layers that run 'horizontally', parallel to the surface of the brain. Within a 'vertical' cortical column, spanning all six layers, the densely interconnected cells share similar response preferences to sensory stimulation and form complex local neural circuits. How exactly the cytoarchitectural, anatomical, and functional organization of the neocortex allows for efficient sensory information processing is still poorly understood.

Over the last decades, considerable efforts have been made towards understanding more about cortical information processing, especially using optical imaging techniques. Wide-field imaging is an excellent method for investigating how information spreads between spatially distributed cortical areas horizontally. However, the previous wide-field imaging techniques – using either intrinsic signals or small molecule voltage- or calcium-sensitive organic dyes – did not allow for chronic *in vivo* studies of large-scale cortical signal flow with high spatiotemporal resolution. Moreover, local circuit computations, established vertically across different cortical layers, and in particular the behavioural role of neurons in infragranular layers within such a processing circuit have remained elusive due to technical limitations. Today, further advances in optical imaging methods in combination with newly developed neuronal activity indicators, as reported here, shed new light on our way towards answering those fundamental questions in neurosciences.

In my thesis, I first present a technique for long-term investigation of cortical map dynamics using wide-field ratiometric fluorescence imaging of the genetically encoded calcium indicator (GECI) Yellow Cameleon 3.60. Wide-field GECI signals reported sensory-evoked activity in the primary somatosensory cortex (‘barrel cortex’) in anaesthetized mouse with high sensitivity, high temporal resolution, and good spatial precision, albeit lacking cellular resolution. Functional maps could be measured repeatedly in separate imaging sessions over multiple weeks. This method opens new possibilities for the longitudinal study of stability and plasticity of cortical sensory representations.

In the second part of this thesis, I present a novel approach that enables *in vivo* calcium imaging of deep, infragranular cortical neurons with cellular resolution. Using two-photon excitation of the sensitive red fluorescent calcium indicator R-CaMP1.07 at 1040-nm through a standard cranial window I demonstrate measurements of whisking-related neuronal activity throughout all layers of somatosensory cortex in awake, head-immobilized mice, down to layer 6. Neuronal activity was heterogeneous in all investigated layers, with only few neurons showing strongly correlated activity with free-air whisking. This method offers a solution for chronic investigations of the functional role of deep neocortical layer 5 and layer 6 neurons in information processing in the mouse brain during specific behaviours. Overall, with these two projects I contributed to the advancement of *in vivo* imaging techniques for enabling deeper studies of neocortical circuit function, locally and across the cortical sheet.

Zusammenfassung

Wissenschaftler sind seit jeher fasziniert vom mysteriösesten Organ der Welt –dem Gehirn. Der Neocortex macht einen grossen Teil des Gehirns aus und ist aufgrund seiner Rolle in der Verarbeitung von Sinnesreizen von besonders grossem Interesse. In Säugern macht der Neocortex einen Grossteil der Oberfläche des Grosshirns aus, darunter fallen verschiedene, primäre Hirnrindenareale, welche verschiedene Modalitäten (z.B. Sehen, Hören, Tasten) verarbeiten. Innerhalb einer alle 6 Schichten umfassenden, kortikalen Säule sind die Nervenzellen stark vernetzt und bilden komplexe lokale neuronale Schaltkreise. Wie jedoch die anatomische und funktionelle Organisation des Neocortexes eine effiziente Verarbeitung von Sinnesreizen ermöglicht, ist jedoch unzureichend verstanden.

Über die letzten Jahrzehnte wurden grosse Anstrengungen unternommen um die Grundsätze der kortikalen Informationsverarbeitung zu verstehen. Dazu wurden hauptsächlich optischen Methoden eingesetzt. Die Weitfeld-Fluoreszenzmikroskopie eignet sich beispielsweise hervorragend dazu die horizontale Signalausbreitung über verschieden Cortexareale zu untersuchen. Die bisherigen Weitfeldaufnahme Techniken basierten auf intrinsischen Signalen oder niedermolekularen, spannungs- bzw. kalziumabhängigen Farbstoffen. Diese liessen allerdings keine chronischen in-vivo Studien mit hoher spatiotemporaler Auflösung zu. Ausserdem konnten neuronale Schaltkreise, welche verschieden Schichten umfassen, aufgrund von technischen Limitationen bis anhin nur unzureichend analysiert werden. Dies trifft vor allem auf die Rolle der Neuronen in den infragranulären Schichten während Verhalten zu. Inzwischen ermöglichen weiterentwickelte, bildgebende Verfahren in Kombination mit neuen neuronale Aktivität Indikatoren, wie sie in dieser Studie angewendet werden, es grundlegende Fragen der Neurowissenschaften besser zu erforschen.

In meiner Doktorarbeit stelle ich zunächst eine neue Methode für Langzeitstudien der Dynamik kortikaler Aktivität vor, die ratiometrische Fluoreszenzmessung mit einem Weitfeld-Mikroskop und dem genetisch kodiertem Kalzium Indikator (GECI) Yellow Cameleon 3.60. Mit dieser Technik konnte ich sensorisch evozierte Aktivität im primären somatosensorischen Cortex („Barrel- Cortex“) von anästhesierten Mäusen, mit hoher zeitlichen Auflösung und guter räumlicher Präzision (jedoch ohne zelluläre Auflösung) messen. Funktionelle Kartierungen konnten anhand von wiederholten Messungen im selben Tier über mehrere Wochen erstellt werden. Diese Methode ermöglicht longitudinale Studien der Stabilität und Plastizität kortikaler Repräsentationen von sensorischen Reizen.

Im zweiten Teil meiner Dissertation stelle ich eine neue Methode vor, welche es ermöglicht in vivo Aufnahmen mit zellulärer Auflösung von Neuronen in den tiefen, infragranulären Cortexschichten zu machen. Durch die 2-Photonen Anregung eines sensitiven rot fluoreszierenden Kalzium Indikators, RCaMP1.07, bei 1070 nm konnte ich somatosensorische neuronale Aktivität in allen kortikalen Schichten (einschliesslich Schicht 6) in wachen, kopffixierten Mäusen messen. Die neuronale Aktivität war heterogen in allen untersuchten Schichten. Wir konnten jedoch einige wenige Zellen ausmachen deren Aktivität stark mit der aktiven Bewegung der Schnurrhaare korrelierte. Die hier präsentierte Methode bietet eine Lösung für longitudinale Studien, welche sich mit der Rolle von kortikalen Neuronen in den Schichten 5 und 6 bei der Informationsverarbeitung im sich verhaltenden Tier befassen. Mit diesen zwei Projekten konnte ich zu der Weiterentwicklung von bildgebenden Verfahren in vivo beitragen, welche lokale und Cortex übergreifende Studien der Funktion neokortikaler Schaltkreise ermöglichen.

1 General Introduction

Rodents are widely used in neuroscience research as a mammalian animal model due to their short life span, high genetic similarity to human genome, small body size as well as the availability of numerous transgenic lines. Like in other mammals, rodent neocortex is a part of the cerebrum and is the grey matter that covers the majority of the brain. The neocortex is associated with many higher brain functions such as sensory information perception and integration, voluntary movement, memory as well as learning. Rodent neocortex can be divided into different regions by cytoarchitecture, connectivity or function. Examples of different sensory areas in the neocortex that receive inputs from different peripheral sensory organs are visual cortex, auditory cortex and somatosensory cortex. Neocortex not only forms tight reciprocal connections within the neocortex, but also with many subcortical structures such as thalamus, striatum, amygdala, hippocampus, etc. (**Figure 1-1**).

Cells within neocortex can be classified into different types and subtypes according to different criteria. There are two main classes of cells in the neocortex: neurons and glia. Both neurons and glia share many structural and molecular characteristics with cells in general. However, the morphological properties of neurons are clearly distinguished by their functional specialization for communicating with other cells precisely and rapidly. Although glia cells do not directly participate in electrical signalling and information processing, it is widely believed that their contributions to information processing are much more important than it is currently appreciated. The glia/neuron ratio is not only species-dependent but also brain region-dependent (Herculano-Houzel, 2014). There are approximately 14 million neurons and 12 million glia in the mature mouse cortex (Herculano-Houzel et al., 2006). Neurons can be further classified according to their location,

morphology, connectivity, physiology, neurotransmitters, molecular properties, etc.

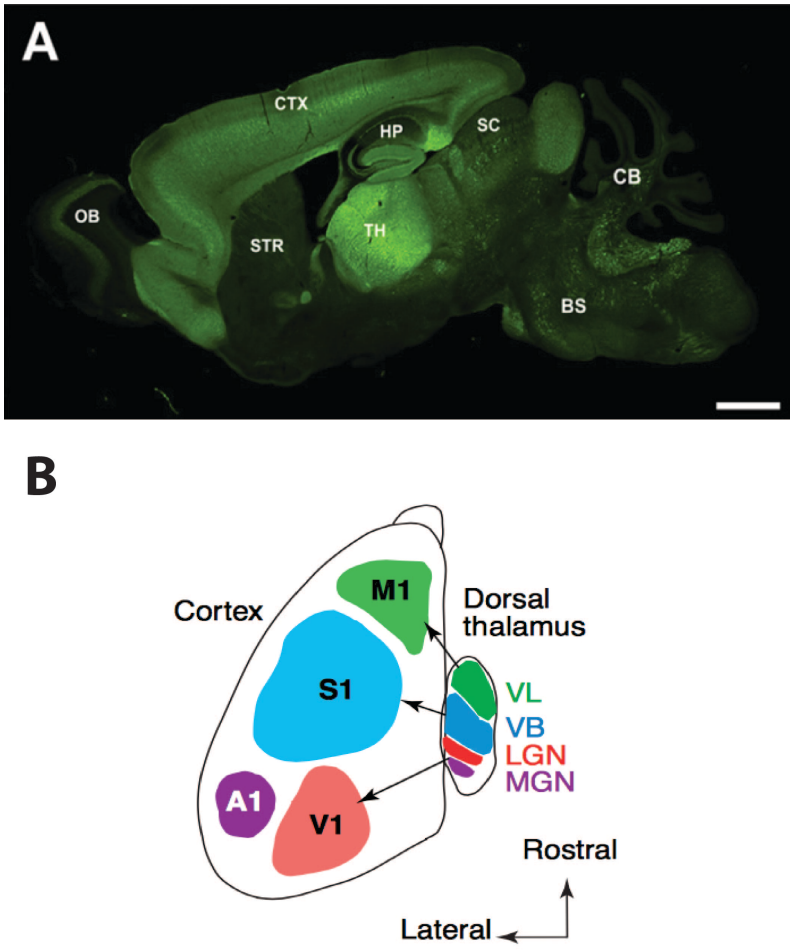

Figure 1-1: Illustration of mouse central nervous system. *(A) A sagittal section of brain from a Thy1-GCaMP3 mouse. OB, olfactory bulb; CTX, cortex; HP, hippocampus; STR, striatum; TH, thalamus; SC, superior colliculus; CB, cerebellum; BS, brain stem. Scale bar in (A) is 1 mm. Adapted from (Chen et al., 2012). (B) Schematic illustration of the connectivity between thalamus nuclei and neocortical primary sensory areas in mouse brain. A1, primary auditory area; V1, primary visual area; S1, primary somatosensory area; M1, primary motor area; MGN, medial geniculate thalamic nucleus; LGN, lateral geniculate nucleus; VB, ventrobasal thalamic nucleus; VL, ventrolateral thalamic nucleus. Adapted from (Vanderhaeghen and Polleux, 2004).*

1.1 Rodent barrel cortex as a model for investigating sensory information processing in mammalian neocortex

Somatosensory information is extremely important for nocturnal species like mice and rats, as somatosensory information can compensate for

the limited visual information. Whiskers on the snouts deliver information about the location and texture of the objects in the surrounding environment. The collected information will be further processed by the primary somatosensory cortex (S1). Rodent S1 has a very unique organization that not only offers the possibility to manipulate sensory inputs according to the experimental designs, but also facilitates the analysis of the underlying neural mechanisms for cortical information processing as well as plasticity. Therefore, rodent S1 is an ideal model for investigating structure-function relationship. Here I will introduce the two major thalamic pathways for whisking in rodents before summarizing what is known about vertical intracolumnar functional connectivity and within the cortical sheet barrel-related long-range connections.

The neurons in S1 are organized in six layers (layer 1, 2/3, 4, 5 and 6). Each layer has different cell density, cell types, cellular morphology, layer thicknesses and gene expression (Lein et al., 2007; Molyneaux et al., 2007). It is, however, worth to notice that there are no absolute laminar boundaries existing between different cortical layers. Neurons are assigned to be in a specific cortical layer according to the location of their somata. Usually their dendrites and axons often extend across many different layers, depending on the specific type of the neuron (**Figure 1-2**).

Layer 1 (L1) is the outermost layer. Unlike other cortical layers that contain many neuronal somata, L1 consists largely of axons and the apical dendrites of pyramidal neurons whose somata reside in L2/3 or L5. Besides, virtually all L1 neurons are inhibitory neurons (Douglas and Martin, 2004; Xu and Callaway, 2009). Small pyramidal cells are the predominant cell type in L2/3. L2 and L3 are commonly treated as a single layer in the mouse cortex, although there is evidence showing the existence of functional segregation between these layers (Bureau et al., 2006). L4 is the most densely populated layer among all six layers. Large pyramidal neurons are commonly observed in L5. These

pyramidal neurons project their axons to many different cortical and subcortical regions (Larsen et al., 2007). The further classification of L5 neurons can be based on many criteria. For example, when based on different connectivity, L5 can be further divided into L5A (corticostriatal) and L5B (corticospinal) (Anderson et al., 2010). L6 occupies a large part of the cortical depth in mice and contains a diverse population of pyramidal neurons.

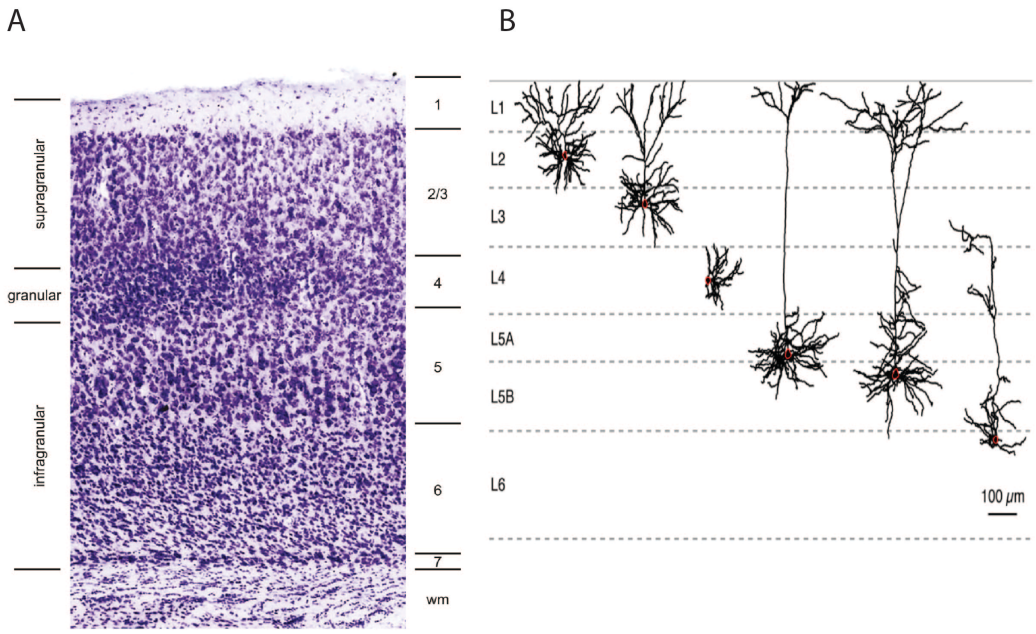

Figure 1-2: Layers of the mouse primary somatosensory cortex. *(A) Nissl stain of RNA reveals different cell densities in different cortical layers. A less discussed layer 7, a thin layer of subplate cells that project to layer 1 and the corpus callosum* (Reep, 2000)*, is shown here as well. Adapted from Dr Erika Gyengesi* (Kirkcaldie, 2012)*. (B) Examples of different dendritic morphologies found in the mouse C2 barrel column. Layer boundaries are drawn to scale at their mean subpial distance. Adapted from* (Lefort et al., 2009)*.*

Two major whisker-related thalamic pathways. Mechanical stimulation of the whiskers opens mechanosensitive ion channels in nerve endings innervating the whisker follicles. These nerve endings are the peripheral branches of trigeminal ganglion (TG) sensory neurons (Dörfl, 1985). A single TG sensory neuron is only responsive to stimulation of one specific whisker. TG neurons send another central branch into the trigeminal nucleus (TN) in the brainstem. The evoked

signals will then travel along this central branch and reach the trigeminothalamic neurons in the brainstem (Clarke and Bowsher, 1962). Trigeminothalamic neurons are organized in a manner that precisely recapitulates the spatial pattern of whiskers on the snouts. This topographic map is named “barrelettes” according to its special shape and arrangement. Each barrelette receives strong input from a single whisker (Ma, 1991).

From TN, sensory signals are relayed first to the thalamus and then to S1 via at least two major parallel pathways: the lemniscal pathway and the paralemniscal pathway. In lemniscal pathway, whisker signals from the principal trigeminal nucleus (PrV) in the brainstem project to the ventral posteromedial nucleus (VPM) nucleus of the thalamus. The previous described somatotopic maps can be observed again and is called “barreloids” in thalamus (Van Der Loos, 1976). By using whole-cell voltage recording and morphological reconstruction, Brecht and Sakmann (Brecht and Sakmann, 2002) found that one barreloid has stronger responses for one “principal” whisker than the others. Axons arising from VPM neurons in the core barreloid innervate predominantly L4 and to a less extent L5B, L6 as well as deep L3 (Bureau et al., 2006; Cruikshank et al., 2010; Oberlaender et al., 2012) (**Figure 1-3**). In S1 L4, a clear somatotopical map that matches the layout of the whiskers on the contralateral snout can be observed. This somatotopical map can be visualized by cytochrome oxidase (COX) staining (Minderer et al., 2012). Barrels are separated from one another by structures called septa. This matrix-like part of S1 is called barrel cortex and each barrel is predominantly related to a single whisker (Woolsey and van der Loos, 1970) (**Figure 1-3**). C2 barrel column in mouse contains about 6500 neurons, of which 11% are inhibitory interneurons (Lefort et al., 2009). In the paralemniscal pathway, whisker signals from the rostral section of the interpolar spinal trigeminal nucleus (SpV) in the brainstem project to the posteromedial nucleus (POm) nucleus of the thalamus. Axons arising from POm neurons project to S1, the secondary somatosensory cortex (S2) as well as the primary whisker motor cortex (wM1).

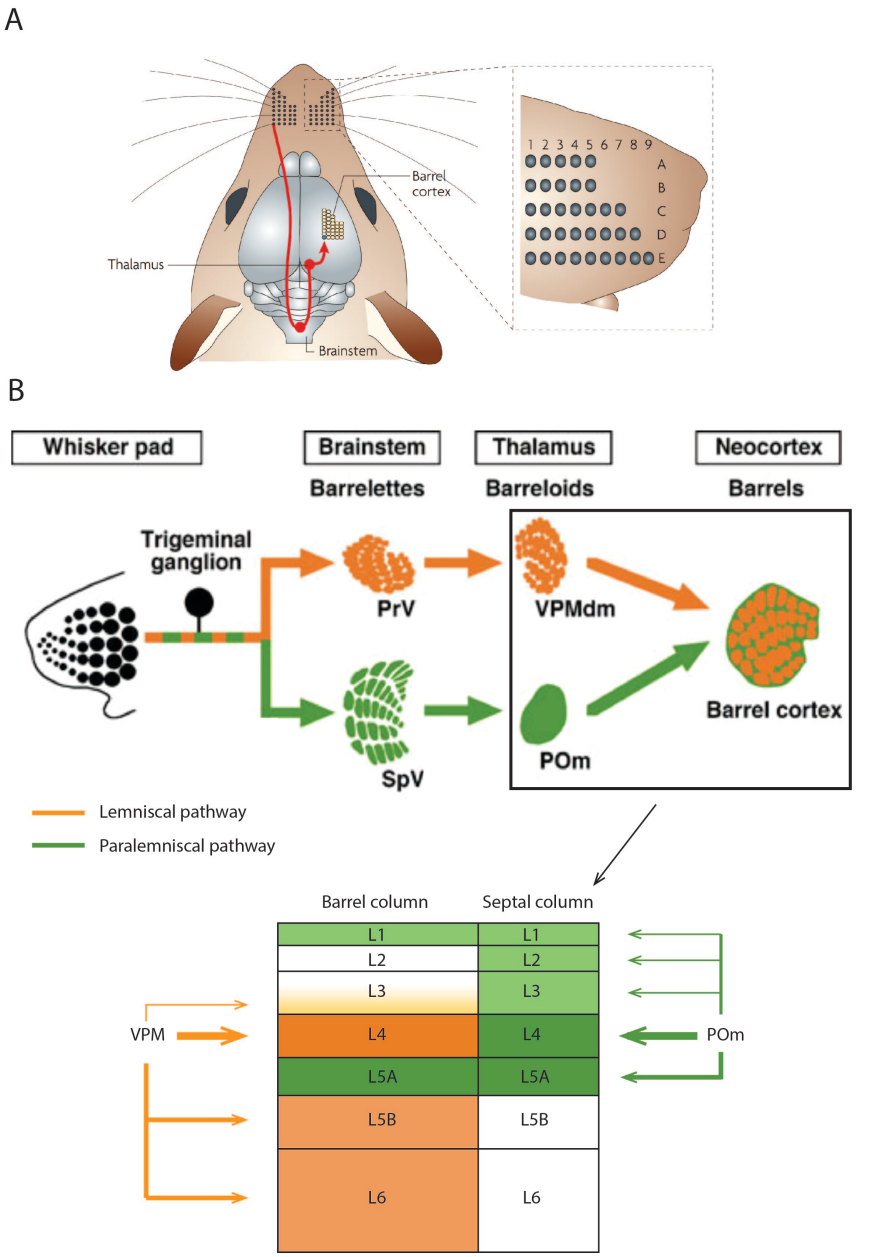

Figure 1-3: Illustration of rodent whisking system. *(A) Schematic top view of the rodent whisking pathway. Sensory information travels from whisker to brainstem, then to thalamus, and finally arrives in S1. (B) Schematic coronal view of the two main whisking pathways from thalamus to S1: the lemniscal pathway (orange pathway) and the paralemniscal pathway (green pathway). Barrels are separated from one another by structures called septa. Adapted from (Alloway, 2008; Diamond et al., 2008; Sehara et al., 2010)*

In S1 septal columns, POm neurons innervate most densely L4 and to a lesser extent L1, L2/3 as well as L5A. In S1 barrel columns, POm neurons innervate predominantly L5A and to a lesser extent L1. (Bureau et al., 2006; Wimmer et al., 2010) (**Figure 1-3**). The distinct yet inter-

connected pathways are the foundation of processing complicated whisker-related information. The lemniscal pathway is associated with whisking-touch signal while the paralemniscal pathway contributes to sensorimotor coordination (Yu et al., 2006). Another pathway, the extralemniscal pathway, also conveys multi-whisker information. It originates from the caudal part of the interpolar SpV, via the tail of the barreloids in VPM terminates in dysgranular S1 and in S2 (Pierret et al., 2000; Veinante et al., 2000a).

Whisking-related information processing within neocortex. In 1957, Mountcastle found that neurons in a vertical cluster share the same tuning for a given receptive field attribute in cat visual cortex (Mountcastle, 1957). Thus, he believed that a vertical functional organization exists in the neocortex, which he called the cortical column. This concept was widely accepted because it allowed studying the extremely intricate cerebral cortex in a more simplified way. Mouse barrels cortex serves as a typical model for studying the microcircuits within a cortical column. Although the functional unit role of the barrel columns is still under debating depending on the definition of a column (Feldmeyer et al., 2013)

After the sensory signals arrive in barrel cortex, the local processing follows the canonical microcircuitry defined by Douglas and Martin (Douglas and Martin, 1991, 2004). Here, I will introduce whisking-related information processing circuitry in mouse neocortex in more detail (**Figure 1-4**). Afferent thalamocortical axons from VPM form axonal clusters at the center of each barrel in L4. Excitatory spiny neurons in L4 surround these axonal clusters as barrel walls and send their dendrites toward the central hollow of the barrel. Here, cells in each column respond to the stimulation of the corresponding whisker with the shortest latency and strongest amplitude (Bruno and Sakmann, 2006; Bureau et al., 2006; Simons, 1978). L4 spiny neurons display a high degree of intralaminar reciprocal connectivity within a barrel column (Feldmeyer et al., 1999). Such reciprocal connections have been proposed to function

as feedback amplifiers of synaptic signals (Douglas et al., 1995). In addition to intralaminar reciprocal connectivity within a barrel column, L4 spiny neurons send intracolumnar axons that target preferentially L2/3 pyramidal cells (Feldmeyer et al., 2002; Shepherd et al., 2005; Silver et al., 2003), and particularly L3 pyramidal neurons in mouse barrel cortex (Bureau et al., 2006). Such translaminar signal flow between L4 and L2/3 neurons is uni-directional and has low synaptic efficacy (Feldmeyer et al., 2002). Moreover, there are evidence showing that individual barrels contain subcolumnar angular tuning domains that show different direction preference (Andermann and Moore, 2006; Bruno et al., 2003). Thus, this L4-L2/3 synaptic connection may function as a "gate" for further local processing as well as long-range communication. In addition to the predominant L4-L2/3 connection, it has been shown that L4 spiny neurons also innervate L5A, L5B and L6 pyramidal neurons, although with a very low connectivity (Lefort et al., 2009).

Before reaching L2/3, the excitatory signal flow is mostly vertical and confined within each barrel column. After the information arriving in L2/3, the local and long-range connections that L2/3 pyramidal neurons form with other neurons enable them to integrate and distribute excitatory signals arriving from L4. One main target of L2/3 pyramidal cells are other pyramidal cells in L2/3 (Feldmeyer et al., 2006). These horizontal connections can be either uni- or bi-directional, can be local connections (with neighbouring L2/3 pyramidal neurons in the home barrel column) or long-range connections (across several barrel columns or with the contralateral barrel cortex) (Petreanu et al., 2007). The longer-range connectivity of L2/3 pyramidal cells (>200um intersomal distance) is dramatically decreased as compared to local connections (Feldmeyer et al., 2006; Holmgren et al., 2003). Other main targets of L2/3 pyramidal cells are L5A and L5B pyramidal cells (Lefort et al., 2009; Petreanu et al., 2009). These vertical connections can be intracolumnar connections (with L5 pyramidal neurons in the home barrel column) or long-range connections (across several barrel columns or with the contralateral barrel cortex) (Petreanu et al., 2007).

Thus, L2/3 pyramidal cells might play a role in integrating and coordinating the activity of the home barrel column with the activity of the surrounding barrel columns as well as the contralateral barrel cortex.

L5 is the main output layer in S1 and have axonal projections to various subcortical brain regions. There are at least two main excitatory cell types in L5. Pyramidal cells featured by slender apical tufts are mainly located in L5A, while pyramidal cells that have thick, elaborate apical tufts locate in L5B. The slender-tufted L5A neurons receive POm thalamic afferents while the thick-tufted L5B pyramidal cells receive VPM thalamic afferents (Oberlaender et al., 2012; Petreanu et al., 2009). The axons of slender-tufted L5A pyramidal cells innervate predominantly L2/3 both within and outside the home barrel column (Larsen and Callaway, 2006; Oberlaender et al., 2011; Shepherd and Svoboda, 2005). They also project to ipsilateral wM1 (Mao et al., 2011) as well as the contralateral S1 (Larsen et al., 2007). Thick-tufted L5B pyramidal cells project to many subcortical regions such as the thalamic nuclei, the superior colliculus, the striatum, and the trigeminal nuclei (Kozloski et al., 2001; Larsen et al., 2007; Mao et al., 2011; Veinante et al., 2000b). Slender-tufted L5A pyramidal neurons show little if any action potential firing after passive touch (Curtis and Kleinfeld, 2009; de Kock and Sakmann, 2009). In contrast, thick-tufted L5B pyramidal cells have been reported to reliably increase action potential firing after passive whisker touch (de Kock et al., 2007). During exploratory behaviour, both lemniscal and paralemniscal pathways are activated. Thus, the thick-tufted L5B pyramidal cells may be depolarized at both basal dendrites (directly *via* the VPM afferents) and the apical dendritic tuft (indirectly via POm inputs to L5A and possibly also L1). This will then result in increased neuronal firing, which is subsequently conveyed to other cortical as well as subcortical targeted regions.

Like L5 pyramidal cells, pyramidal cells in L6 can also be subdivided into at least two groups according to their axonal projection patterns: corticocortical and corticothalamic neurons (Kumar and Ohana, 2008;

Oberlaender et al., 2012; Tanaka et al., 2011). According to a morphological study (Tanaka et al., 2011), it has been shown that L6 corticothalamic neurons are densely connected with themselves within a barrel column, whereas L6 corticocortical neurons connect with corticothalamic neurons horizontally beyond the barrel column. Besides, L6 corticothalamic neurons also receive strong connections from L4 neurons in the same barrel column and to a less extent from L5A and L5B neurons. Thus, L4 neurons may have an important role in shaping the cortical modulation of thalamic relay neurons through cortical thalamic neurons. To summarize, both L5 and L6 not only play direct and indirect roles in modulating the thalamic activity in different thalamocortical pathways, but also are important elements in feedforward signalling from S1 to S2 and wM1.

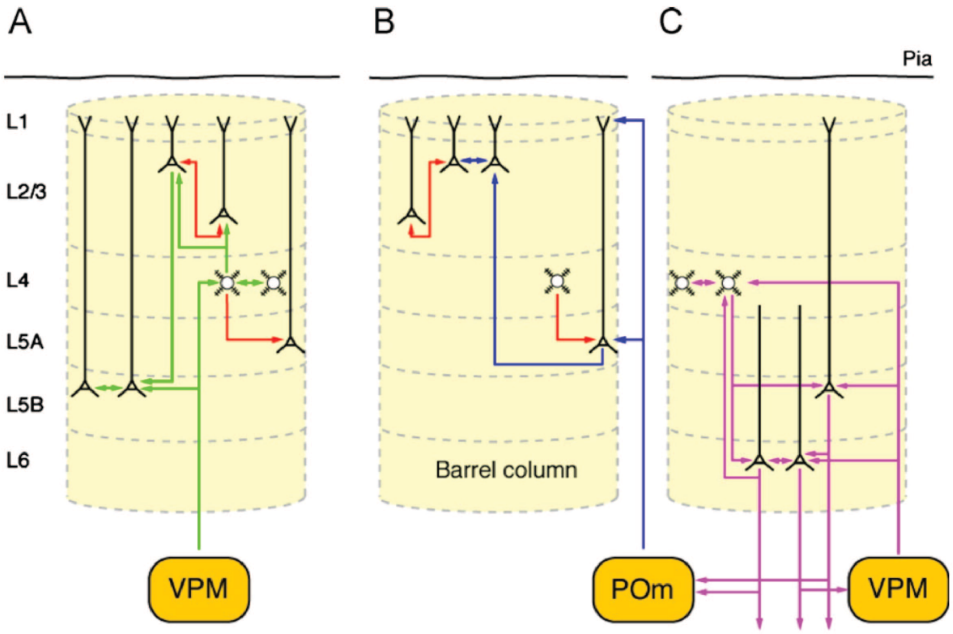

Figure 1-4: Simplified scheme of parallel cortical microcircuits in the barrel cortex. *(A) The 'canonical' microcircuits receiving lemniscal thalamic input from the ventroposterior medial nucleus (VPM) predominantly in layer 4 (and to lesser degree in layer 5B. (B) Intracortical microcircuits involved in the processing of signals arriving from the paralemniscal pathway (inputs from the posterior medial thalamic nucleus, POm, to L5A pyramidal neurons). (C) Synaptic connections involved in the thalamocortical-cortictohalamic feedback circuit between L4 spiny neurons, L6 pyramidal cells and the thalamic nuclei. Color code: Green: 'canonical' microcircuit, blue: 'paralemniscal' pathway, red: intracortical microcircuits interdigitating 'lemniscal' and 'paralemniscal' microcircuits,*

violet: thalamocortical-corticothalamic loop. Adapted from (Lübke and Feldmeyer, 2007).

As mentioned at the beginning of section 1.1, whisking behaviours are complicated behaviours that deliver information about the location and texture of the objects in the surrounding environment. Whisking behaviours can occur at different frequencies, but typically around 5-12 Hz (Brecht et al., 2006). Whiskers on both sides of the snouts can either move synchronously or asynchronously (Mitchinson et al., 2007). It has been observed that even the whiskers on the same side can move in different direction in order to fully explore an object (Sachdev et al., 2002). Interactions between S1, S2 and wM1 are important not only for object localization and texture discrimination but also to modulate and coordinate the whisker movement.

Within the barrel cortex, the horizontal axon collaterals of L2/3, L5 and a subset of L6 pyramidal neurons run predominantly along the barrel rows and less along the barrel arcs (Adesnik and Scanziani, 2010; Bruno et al., 2009). Another recent morphological study showed that in rat barrel cortex the majority of intracortical axon projections are transcolumnar. These transcolumnar projections are asymmetric (innervate columns of either the same whisker row or arc) and divide rat barrel cortex into two orthogonal supragranular and infragranular strata (Narayanan et al., 2015). Such an organisation might play an important role in the modulation of the home column activity with respect to its neighbouring columns. Intrinsic optical imaging has been used to study the experience-dependent functional map plasticity in barrel cortex over long periods of time in the same awake behaving animal (Polley et al., 1999). However, this method cannot offer the sufficient spatiotemporal resolution for a better understanding of the experience-dependent reorganization of cortical synaptic circuits. A Channelrhodopsin-2 (ChR2)-assisted circuit mapping study showed that in addition to the predominant connections between the S1 L2/3 pyramidal cells and the contralateral S1 L2/3, L5A, and L5B pyramidal cells, a few connections with L6 neurons also existed (Petreanu et al., 2007). As compared to

S1, the structure and function of S2 is far less understood and explored, it likely plays an essential role in multisensory integration. Axonal projections from barrel cortex to the ipsilateral S2 are topographic and reciprocal (Aronoff et al., 2010). They mainly arise from pyramidal neurons in L2/3, L5A and to a lesser degree L5B and L6 (Chakrabarti and Alloway, 2006). Ipsilateral S1-to-wM1 projections are also somatotopically arranged. The projections arise from a subset of L2/3 and L5A pyramidal neurons in S1 and target L2/3 and L5A neurons in wM1 (Aronoff et al., 2010; Mao et al., 2011; Sato and Svoboda, 2010). Conversely, ipsilateral wM1-to-S1 connections innervate L2/3 and L5 pyramidal neurons in S1 via axon collaterals that arise from wM1 L5, L6 as well as L1 (Mao et al., 2011; Petreanu et al., 2009; Veinante and Deschênes, 2003).

In summary, our knowledge about barrel cortex function has been mostly gained by anatomical tracing studies (classical tracer substances and or more recently viral vectors coupled to fluorescent markers), electrophysiological studies (*in vitro* paired recording) and optical studies (intrinsic imaging, photo-activation of caged glutamate or ChR2 or calcium or voltage-sensitive dye imaging). Based on the available studies it can be stated that the whisker-related sensory information processing in neocortex has a 'vertical' component across the layers within a barrel column and a 'horizontal' (transverse) component governing activity spread between columns and to various cortical areas. Although the application of two-photon calcium imaging has been a powerful tool for imaging neuronal activity in living tissues, most *in vivo* two-photon studies were limited to the superficial 400 µm in the scattering mammalian brains. Thus, the depth of infragranular cells (L5 and L6) has hindered the investigation of their functional roles during different behavioural states in awake animals. Moreover, due to technical limitations, only little is known about sensory information transformation between spatially distributed cortical areas horizontally over long periods of time.

1.2 Genetically-encoded calcium indicator (GECI)

Intracellular calcium dynamics. The cell membrane, a phospholipid bilayer, isolates the cytosol of the neuron from the extracellular fluid. H_2O is an important component in both cytosol and extracellular fluids. It is a polar molecule that held together by polar covalent bonds. This property makes H_2O an effective solvent of other charged or polar molecules, for example Na^+, K^+, Cl^- and Ca^{2+}. These ions are the most important charge carriers involved in the conduction of electricity signals in neurons. At rest, ion pumps such as the sodium-potassium pump and the calcium pump in the cell membrane ensure that K^+ has higher intracellular concentrations than outside, while Na^+ and Ca^{2+} have higher extracellular concentrations than inside. During an action potential (AP), the electrical charge is redistributed along the membrane. The activation of the voltage-gated sodium channels results in Na^+ influx and plays an important role during the fast rise of the AP. The inactivation of the voltage-gated sodium channels as well as the activation of the voltage-gated potassium channels (K^+ efflux) are responsible for the falling phase of the AP (Purves D, Augustine GJ, Fitzpatrick D, et al., 2001). Besides, APs are observed to tightly coupled to large and rapid intracellular free calcium concentration increase as well. The estimated free calcium concentration change companying a single AP for cortical pyramidal neurons is 150-300 nM (Helmchen et al., 1996).

There are many factors that can influence intracellular calcium concentration. For example, voltage-gated calcium channels (VGCCs) are the main contributor of somatic calcium influx. AP back propagation and synaptically mediated depolarization can effectively activate VGCCs in the dendrites and spines (Bloodgood and Sabatini, 2007; Reid et al., 2001; Spruston et al., 1995; Waters et al., 2005). The extreme difference between the intracellular calcium concentration (50 – 100 nM) and the extracellular calcium concentration (about 1.2 mM) creates a large inward driving force that pushes Ca^{2+} into neurons through the

activated VGCCs (Berridge et al., 2000; Purves D, Augustine GJ, Fitzpatrick D, et al., 2001). According to the voltage-dependent activation threshold, VGCCs are generally categorized in to two classes: high-voltage-activated (HVA) channels and low-voltage-activated (LVA) channels (Catterall, 2000). HVA channels can be activated only at membrane potentials above -10 mV. Based on biophysical, pharmacological, and molecular features, HVA can be further classified into different subtypes: L-, P/Q-, N-, and R-type. Different neuron types and different cellular subcompartments express different types of VGCCs. For example, L-type and predominantly R-type VGCCs are abundant in spines of proximal dendrites (Berridge et al., 2000; Catterall, 2000). P/Q- and N-type channels are found in many nerve terminals, thus are involved in synaptic neurotransmitter release (Catterall, 2000). T-type LVA channels are commonly found in thalamic neurons (Coulter et al., 1989). In addition to VGCCs, synaptic input directly gates Ca^{2+} through neurotransmitter-gated ion channels (Müller and Connor, 1991), primarily ionotropic N-methyl-D-aspartate (NMDA) glutamate receptors and nicotinic acetylcholine receptors (nAChR). Ca^{2+} influx through neurotransmitter-gated ion channels plays an important role in synaptic plasticity (Zucker, 1999), memory consolidation on behavioural level (Carafoli, 2003) as well as gene expression.

In addition, calcium ions can also be released from internal calcium stores, most prominently the endoplasmatic reticulum (ER). This process is mediated by inositol trisphosphate receptors (IP_3Rs) and ryanodine receptors (RyRs) (Berridge, 1998). IP_3Rs can be generated by the activation of metabotropic glutamate receptors (mGluRs) (Niswender and Conn, 2010). RyRs can be activated by elevations of the cytosolic calcium concentration and RyR-mediated calcium release contributes to the amplification of the AP related calcium influx (Berridge, 1998; Kano et al., 1995). Moreover, mitochondria can act as calcium sink and are important for neuronal calcium homeostasis. They take up calcium during cytosolic calcium elevations through the calcium

uniporter and then release calcium back to the cytosol slowly through sodium-calcium exchange (Duchen, 1999).

Because of the rapid calcium influx, AP evoked calcium transients typically display a sharp rise. The sharp rise is followed by a relatively slow exponential decay due to calcium buffering and slow extrusion of calcium out of the cytosol. The calcium extrusion requires energy, either directly by consuming adenosine triphosphate (ATP) in the Ca^{2+}-Mg^{2+}-ATPase or secondary via the Na^{+}-Ca^{2+}-exchanger (Berridge et al., 2003).

In summary, APs are tightly coupled to large and rapid intracellular free calcium concentration increases. Thus, intracellular calcium dynamics can be used to read out neural activity with appropriate calcium indicators. The exact shape of the calcium transient not only depends on calcium influx and efflux, but also depends on the exchange of calcium with internal stores, the presence of endogenous calcium buffering proteins like parvalbumin, calbindin-D28k (Schwaller, 2010) as well as the presence of exogenous calcium indicators, which themselves act as buffers (Helmchen et al., 1996).

Calcium indicators. The first Ca^{2+}-sensitive bioluminescent protein used to visualize intracellular Ca^{2+} changes was aequorin (Shimomura et al., 1962). Aequorin-based recording has it own advantages and disadvantages. The advantages include that it has a high signal-to-noise ratio and it does not require complicated external illumination sources. However, some of its disadvantages such as low spatial resolution resulted by the low amount of emitted light as well as the high consumption rate of aequorin during long experiments drove scientists to look for other calcium sensitive indicators. Synthetic calcium indicators, for example fura-2, fluo-4 and Oregon Green 488 BAPTA-1 (OGB-1) (Gee et al., 2000; Grynkiewicz et al., 1985; Tsien, 1980), change their intramolecular conformation upon calcium binding. The conformation change can lead to a change in the emitted fluorescence. These synthetic dyes are bright, photostable, have a high affinity, and

show very large Ca^{2+}-dependent fluorescence changes. Their application is, however, limited because of disadvantages such as invasive dye loading process, dye leakage as well as non-selective labelling. Thus, the need of performing less invasive, long-term repeated measurements, and better targeted investigations in awake, free behaving animals led to the development of genetically-encoded calcium indicators (GECIs).

GECIs are highly desired due to the possibilities to achieve long-term targeted expression with minimal invasiveness. In general, GECIs consist of a calcium-binding domain and one or two fluorescent proteins (FPs). Thus, GECIs can be categorized into two groups according to the number of FP (**Figure 1-5**). GECIs that contain only one FP are usually single-wavelength non-ratiometric indicators. GECIs that contain two FPs are Förster resonance energy transfer (FRET) ratiometric indicators. FRET-based ratiometric indicators can be further classified into two groups according to different calcium-binding domains: calmodulin-based calcium indicators and troponin C-based calcium indicators. The very first generation of GECIs, Cameleons, are ratiometric calmodulin-based GECIs (Miyawaki et al., 1997). Here I take Yellow Cameleon 3.60 (YC3.60) (Nagai et al., 2004) as an example to illustrate the working principle of FRET-based ratiometric GECIs. When the distance between an excited donor fluorophore and an acceptor fluorophore is less than 10nm, non-radiative energy can transfer from the excited donor fluorophore to the acceptor fluorophore (Jares-Erijman and Jovin, 2003). In YC3.60, the donor fluorophore is an enhanced cyan fluorescent protein (ECFP) and the acceptor fluorophore is a circularly permuted Venus protein (cp173Venus). These two FPs are linked together by a linker sequence that consists of the calcium-binding protein calmodulin and the calmodulin-binding peptide M13 (CaM-M13) (Nagai et al., 2004). In the absence of calcium ions, the emission is dominated by the blue ECFP fluorescence (480 nm). Calcium binding to calcium binding domain can lead to intramolecular conformational changes. Such conformational changes reduce the spatial distance

between the two FPs, which in turn results in the energy transfer from ECFP to cp173Venus and cp173Venus emits photons of about 530 nm (yellow). The read out calcium signal is expressed as a ratio between cp173Venus and ECFP fluorescence. Linker mutagenesis (elongation) of YC3.60 calcium binding domain produced a series of very high-affinity indicators -- YC-Nanos (Horikawa et al., 2010). Calcium buffering effect (Helmchen et al., 1996) and potential long-term cytotoxicity should be taken into consideration when using GECIs that have such high Ca^{2+} affinity. In troponin C-based calcium indicators, calmodulin is replaced by troponin C variants. Because troponin C is the calcium-binding protein in the cardiac and skeletal muscle cells, it has very low probability to interact with endogenous proteins in neurons. Example of troponin C-based calcium indicators are TN-XXL (Mank et al., 2008) and Twitch (Thestrup et al., 2014).

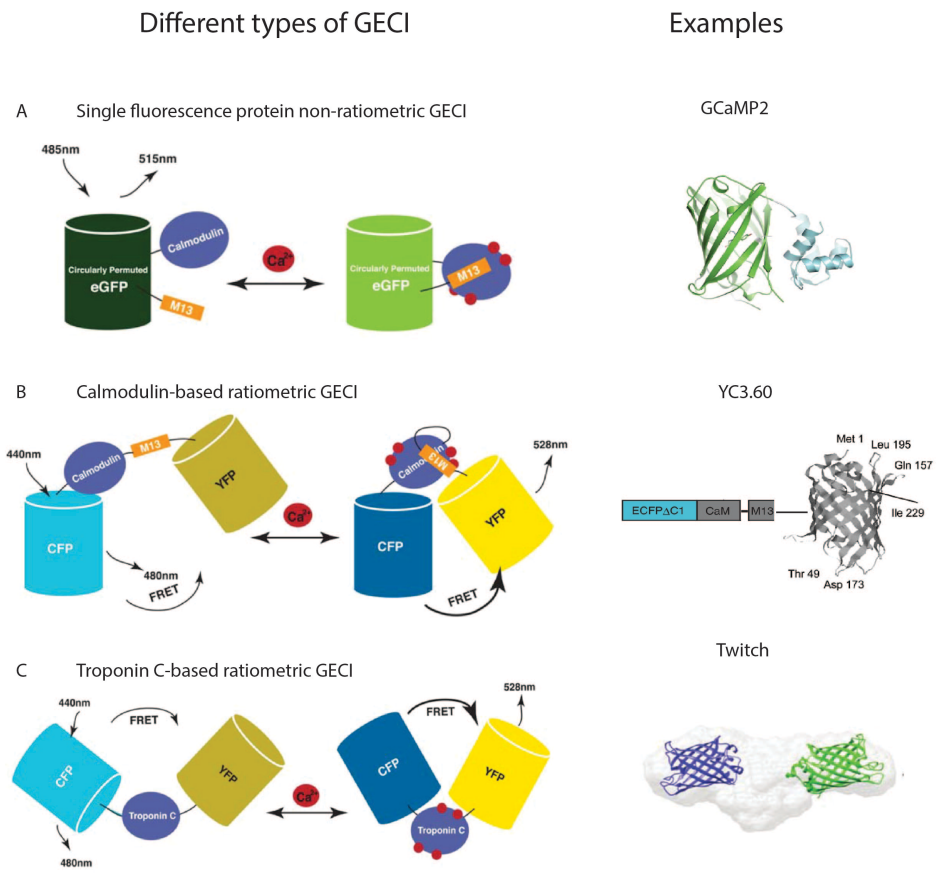

Figure 1-5: Most commonly used green GECIs. *A). Schematic representation of GCaMP sensing mechanism (left). Upon calcium binding, conformational change of Calmodulin increases the fluorescence of the circularly permuted GFP; crystal structure of calcium-free GCaMP2*

(right). B). Schematic representation of calmodulin-based indicators sensing mechanism (left). A conformational change of Calmodulin-M13 upon calcium binding brings CFP and YFP closer, this conformational change would allow the energy transfer from the CFP onto the YFP; the structure of YC3.60 (right). C). Schematic representation of troponin C-based indicator sensing mechanism (left). The conformational change upon calcium binding results in an increase in FRET acceptor emission; the structure of Twitch (right). Adapted from (Akerboom et al., 2009; Hires et al., 2008; Nagai et al., 2004; Thestrup et al., 2014).

A good representatives of single-wavelength non-ratiometric indicators is the GCaMP family, which has been developed over the years by several groups (T.-W. Chen et al., 2013; Nakai et al., 2001; Ohkura et al., 2005; Tian et al., 2012, 2009). Here I take GCaMP2 as an example to illustrate the working principle of single-FP non-ratiometric GECIs (Akerboom et al., 2009). GCaMP2 consists of a circularly permuted enhanced green FP (cpEGFP), calcium-binding protein calmodulin (CaM) and the calmodulin-binding peptide M13. In the absence of calcium ions, cpEGFP has low baseline fluorescence. Calcium binding to the binding domain will change the conformation of CaM-M13 complex (protect the cpEGFP chromophore from the aqueous environment). Such conformational change will further results in an increased fluorescence emission. (Akerboom et al., 2009)

Recent years, the improvement of the performance of GCaMP family GECIs have been focusing on increasing the brightness and response dynamics upon calcium binding. Examples for the most advanced GECIs that belong to GCaMP family are GCaMP5 (Akerboom et al., 2012), GCaMP6 (T.-W. Chen et al., 2013), GCaMP7 (Muto et al., 2013) and GCaMP8 (Ohkura et al., 2012b).

Spectral properties, response kinetics, calcium affinity, dynamic range as well as specific experimental conditions are some important factors to consider when choosing the appropriate GECI for a specific experiment (Hendel et al., 2008). Dissociation constant (K_d) describes the propensity that an indicator-calcium complex will separate. It corresponds to the calcium concentration at which half of the GECIs are bound to calcium. Notably, many factors such as pH, temperature, Mg^{2+}

concentration can affect the results of K_d measurement in a specific experiment (Hires et al., 2008; Oliver et al., 2000). A high K_d indicates a low calcium affinity due to the inversely dependent relationship between the two parameters (Mank et al., 2006). A low-affinity GECI provides less buffering effect, faster rise and decay times (Helmchen et al., 1997) as well as a greater effective dynamic range. Thus, it is the indicator of choice for quantitative measurement of larger calcium transients. On the other hand, in cases of monitoring small calcium transients, a high-affinity indicator is preferred. However, high-affinity indicators saturate more easily at high calcium concentration and have stronger buffering effect. As compared to ratiometric indicators, non-ratiometric indicators have faster kinetics and larger dynamic ranges (Lütcke et al., 2010; Tian et al., 2009). However, ratiometric indicators are less sensitive to tissue movement, optical path length changes, excitation light intensity changes as well as GECI expression level in long-term *in vivo* imaging due to their ratiometric readout.

So far the most widely used YFP/GFP-based GECIs are not optimized for imaging deeper tissues *in vivo*. Here I will explain the reason in more detail. Tissue scattering and light absorption by blood vessels are the two major obstacles when imaging deeper structures *in vivo*. The longer the wavelength, the lower the probability of photons straying away from their ballistic path during imaging. Besides, light that has longer wavelengths are less affected by haemoglobin absorption. Red light has longer wavelength, therefore, red light is less affected by tissue scattering as well as blood absorption. This property of red light as well as the desire to image deeper tissues *in vivo* steered the development of red-shifted GECIs (Akerboom et al., 2013; Ohkura et al., 2012a) (**Figure 1-6**). RCaMP1a-h and RCaMP1.07 are the two commonly used red GECIs groups (Akerboom et al., 2013). RCaMP1a-h are developed by replacing the GFP in GCaMP3 with a circularly permuted version of mRuby whereas RCaMP1.07 is developed by mutagenesis screening after replacing the GFP in GCaMP3 with mApple (Ohkura et al., 2012a; Zhao et al., 2011).

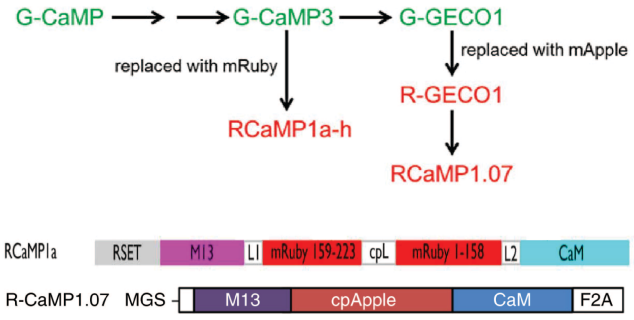

Figure 1-6: The development of red GECIs. *Adapted from* (Akerboom et al., 2013; Inoue et al., 2014; Sasaki, 2015).

1.3 Expression of fluorescent calcium indicators in the mouse brain

In order to deliver a fluorescent calcium indicator into cells in culture, brain slices or even in the brains of living animals, neuroscientists have developed different categories of delivery methods: physical, chemical, viral and transgenic methods. The method of choice is based on specific experiment designs and purposes.

1.3.1 Physical and chemical methods

Physical methods are efficient for delivering fluorescent calcium indicator without limitations on the cell type, however they have the potential to harm cells. Commonly used physical methods for loading targeted cells with fluorescent dyes are: microinjection and electroporation. Under a microscope, dissolved synthetic dyes can be microinjected or loaded into a target cell by using a glass micropipette both *in vitro* (Helmchen et al., 1996; Jaffe et al., 1992) and *in vivo* (Borst and Egelhaaf, 1992; Eilers and Konnerth, 2009; Helmchen et al., 1999). This method can only target one cell per injection, which can either be an advantage or disadvantage depending on the specific experiment purpose. However, the substantial stress caused by the membrane

penetration can result in a relatively low survival rates for injected neurons. As compared to microinjection, electroporation can be used for both single cell and multiple cells labelling (Bonnot et al., 2005; Briggman and Euler, 2011). Applying an electrical field can temporarily increase cell membrane permeability by forming electropores, thus fluorescent calcium indicators can defuse into the affected cells through the formed electropores driven by the electroporation field (De Vry et al., 2010). Single-cell electroporation for expressing calcium indicators *in vivo* can be achieved by targeting a neuron using a glass pipette after negatively staining the cell (Nevian and Helmchen, 2007). Expressing GECIs by using in utero electroporation has its special advantages, as it has no strict limitation on transgene size, can target on specific cell types and can be applied in species where transgenic technology is less developed (Gee et al., 2015; Grienberger and Konnerth, 2012).

Chemical methods usually express fluorescent dyes in the targeted cells by increasing cell membrane permeability biochemically. Commonly used chemical methods for loading targeted cells with fluorescent dyes are: acetoxymethyl (AM) ester loading and dextran-conjugated loading. Cell membranes are not permeable to most of the chemical fluorescent dyes. However, the AM form of the indicator can diffuse through the cell membranes and the entered indicators will be trapped within the cell due to its impermeability after cytosolic esterases cleaving the AM groups off (Tsien, 1981). This method is suitable for labeling population of cells and has been successfully applied in *both in vitro* (Berger et al., 2007) and *in vivo* (Stosiek et al., 2003). Dextran-conjugate loading is another method suitable for labeling population of cells. Locally injected dextran-conjugated organic calcium indicators results in both retrograde and anterograde dye uptake (Gelperin and Flores, 1997; O'Donovan et al., 1993), which makes the investigation of the cells projecting to a specific region of interest possible.

1.3.2 Viral-mediated transduction

The natural processes and ability of a virus to infect a host cell in order to cause expression of their own genetic information within the host cell environment can be used for expressing fluorescence protein in targeted cells both *in vitro* and *in vivo*. This method offers the possibility to achieve cell-type specific labelling and long-term expression. However, there are limitations such as construct sizes, possible immune responses and some safety concerns. There are four commonly used viral vectors in Neuroscience: lentivirus, Herpes Simplex Virus (HSV), Adenovirus and Adeno-associated virus (AAV). Different viral vectors have different advantages and drawbacks. Researchers usually choose specific viral vector types according to the experimental purposes and requirements.

Lentivirus is able to integrate into the host cell genome. Thus, it is suitable for experiments that require long-term expression. Lentivirus have a insert capacity of 9 kb (Kumar et al., 2001) and their expression pattern are more localized surrounding the injection sites as compared to AAVs' (Yizhar et al., 2011). HSVs are neurotropic viruses that do not integrate into the host cell genome. It has a large insert capacity and can spread transsynaptically to soma (retrograde labeling) (Simonato et al., 2000). Its cellular toxicity and the difficulty to engineer limit its usage in neuroscience research. Adenovirus have a insert capacity of 27 kb (Soudais et al., 2004) and because they do not integrate into the host cell genome, they can only express the introduced gene transiently. It should be noticed that Adenovirus could cause strong immune responses in *in vivo* conditions (Lowenstein et al., 2007).

Among all the viral vectors, AAV vectors are the most commonly used one for delivering GECIs into neurons in the living animals. The recombinant viral vectors derived from AAV are widely used in neuroscience studies for expressing GECIs in neurons due to its low immunogenicity, nonpathogenicity. AAV virus that carry GECI sequences can be stereotaxically injected into the target brain regions

(Cetin et al., 2006) to achieve regional gene expression, and there are evidence showing that combined injection of recombinant AAVs with mannitol can enhance the gene expression in rodent brains (Mastakov et al., 2001). Besides, unlike adenovirus, AAVs integrate into the host cell genomes, which allows high expression levels over long periods of time. Some drawbacks of this vectors are the onset of AAV-mediated gene expression usually takes two to three weeks after the injection, which is longer than using other viral vectors and AAVs only has a insert capacity of about 4.7kb (Dong et al., 1996).

Specific labelling of targeted neuron types/subtypes can be achieved by using specific combination of AAV serotypes and promoters or in combination with Cre-activated viral gene expression.

Serotypes. The most commonly used AAV serotypes in neuroscience studies are 1, 2, 5, 6, 8 and 9 (Aschauer et al., 2013). Different AAV serotypes have different capsid proteins. Capsid proteins can determine the infection efficiency of specific serotypes by interacting with different receptors on target cell membranes (Buning et al., 2008). For example, evidence suggests that with the same promoter AAV5 have a broader gene expression pattern than AAV2 in hippocampus region (Aschauer et al., 2013; Burger et al., 2004); AAV8 is particularly efficient to drive transgene expression in astrocytes while AAV9 is very efficient for labelling neocortical neurons (Aschauer et al., 2013). Scientists have been working on targeted labelling of specific cell populations by developing novel capsid sequences (Klimczak et al., 2009). Besides, the infectivity for different cell types of each AAV serotypes are dose dependent (Klein et al., 2002).

Promoters. Better cell-type specificity can be achieved by combining specific serotype and promoter. Given to the insert capacity of AAV is only about 4.7kb, not all cell-specific promoter can be insert into AAV vector together with a GECI. The most commonly used ubiquitous promoters which can drive robust gene expression in neurons are: human elongation factor-1α (EF-1α) (Tsuchiya et al., 2002) and

cytomegalovirus early enhancer/chicken β-actin (CAG) (Weitz et al., 2013); the most commonly used neuron specific promoters are: human synapsin 1 (hSyn1) for labeling neurons (Kügler et al., 2003; Minderer et al., 2012), and calcium/calmodulin-dependent protein kinase IIα (CaMKIIα) for labeling only excitatory pyramidal neurons (Inoue et al., 2014); and promoter for labeling astrocytes is glial fibrillary acidic protein (GFAP) (Akerboom et al., 2013). Using short inhibitory neuron specific promoters to label interneurons, however, can be very challenging (Nathanson et al., 2009).

In combination with Cre-activated viral gene expression. Given to the limited insert capacity of AAV vectors, scientists need to find other methods in order to label specific cell types or even subtypes.

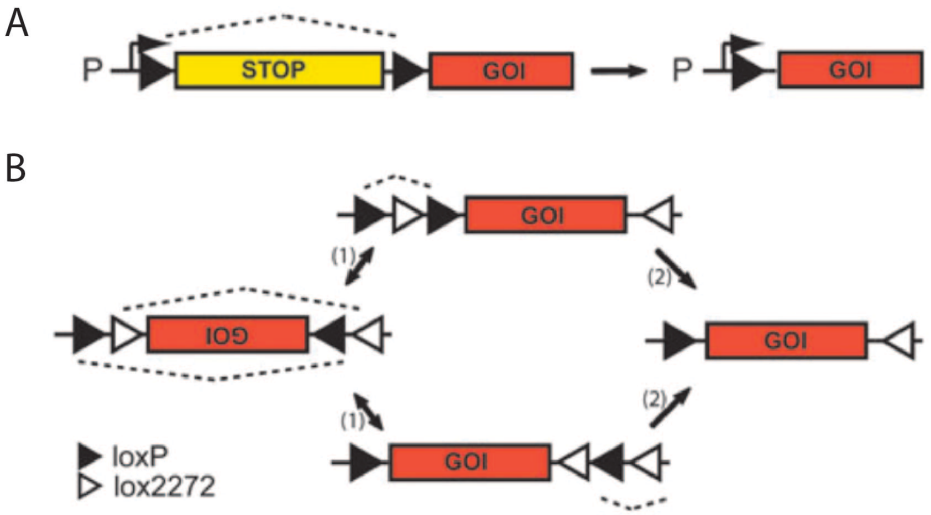

Figure 1-7: Cre-activated viral gene expression switches. *A). Stop cassette regulated expression of a gene of interest (GOI). In the presence of Cre, the stop cassette that is flanked by two recombinase recognition sequences loxP sites is excised (one loxP site remains). Thus allow the transcription of the GOI. B). FLEX switch regulated expression of a GOI. The GOI is inverted between two pairs of heterotypic, antiparallel lox-type recombination sites (loxP and lox2272). In the presence of Cre, the originally inverted GOI will first undergo an inversion and then an excision of two sites. The resulted recombination sites will lead to the expression of the GOI and further recombination will be impossible. Adapted from Betley et al.* (Betley and Sternson, 2011).

Cre-activated viral gene expression method that combining a Cre recombinase driver mouse or rat line (Gong et al., 2007; Witten et al.,

2011) with a Cre-dependent viral vector is one of them. With this method, the cell-type specific expression of Cre is under the control of large upstream promoter regulatory regions in the transgenic mouse genome (Gong et al., 2007). Thus, the robust expression of the gene of interests in cells that express Cre-recombinase can be achieved by using recombinase-dependent rAAV vectors containing a ubiquitous, strong promoter (Kuhlman and Huang, 2008). There are two strategies for achieve targeted expressions by using Cre-activated viral gene expression method (**Figure 1-7**). One is to introduce a Cre-dependent transcriptional stop cassette place in between the promoter and the gene of interest. However, this strategy puts an extra limit on the size of the promoter and the gene of interest (Kuhlman and Huang, 2008). Another strategy involves a flip-excision (FLEX) switch. Due to the inverted orientation of the gene of interest in the absence of Cre, this method can avoid the expression "leakage" that are observed using the first "stop cassette" strategy (Kuhlman and Huang, 2008).

1.4 Imaging cortical activity *in vivo*

Over the last decades, considerable efforts have been made towards understanding more about cortical information processing. Wide-field imaging is an excellent method for investigating how information spreads between spatially distributed cortical areas horizontally. The development of two-photon imaging using GECIs offers a great opportunity to study cortical activity with cellular resolution at different vertical depths in living animals. Here I discuss the most commonly used calcium imaging methods for achieving the goals of imaging neuronal activity on a larger scale or in a deeper depth.

1.4.1 *In vivo* wide-field imaging

Repeated large-scale imaging from the same subjects over long periods of time is essential for a better understanding of cortical function. Intrinsic optical signal (IOS) imaging is a dye-free imaging technique that uses intrinsic signals to read out cortical activity (Malonek and Grinvald, 1996). It is based on the fact that neuronal activity in cerebral cortex is accompanied by corresponding haemodynamics, which can affect the light reflectance patterns of the living brain (Erinjeri and Woolsey, 2002; Kalatsky and Stryker, 2003). One major advantage of IOS imaging is that it allows longitudinal experiments in individual animals over long periods of time. Thus, it is a useful technique for studying experience-dependent cortical plasticity (Polley et al., 2004). However, because the intrinsic signals measured with IOS imaging lack the millisecond time resolution and have an indirect relationship to neuronal activity, IOS imaging cannot offer sufficient temporal resolution to capture signal onset kinetics and is not an ideal method for investigating the details of high-frequency responses.

Other optical methods using organic voltage- or calcium-sensitive indicator dyes allow recording the fast dynamics of cortical activity on large-scale level (Berger et al., 2007). Voltage-sensitive dyes (VSDs) are dyes that insert into the neuronal plasma membrane and change their fluorescence intensity depending on the membrane potential changes across the membrane. Classic VSD optimized for *in vivo* recording such as RH1691 can achieve millisecond and subcolumnar resolution when used in combination with advanced charged coupled detector (CCD)/complementary metal-oxide semiconductor (CMOS)-based cameras (**Figure 1-8**) (Berger et al., 2007; Shoham et al., 1999). VSDs imaging can provide more direct and complete information about electrical events happening in neurons as compared to other optical methods, as it is sensitive to subthreshold membrane potential changes. However, this method offers a small signal-to-noise ratio (SNR) because of the small fluorescence changes. In contrast, imaging with calcium-

sensitive dyes (CSDs) provides larger SNR as compared to VSD imaging. CSDs respond to the cytosolic free Ca^{2+} concentration changes with temporal precision of a few milliseconds and mainly report suprathreshold neuronal responses. Due to the slow kinetics of calcium unbinding as well as the slower cytosolic calcium transients changes as compared to membrane potential changes, CSD signals typically are slower than VSDs imaging. Although both organic voltage- and calcium-sensitive indicator dyes are powerful imaging tools with relatively high temporal resolution, yet organic dyes have their limitations. They not only suffer to a variable degree from phototoxicity and non-specific labelling, but they also are not optimal for longitudinal studies because repeated tissue staining in consecutive imaging session has proven difficult (Andermann et al., 2010; Slovin et al., 2002). The previously introduced GECIs could provide an alternative to CSDs as they should be able to report large-scale cortical map dynamics chronically over long periods. In my thesis I have explored this type of application, which had not been explored before.

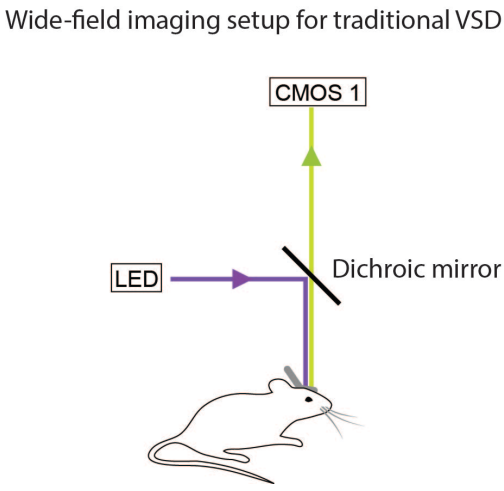

Figure 1-8: Schematic illustration of wide-field microscopy using complementary metal-oxide semiconductor (CMOS)-based detection unit. *Adapted from Minderer and Liu, et. al. (Minderer et al., 2012).*

1.4.2 Two-photon calcium imaging

Before the establishment of two-photon microscopy (Denk et al., 2008), single-photon excitation methods such as confocal microscopy were widely used for in vitro imaging. The light-matter interaction in single photon excitation is linear. It is based on molecular absorption of single photons, thus it relates linearly to the laser intensity. In single-photon excitation, a fluorophore accomplishes the transition from its ground state to an excited state by the absorption of a single photon. After the excitation, the fluorophore relaxes to its ground state by emission of a photon. In confocal imaging, large parts of the specimen below and above the focal plane are illuminated. In order to selectively collect the fluorescence emanating from the focal plane, a pinhole is placed before the photomultiplier tube (PMT) for blocking the out-of-focus fluorescence (**Figure 1-9**). However, confocal imaging cannot distinguish the focal planed emitted photons that scattered on their way back through the optical path from the real out-of-focus fluorescence, especially in highly light scattering tissues such as brain tissues.

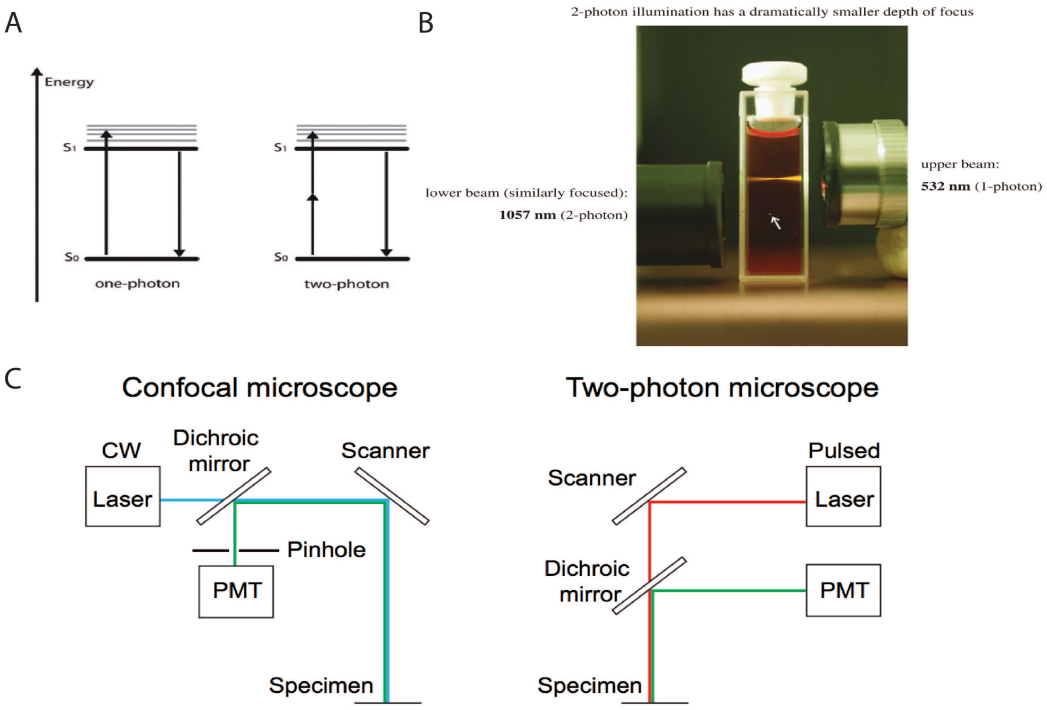

Figure 1-9: Confocal and two-photon microscopy comparison. *(A). Jablonski diagram of one-photon (left) and two-photon (right) excitation.*

(B). Illumination comparison using single photon and two photon wavelengths. White arrow indicates the focal spot of two-photon illumination. (C). Schematic illustration of commonly used confocal and two-photon microscopy. Adapted from Ustione and Piston, Homma et. al. and Grienberger and Konnerth. (Grienberger and Konnerth, 2012; Homma et al., 2009; Ustione and Piston, 2011).

In two-photon excitation, the transition from the ground state to an excited state of a fluorophore is achieved by near-simultaneous (within ~10^{-16} s) absorption of two photons (**Figure 1-9** A right). Thus, two low-energy near-infrared (IR) photons together can make an excitation quantum event occur. Because the process of two-photon absorption is nonlinear, the excitation is highly unlikely to occur outside the focal point of the laser light. This property of two-photon excitation can significantly reduce the out-of-focus excitation and bleaching as compared to single photon excitation (**Figure 1-9** B). Thus a pinhole as used in confocal imaging is not required in two-photon microscopy and the concentration of the excitation light source is achieved by the usage of high numerical aperture (NA) objectives and ultra-short (about 100 fs duration), pulsed laser light. Besides, the longer excitation wavelengths used in two-photon excitation have better tissue penetration power and are less scattered in the brain (Oheim et al., 2001). For all those reasons, the application of two-photon microscopy in neuroscience allows structural and functional investigations of neuronal activity in scattering brains *in vivo* with high spatiotemporal resolution.

Although two-photon microscopy has become a powerful technique for monitoring morphological and functional changes of the scattering brains since its invention decades ago (Denk et al., 2008), most studies using two-photon microscopy to investigate mammalian brains *in vivo* have been limited to supragranular layers. One reason for this depth limit is optical aberration. Aberration is caused by the refractive index differences between window, immersion solution as well as within brain tissues. Brain tissue induced aberration increases with imaging depth increase. Aberration could be reduced by using adaptive optics (AO) techniques (Ji et al., 2010; Rueckel et al., 2006) and by positioning the

imaging site as perpendicular to the optical axis of the microscope objective as possible. In addition to aberration, another main reason that limits the imaging depth is light attenuation caused by absorption and scattering. Both absorption and scattering reduce light intensity exponentially with depth increase. Despite the difficulty, attempts have been made for imaging infragranular layers. For example, Mittmann et al. managed to image L5 neuronal somata in mouse somatosensory cortex *in vivo* by using two-photon microscopy with a regenerative amplifier in combination with GCaMP3 (Mittmann et al., 2011). The use of a regenerative amplifier can increase the efficiency of two-photon excitation by amplifying a selected subset of laser pulses. In another study, red fluorescent protein-labelled neurons in the stratum pyramidale of a B6.Cg-Tg(Thy1-Brainbow1.0)HLich/J mouse can be seen 1,060–1,120 mm below the surface of the brain by using three-photon fluorescence microscopy (Horton et al., 2013). In addition, by using a right-angle view through a chronically implanted glass microprism in combination with GCaMP3, calcium signals were recorded from all six layers in visual cortex of awake mice (Andermann et al., 2013). However, the introduction of a microprism into the brain tissue is highly invasive. Despite these significant technical progress, the methods for investigating the functional role of all six cortical layers during sensory information processing and integration in awake behaving animals need to be further optimized. As mentioned in Section 1.2, red light has longer wavelength, thus it has a lower probability of photons scattering away from their ballistic path during imaging and they are less affected by haemoglobin absorption. Therefore, red light is less affected by tissue scattering as well as blood absorption. Therefore, deeper cortical layer imaging could be improved by using red-shifted fluorescent dyes, which are currently under development. In addition, the newly developed layer-specific labelling transgenic mouse lines may help to improve image quality in deeper cortical layers by minimizing the fluorescence staining of upper layer neurons. In my thesis I aimed to advance imaging deeper along the vertical dimension of neocortex by applying a novel red-shifted GECI.

1.5 Goals of this thesis

Methods that allow the chronic investigation of information processing between distant cortical regions horizontally as well as across different cortical layers vertically in mouse cortex will facilitate our understanding of the structure–function relationship in complex brain networks. However, previous existed methods are not optimized for studying the cortical sensory representations dynamics over long periods of time. In addition, most previous *in vivo* studies using optical methods are limited to the superficial cortical layers, and the investigation of deeper layer neurons in intact brains are generally hindered by their depth. In this thesis, I present two projects that use optical tools in combination with newly developed GECIs to tackle the challenges of chronic wide-field calcium imaging with high spatiotemporal resolution as well as calcium imaging in behaving mice across the entire neocortical layers in mouse barrel cortex.

1.5.1 Goals project I

Large-scale, chronic imaging from the same subjects over long periods of time is essential for a better understanding of cortical function. While chronic imaging is well established using dye-free methods such as intrinsic optical imaging, intrinsic optical imaging has slow dynamics and an indirect relationship to neuronal activity. Although having faster dynamics, other methods using organic voltage- or calcium-sensitive indicator dyes suffer from phototoxicity and non-specific staining. In addition, organic dyes are not optimal for chronic experiments because they require repeated tissue staining.

In the first project of this thesis, I present a method using wide-field calcium imaging in combination with ratiometric GECI YC3.60 to repeatedly measure fast dynamics of sensory-evoked spatiotemporal activity across large areas of mouse somatosensory cortex over multiple

weeks in the same animal. To be more specific, the main goals of the first project were:

- To establish a method that enable chronic investigation of large-scale cortical activity with the temporal resolution necessary to capture signal onset kinetics and high-frequency responses using GECI YC3.60.

- To investigate with this method how stable the functional map is in mouse barrel cortex.

1.5.2 Goals project II

A better understanding of cortical infragranular layers is dispensable to the investigation of cortical information integration and processing. Although two-photon fluorescence microscopy has become an essential tool for imaging of neurons at cellular spatial resolution in scattering brains, however, most *in vivo* two-photon studies are limited to the superficial cortical layers. Despite the efforts to image deep layer neurons, how sensory information are processed and integrated across cortical layers in intact brains of awake behaving animals are still largely unknown. The current popularly used GFP/YFP-based GECIs are not optimized for imaging the deep cortical infragranular layers, because tissue scattering, a main and difficult factor that limits two-photon imaging depth, is weaker when using GECIs that have longer excitation wavelengths.

In the second project of this thesis, I present a method using two-photon calcium imaging in combination with a newly developed red GECI R-CaMP1.07 to measure calcium signals from cells located in L5 at 550-750 micron depths and even L6 cells at depth greater than 800 micron in head-fixed, awake mice during free-air whisking behaviour. To be more specific, the main goal of the second project is:

- To achieve larger imaging depths by using excitation of a red GECI R-CaMP1.07 at 1040-nm wavelength with a compact, high-power, low-cost femtosecond laser

- To collect two-photon calcium imaging data from all cortical layers in barrel cortex in head-fixed, awake mice during free-air whisking behaviour to reveal the vertical profile of columnar activity.

2 Chronic imaging of cortical sensory map dynamics using a genetically encoded calcium indicator

Matthias Minderer*, Wenrui Liu*, Lazar T. Sumanovski, Sebastian Kügler, Fritjof Helmchen and David J. Margolis

Original article published in: The Journal of Physiology. 2012 Jan 1;590 (Pt 1):99-107.

* M. Minderer and W. Liu contributed equally to this work.

Own contributions: I made the DNA plasmids, performed the AAV injections. and I was responsible for imaging experiments and participated in the data analysis.

2.1 Abstract

In vivo optical imaging can reveal the dynamics of large-scale cortical activity, but methods for chronic recording are limited. Here we present a technique for long-term investigation of cortical map dynamics using wide-field ratiometric fluorescence imaging of the genetically encoded calcium indicator (GECI) Yellow Cameleon 3.60. We find that wide-field GECI signals report sensory-evoked activity in anaesthetized mouse somatosensory cortex with high sensitivity and spatiotemporal precision, and furthermore, can be measured repeatedly in separate imaging sessions over multiple weeks. This method opens new possibilities for the longitudinal study of stability and plasticity of cortical sensory representations.

2.2 Introduction

Optical imaging techniques have enabled important advances in systems neuroscience by allowing investigation of spatiotemporal activity dynamics over large areas of cortex. Chronic, repeated imaging from the same subjects over long time periods is essential for longitudinal studies of cortical function, but presents additional technical challenges. While chronic imaging is well established using dye-free methods such as optical imaging of intrinsic signals (Masino and Frostig, 1996), intrinsic signals, including autofluorescence (Shibuki et al., 2003), have slow dynamics and an indirect relationship to neuronal activity. Fast dynamics of cortical activity can be visualized using fluorescence imaging of organic voltage- or calcium-sensitive indicator dyes on the wide-field (WF) (Berger et al., 2007; Grinvald and Hildesheim, 2004) and local population levels (Grewe and Helmchen, 2009). However, organic dyes suffer from photo-toxicity and non-specific staining, and critically, are not optimal for chronic experiments because they require repeated

tissue staining before each imaging session (Andermann et al., 2010; Slovin et al., 2002).

Fluorescent protein indicators are well suited for chronic imaging. Genetically encoded calcium indicators (GECIs), pH- and voltage-sensitive proteins have been used for WF mapping of neuronal activity *in vivo* (Akemann et al., 2010; Bozza et al., 2004; Hasan et al., 2004), but methods have not been optimized to record fast spatiotemporal dynamics of sensory representations repeatedly in longitudinal studies. While GECIs have emerged as powerful tools for chronic two-photon imaging of action potential (AP)-related neuronal activity with cellular resolution (Andermann et al., 2010; Mank et al., 2008; Tian et al., 2009) their capacity for reporting large-scale cortical map dynamics has not been fully investigated.

Among GECIs, Yellow Cameleon (YC) 3.60 is a good candidate for long-term cortical mapping because it is a ratiometric FRET (fluorescence resonance energy transfer) indicator (Nagai et al., 2004), and therefore less influenced by optical path changes and brain motion than single wavelength indicators. Furthermore, YC3.60 expression and functional properties are stable in mouse cortical neurons over months (Andermann et al., 2010; Margolis and Al., 2010), and *in vivo* cellular signals sensitively report AP firing (Lütcke et al., 2010). Previous studies that imaged WF GECI signals (Hasan et al., 2004; Lütcke et al., 2010) used non-ratiometric systems with limited spatial and/or temporal resolution and therefore did not capture detailed spatiotemporal activity dynamics. Chronic WF mapping of cortical activity using GECIs has not been achieved.

Here we present a method based on WF imaging of virally expressed YC3.60 for measuring fast dynamics of sensory-evoked spatiotemporal activity across large areas of mouse somatosensory cortex, using a preparation that enables long-term repeated imaging.

2.3 Methods

2.3.1 Animals

Experiments used male or female C57BL/6 mice, 6–10 weeks old at time of adeno-associated viral (AAV) injection, and were approved by the Zurich Cantonal Veterinary office. Presented data include 13 imaging sessions from five mice.

2.3.2 Viral-mediated expression

YC3.60 was expressed in neurons by intracortical injection of AAV-1/2 hybrid serotype vector AAV-1/2-hSyn-YC3.60 (2×10^8 transducing units μl^{-1}), as in previous work (Lütcke et al., 2010). Under isoflurane anesthesia (4% induction, 1–2% maintenance), 100–150nl virus mixed 1:1 with 20% D-mannitol (200–300nl total volume) was injected through a glass pipette (5–8 µm open tip diameter) 300–500 µm below the pia at 1–3 sites into primary somatosensory cortex (mm from bregma; posterior, lateral): barrel 1 (−1, 3.3), barrel 2 (−0.8, 3.5), hind- limb (−0.5, 1.5).

2.3.3 Chronic cranial window

1–3 weeks after viral injection, mice were re-anaesthetized with isoflurane and implanted with a head post and cranial window. Open-skull windows (Holtmaat et al., 2009) used 3 mm × 3 mm no. 1 thickness square cover glass (UQG Optics or Bullen Inc.). One mouse was implanted with a polished-and-reinforced-thinned-skull window (Drew et al., 2010) using 5 mm no. 1 round cover glass (Menzel Gläser); data from both window types was pooled. Mice recovered for >14 days.

2.3.4 Histology

Mice were intracardially perfused and brains fixed in 4% paraformaldahyde. The entire cortex from the imaged hemisphere was dissected and flattened between microscope slides during post-fixation. Tangential 100 µm sections were cut on a cryotome and stained for cytochrome oxidase. Bright field images were acquired with a stereoscope and aligned to *in vivo* images in Adobe Illustrator.

2.3.5 Imaging setup

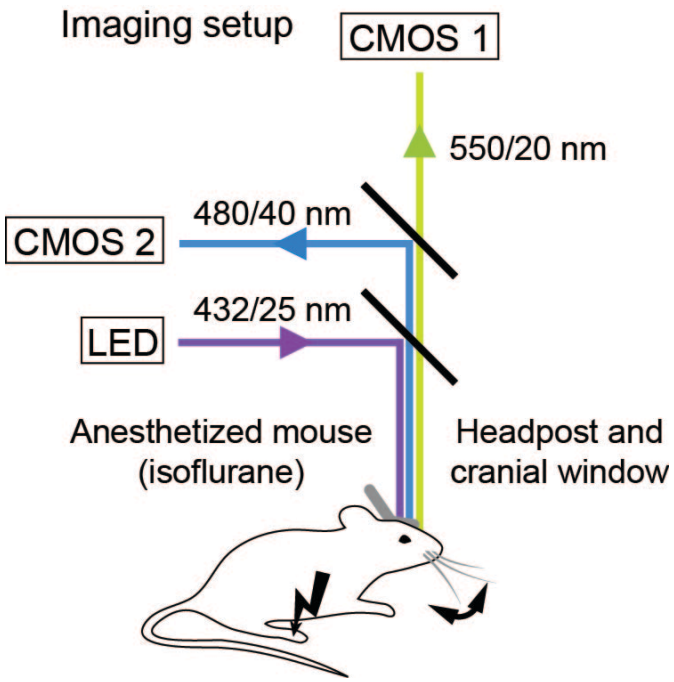

Figure 2-1: Schematic diagram of two-camera high-speed fluorescence imaging setup for in vivo WF GECI imaging.

Our custom tandem-lens fluorescence macroscope (**Figure 2-1**) incorporated two identical high-speed cameras (100 pixel×100 pixel CMOS sensor; MiCam Ultima-L, Brain Vision Inc.) to visualize FRET between the cyan and yellow fluorophores of YC3.60. Fluorescence was excited through a 432-nm/25-nm excitation filter (Chroma) with a high power 60-chip 435-nm LED (±15-nm half-width; Roithner Lasertechnik) driven by a stabilized current driver (Prizmatix). Excitation light was

reflected by a 50-mm dichroic mirror (Q470lp, Chroma) and focused through a 17 or 25 mm f0.95 lens (D-1795 or D-2595; Navitar). Fields of view with these lenses were 3.0 or 4.4 mm (33 or 49 μm pixel width), respectively. Cyan fluorescent protein (CFP) fluorescence emission was reflected to CMOS2 by a second dichroic mirror (DC-Blue, Linos) mounted on a kinematic platform (Thorlabs) to aid alignment, emission filtered (480-nm/40-nm; Chroma) and collected by a 50 mm f0.95 lens (D-5095; Navitar). Yellow fluorescent protein (YFP) fluorescence passed the second dichroic, an emission filter (550-nm/20-nm; Chroma), and was imaged onto CMOS1 by a second 50 mm f0.95 lens. Cameras were synchronized and acquisition controlled by MiCam Ultima imaging system (Brain Vision, Inc.).

2.3.6 Electrophysiology and intracortical microstimulation

Local field potential (LFP) was recorded using a glass pipette (tip diameter ~5 μm) filled with Ringer solution (in mM: 135 NaCl, 5.4 KCl, 1 $MgCl_2$, 1.8 $CaCl_2$ and 5 Hepes) and inserted through the dura mater into layer L2/3. Signals were amplified (ELC-03XS; NPI), bandpass-filtered (0.3–500 Hz), digitized at 20 kHz (ITC-18, Instrutech) and recorded using custom software (Igor Pro, Wavemetrics). Intracortical microstimulation (ICMS) current pulses from a stimulus isolator were delivered through a glass pipette (tip diameter ~5 μm) filled with Ringer solution inserted into L2/3.

2.3.7 Sensory stimulation

Current pulses were delivered by a stimulus isolator to the contralateral hindpaw through a subcutaneous bipolar needle electrode. For whisker stimulation, individual whiskers were inserted into a metal tube glued to a piezo bending element (to ~3 mm from fur) and mechanically deflected by ~0.5 mm (~14 degrees).

2.3.8 Imaging and data processing

Mice were anaesthetized with 0.5–1.5% isoflurane so that breathing rate was >1Hz and heart rate was typically 6–10 Hz (~350–600 beats min^{-1}). Acquisition of each trial (movie) was triggered on the electro-cardiogram (ECG) using a window discriminator. To isolate stimulus-related signals, alternate heartbeat-triggered movies were acquired with (Stim) and without (NoStim) stimulation and subtracted after $\Delta R/R$ calculation. The ratiometric FRET signal (% $\Delta R/R$) was calculated as the change in (YFP:CFP) fluorescence ratio (ΔR) relative to baseline ratio (R; averaged 50–480 ms before stimulation) after detector-offset subtraction. Calcium signals are reported as % $\Delta R/R$ (Stim – NoStim) except in (**Figure 2-3**), where we show relative fluorescence changes separately for each channel ($\Delta F/F$).

2.3.9 Data analysis

Raw 16-bit images were analysed in ImageJ (http://rsbweb.nih.gov/ij/) using custom routines. To calculate calcium signal ($\Delta R/R$) time series, signals were spatially averaged from regions of interest (ROIs; typically containing 25–100 pixels, about 0.03–0.1 mm^2) defined by hand or by contour level relative to signal peak. No further temporal or spatial filtering was used for time series analysis or display. To estimate signal onset location, the first four frames (40 ms) after signal onset were averaged and spatially filtered; the signal onset location was then defined as the maximum pixel in the filtered image. Signal-to-noise ratio (SNR) was defined as the initial peak amplitude after temporal averaging (50-ms window) divided by the SD of a 50-ms pre-stimulus baseline. Decay time constants were measured from single-exponential fits.

2.4 Results

To image WF GECI signals *in vivo*, we built a macroscope using two high-speed cameras for simultaneous measurement of cyan and yellow fluorescence emission from neurons expressing YC3.60 (**Figure 2-1**; see Methods). Cortical expression areas resulting from one to three intracortical AAV injections spanned millimeters of sensory cortex and contained densely labelled neuronal somata and neuropil (**Figure 2-2**).

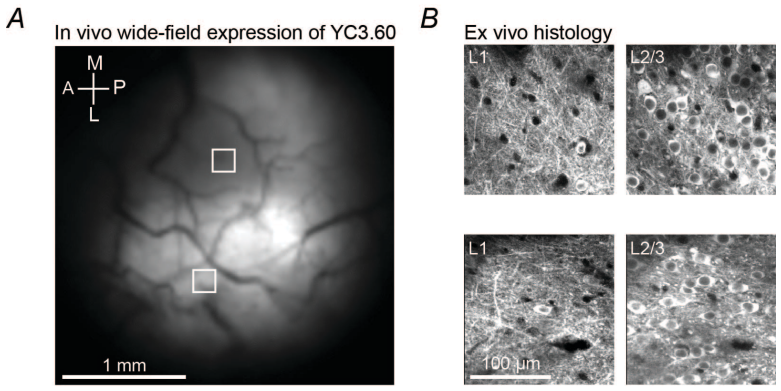

Figure 2-2: *(A) Yellow channel image of YC3.60 expression area in somatosensory cortex of an anaesthetized mouse 115 days after AAV injection. (B) Ex vivo two-photon images of YC3.60 expression in neurons and neuropil of L1 and L2/3, from the same mouse as in A (fixed tissue; locations marked by squares).*

Mice were anaesthetized with isoflurane and the cortex was imaged through a chronic cranial window. YC3.60 fluorescence signals were modulated with the heartbeat in both emission channels due to absorption by haemoglobin (e.g. Akemann et al. 2010), confounding the functional signals. This blood flow artifact was eliminated by triggering image acquisition on the ECG followed by subtraction of trials with and without stimulation (Stim – NoStim; see Methods) (**Figure 2-3** A). After this correction procedure, we readily resolved simultaneous increases in yellow and decreases in cyan fluorescence, as expected from a FRET indicator (**Figure 2-3** A, right). Single-trial ratiometric calcium signals ($\Delta R/R$) in hindlimb primary somatosensory cortex (HL) evoked by brief hindpaw stimulation (1 ms, 300 µA) could be resolved with high signal-

to-noise ratio (SNR) (**Figure 2-3** B). On average, SNR was 9.7 ± 6.4 for single trials and 25.3 ± 11.1 for 10-trial mean responses (mean ± SD; n = 5 mice, including whisker and HL stimuli). Spatiotemporal dynamics of the sensory-evoked response could be visualized at high frame rates (>500 Hz) as a localized initial response that subsequently spread over a larger area (**Figure 2-3** C).

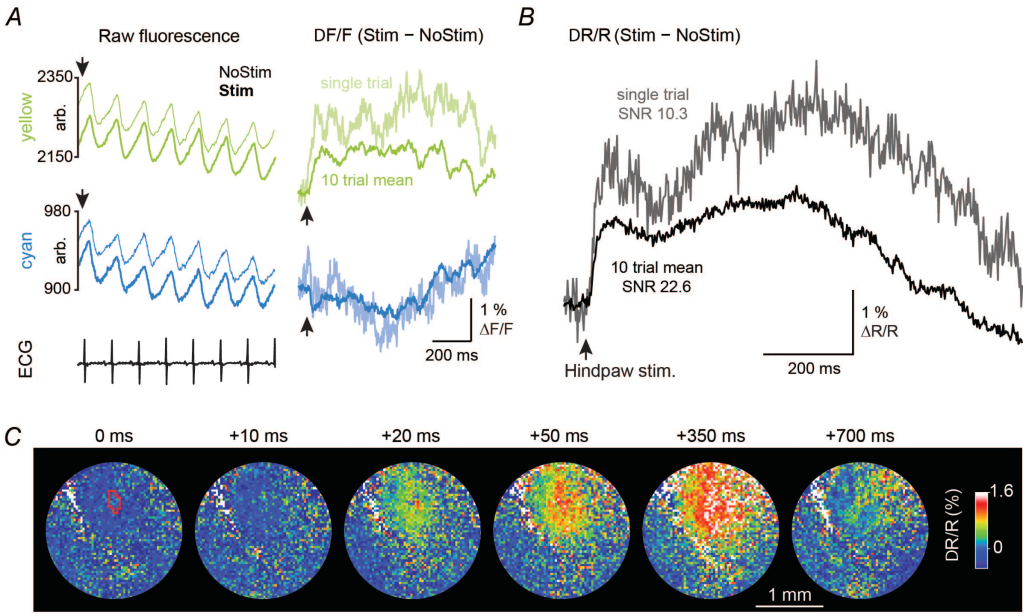

Figure 2-3: *(A) Left, single-trial raw fluorescence traces from each channel before (NoStim) and during (Stim) hindpaw stimulation (1 ms, 300 µA; arrows); right, single trial (thin lines) and mean (thick lines; 10 trials) ΔF/F for each channel. (B) Single-trial and mean ΔR/R (10 trials) for the same data as in A. (C) Movie frames corresponding to the data in A. Red contour on first frame indicates ROI used for spatial averaging of time series. Frame rate 500 Hz in A–C.*

To measure the signal onset kinetics, we compared responses in HL cortex evoked by sensory stimulation or direct intracortical microstimulation (ICMS) imaged at 1000 Hz. While both signals rose quickly (maximum slope, mean ± SD: HL, 87 ± 36% ΔR/R s^{-1}; ICMS, 98 ± 15% ΔR/R s^{-1}; n = 20 trials each), the expected ~10 ms difference in latency between the sensory-evoked (HL) and direct (ICMS) responses was clearly resolvable (**Figure 2-4** A). Time-to-peak from signal onset was ~60 ms for both HL and ICMS responses (mean ± SD: HL, 58 ± 20

ms; ICMS, 57 ± 13 ms; n = 20 trials each). The decay time constant (τ) pooled across ICMS and whisker-evoked responses was 274 ± 27 ms (mean ± SD; n = 20 trials ICMS, n=80 trials 10Hz whisker stimulation). These data indicate that high-speed WF GECI imaging captures rapid cortical dynamics.

To determine the relationship of WF GECI signals to sensory-evoked neuronal activity, we made simultaneous optical and local field potential (LFP) recordings. Optical and electrical signals in response to HL stimulation of three different intensities (50, 100, 300 μA; 1 ms) on average showed close correspondence, both in peak amplitude and timing (**Figure 2-4** B, left). Furthermore, single-trial LFP amplitude and single-trial WF signal amplitude were highly correlated (r = 0.847; P < 10^{-4}) (**Figure 2-4** B, right), demonstrating that WF GECI signals report local electrical neural activity with high fidelity, even on the single trial basis.

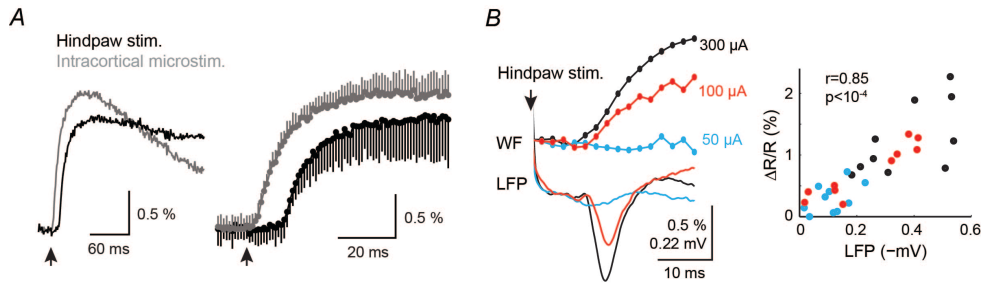

Figure 2-4: *(A) Left, comparison of responses to hindpaw sensory stimulation and intracortical microstimulation (1 ms, 500 μA for each; 1000 Hz frame rate); right, same data on expanded time scale (error bars, 1 SD). (B) Simultaneously recorded LFP and WF YC3.60 signals (frame rate 500 Hz): left, mean of 10 trials at three stimulation intensities (50, 100, 300 μA); right, single-trial correlation between LFP and WF signals for 10 stimuli each at 3 different intensities, as at left (Pearson's linear correlation coefficient, r = 0.85; P < 10−4). Data in **Figure 2-3** and **Figure 2-4** are from the same mouse.*

The high sensitivity and SNR of WF GECI signals allowed imaging of responses to more subtle sensory stimuli. In the whisker-related barrel cortex, we compared signal dynamics evoked by different types of single-whisker stimulation, as illustrated in one example mouse (**Figure 2-5** A and B). A 10 ms whisker deflection elicited a sharp transient with

onset kinetics resembling the ICMS and HL responses of **Figure 2-4** (**Figure 2-5** A, top, and **Figure 2-5** C). During a 1 s step deflection, a clear transient was evoked at stimulus onset and, after adaptation during the holding phase, again at stimulus offset (**Figure 2-5** A and B, middle). During a 10Hz, 1s train of deflections, each of the 10 transient bumps could be resolved (**Figure 2-5** A, bottom) as well as a larger extent of spatial activation (**Figure 2-5** B, bottom).

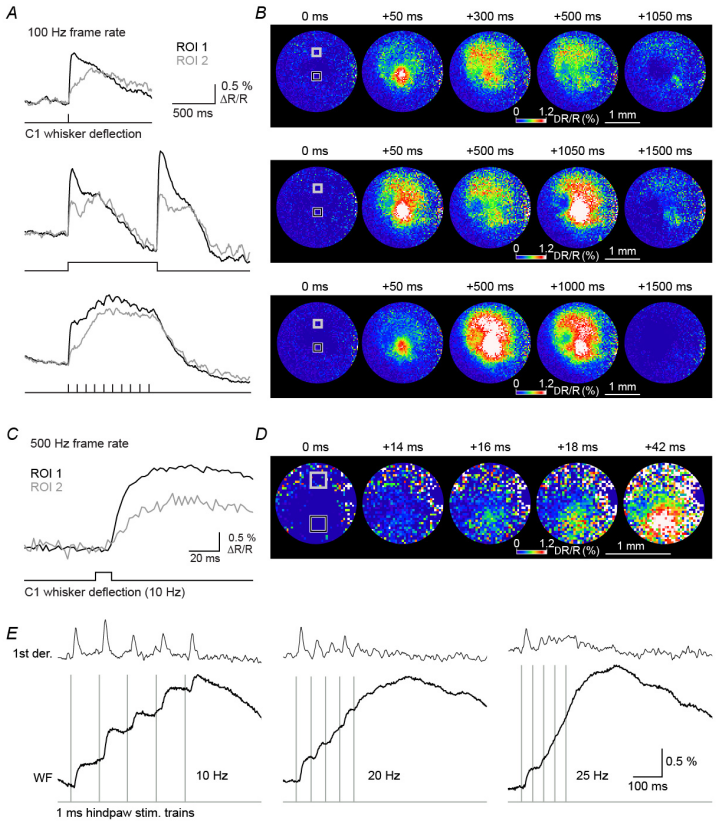

***Figure 2-5: Sensory-evoked dynamics of WF GECI signals**. (A) Responses in barrel cortex of one mouse evoked by three types of whisker deflections: single 10 ms (top, mean of 20 trials), 1 s step (middle, mean of 20), or 10 Hz for 1 s (bottom, mean of 40). 100 Hz frame rate. (B) ΔR/R movie frames corresponding to A. Squares indicate ROI positions for data in A. (C) and (D) Signal onset imaged at 500 Hz in same session (different sweeps to those in A). (E) Responses in HL cortex (different mouse to that in A–D) to hindpaw stimuli of varying frequency. First derivative of smoothed WF signal shown above each trace. 500 Hz frame rate.*

To determine the maximum temporal resolution of WF GECI signals, we measured responses evoked by brief HL electrical stimulation at frequencies from 1 to 50 Hz (different mouse to that in A–

D). Responses to individual pulses could be resolved during stimulus trains at frequencies up to 20 Hz but merged at higher frequencies (**Figure 2-5** E), setting a practical upper limit for imaging high-frequency sensory responses. Together, these data demonstrate the capacity of WF GECI imaging to resolve the spatiotemporal dynamics of sensory-evoked cortical activity.

To investigate spatial and temporal properties of sensory maps over time, we performed repeated imaging through chronically implanted cranial windows, allowing mice to wake up and return to their home cage between each session. As illustrated in **Figure 2-6** A and B, the spatiotemporal dynamics of responses to 10 Hz, 1 s stimulation of whisker C1 were highly reproducible in the same mouse for up to 7 weeks. In a different mouse, we mapped five individual whiskers on one session using single 10-ms deflections (**Figure 2-6** C). Signal contours at the 90% peak level approximated the size and position of the whisker barrels as defined by post hoc histology (**Figure 2-6** C–E). Over the next 6 weeks, we tracked responses to whiskers D1 and D2 (**Figure 2-6** F). Response amplitude and dynamics showed no degradation over time, although map position and shape as well as signal dynamics appeared more variable for the D1 than the D2 whisker, even though responses were imaged in the same sessions under identical experimental conditions (**Figure 2-6** F, G and H). These results illustrate the use of WF GECI imaging for measuring spatiotemporal features of cortical sensory maps over a time scale of multiple weeks, and suggest the importance of longitudinal experiments for understanding long-term cortical map dynamics.

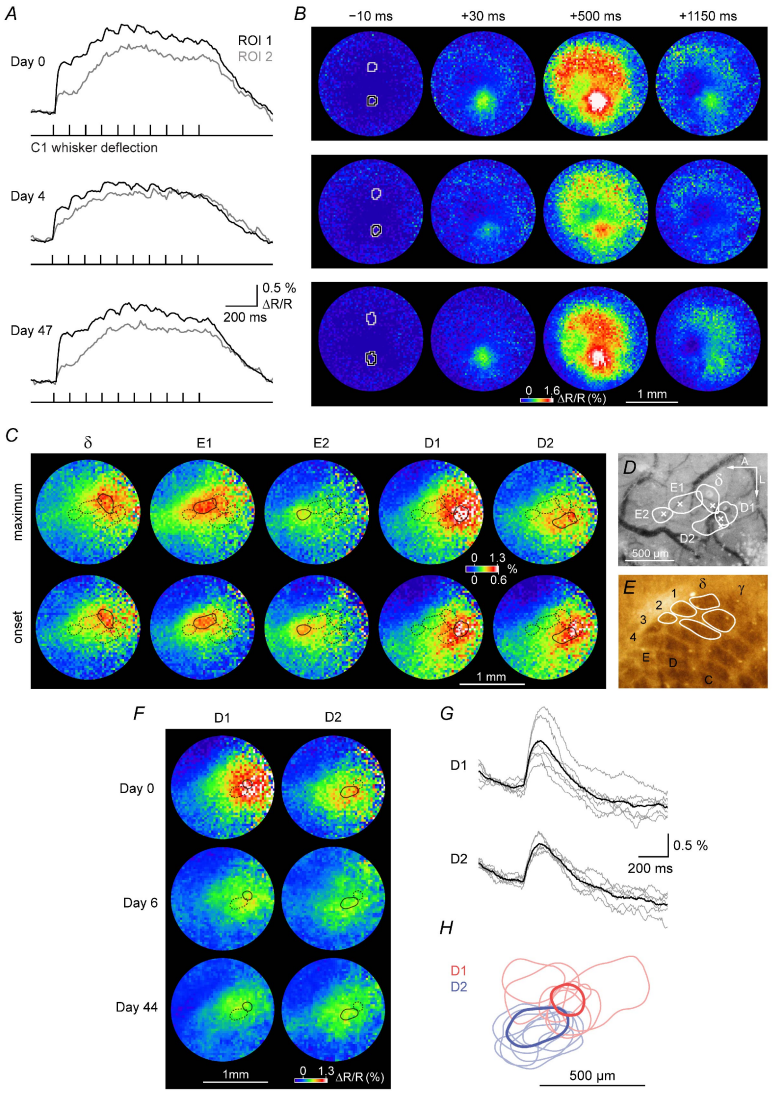

Figure 2-6: Long-term imaging of spatiotemporal map dynamics. *(A) Responses in barrel cortex (mean 40 trials each) from two ROIs (indicated on first frame in B) to 10 Hz whisker stimulation in the same mouse imaged in three sessions over 47 days (same mouse as in Fig. 2A and B). (B) Movie frames corresponding to responses in A; field of view shift over days is uncorrected. Time of individual frames relative to first stimulus shown above. (C) Maximum and onset response to five individual whiskers imaged in a single session (different mouse to that in A and B). 90% contours of all whiskers are overlaid (solid line indicates stimulated whisker). Stimulus was a single 10 ms deflection; mean of 20 trials each. (D) 90% contours overlaid on picture of blood vessels imaged through thinned-skull window 33 days after implant (49 days after virus injection). (E) Cytochrome oxidase barrel map of the same mouse (same scale as in D). (F) Maximum response images for whiskers D1 and D2 from three sessions over 44 days. (G) Signal dynamics and (H) 90% contour maps of D1 and D2 whisker-evoked responses over six sessions. Thick lines indicate all-session means (also overlaid in F). Frame rate 100 Hz in A–H.*

2.5 Discussion

Our data demonstrate that WF optical imaging of the GECI YC3.60 enables chronic *in vivo* investigation of the spatiotemporal dynamics of cortical activity in the anaesthetized mouse. Sensory maps can be imaged in the same mice over weeks and months, opening the possibility for longitudinal studies of stability and plasticity of large-scale cortical map dynamics.

Our method extends established cortical mapping techniques based on WF fluorescence imaging of synthetic voltage- and calcium-sensitive dyes (Berger et al., 2007; Grinvald and Hildesheim, 2004) to GECIs. The key advantage is the capability to image maps with high SNR and spatiotemporal precision longitudinally without the need to re-apply the indicator. Indicator-free techniques such as intrinsic signal or autofluorescence imaging, while useful for long-term mapping experiments, lack the temporal resolution necessary to capture signal onset kinetics and high-frequency responses, as we demonstrate with WF GECI imaging. Synthetic voltage-sensitive dyes can also be used in long-term studies (Slovin et al., 2002), but the need for tissue re-staining makes this approach less practical. Our approach of chronic WF imaging through a cranial window preparation should also be readily applicable to other types of GECIs and recently developed probes such as genetically encoded voltage indicators (Akemann et al., 2010) that have so far only been used in acute experiments.

A major advantage of genetic indicators is the ability to label specific cell populations. The neuronal-specific expression we achieved using AAV-1/2 hybrid serotype with the synapsin promoter (AAV-1/2-hSyn) confines labelling to local neuron populations and avoids non-specific labelling of glia or processes of remote cells (Lütcke et al., 2010). In addition to neuronal somata, the neuropil (dendrites and axons) is strongly labelled (**Figure 2-2** B) and gives rise to a prominent bulk signal thought to be axonal in origin (Berger et al., 2007; Kerr et al., 2005; Lütcke et al., 2010) that probably dominates the WF GECI signal. In this way, WF

GECI imaging is more similar to fiber optic fluorescence imaging than two-photon cellular-resolution imaging (Lütcke et al., 2010), with the additional feature that the spread of activity can be visualized at high frame rate over large areas of cortex. Because GECIs report spiking activity rather than subthreshold membrane potential (at least at the soma and proximal dendrite) (Lütcke et al., 2010; Tian et al., 2009), and because AAV-1/2-hSyn expression labels cells primarily in L2/3 and L5 but not L4, we propose that the WF GECI signal represents population spiking activity of predominantly L2/3 pyramidal neurons. The supra-threshold nature of WF GECI signals probably explains why our whisker maps are more spatially restricted than voltage-sensitive dye signals. Maps of spiking activity will be advantageous for localizing cortical areas specifically involved in suprathreshold neuronal signal transmission.

In the future, expression could be further restricted to subtypes of neurons, such as excitatory and inhibitory cells, providing cell-specific WF activity maps. We anticipate that chronic WF GECI imaging of defined neuronal networks will provide a bridge between systems and cellular neuroscience for the longitudinal study of cortical sensory processing and plasticity in both health and disease.

3 Red-shifted two-photon calcium imaging reveals across-layer profile of behaviour-related neocortical activity

Stefano Carta*, Wenrui Liu*, Yaroslav Sych, Andreas Stäuble, Jerry Chen, Fabian F. Voigt, Bernard Schneider, Masamichi Ohkura, Junichi Nakai[4], Asli Ayaz, Fritjof Helmchen

Manuscript in preparation.

* S. Carta and W. Liu contributed equally to this work.

Own contribution: I was responsible for AAV injections, window preparations, and functional imaging experiments. I also participated in the data analysis and manuscript preparation.

3.1 Abstract

Neurons in infragranular layers of neocortex crucially contribute to information processing, however, their deep location so far retarded functional characterization of their behaviour-related activity using calcium imaging. Here, we demonstrate *in vivo* Ca^{2+} imaging of whisking-related neuronal activity throughout all layers of mouse somatosensory cortex, including upper layer 6, using viral expression of the red fluorescent Ca^{2+} indicator R-CaMP1.07. We utilized a high-power solid state laser for efficient two-photon excitation of R-CaMP1.07 at 1040-nm wavelength, with two-fold increased scattering length compared to 740 nm. Using simultaneous electrophysiological recordings we find that R-CaMP1.07 is a sensitive reporter of action potentials *in vivo*. We monitored excitatory neuronal population activity throughout layers 2, 3, 5, and 6 in awake, head-fixed mice during spontaneous, voluntary whisking and analysed the cross-layer profile of whisking-related activity. Our study showed that the combination of new lasers operating above 1000 nm with red fluorescent proteins like R-CaMP1.07 enables calcium imaging in behaving mice throughout the entire neocortical layers.

3.2 Introduction

Layer 5 (L5) pyramidal neurons integrate widespread synaptic information inputs from different cortical layers and serve as the major output cell type. Layer 6 (L6) is the deepest layer in mammalian cerebral cortex and is essential for corticocortical and corticothalamic network interactions, respectively. Thus, the thorough investigation of cortical infragranular layers is dispensable for complete understanding of cortical information integration and processing. Although two-photon microscopy (Denk et al., 2008) has become a fundamental tool for neuroscience research because it allows comprehensive measurements

of neural network dynamics with high spatial-temporal resolution in living tissues (Grienberger and Konnerth, 2012; Helmchen and Denk, 2005), most *in vivo* two-photon microscopy studies are limited to the superficial cortical layers (J. L. Chen et al., 2013). Thus the investigation of L5 and L6 neurons mainly relies on morphological and electrophysiological studies in vitro (Briggs, 2010; Larkum et al., 1999; Ledergerber and Larkum, 2010; Marx and Feldmeyer, 2013; Oberlaender et al., 2011; Schubert et al., 2006) and relatively few work has been carried out *in vivo* (Constantinople and Bruno, 2013; Jacob et al., 2012; Manns et al., 2004).

Despite the limitation of conventional two-photon microscopy in imaging depth, several studies have performed *in vivo* calcium imaging from dendrites of L5 neurons (Helmchen et al., 1999; Mittmann et al., 2011; Xu et al., 2012). Recent work pushes the limits of imaging depth by using regenerative laser amplifiers (Mittmann et al., 2011; Theer et al., 2003), long-wavelength (1700 nm) lasers (Horton et al., 2013), or microprisms (Andermann et al., 2013) to the somata of infragranular layer neurons. Despite the significant technical progress, how the orchestrated activities of all six cortical layers integrate and process sensory information inputs as well as how they generate cortical outputs and communicate with other cortical areas or subcortical brain regions in awake behaving animals are still largely unknown.

Tissue scattering is the major complicating factor that limits two-photon microscopy imaging depth, and tissue scattering is weaker at longer wavelengths. However, the current popularly used green fluorescent protein based genetically-encoded calcium indicators (GECIs) (T.-W. Chen et al., 2013; Nagai et al., 2004) are not optimized for imaging the deep cortical infragranular layers. Thus, efforts have been made to develop GECIs that have longer excitation wavelengths (Akerboom et al., 2013; Inoue et al., 2014; Ohkura et al., 2012a). The use of red-shifted fluorescent dyes should improve deeper cortical layer imaging. Besides, the newly developed Cre-dependent virus or layer-

specific labelling transgenic mouse lines can help to improve image quality in deeper cortical layers by minimizing the fluorescence staining of upper layer neurons.

Here in this study, we readily measured calcium transients in L5 at 550-700 μm depths and also at depth greater than 800 μm, corresponding to L6, in head-fixed, awake mice during free-air whisking behaviour by exciting a red fluorescent calcium indicator at 1040-nm wavelength with a compact, high-power, low-cost femtosecond laser. The combination of new lasers operating above 1000 nm with red fluorescent proteins like R-CaMP1.07 offers an affordable approach and new opportunities for chronic investigations of the functional role of deep neocortical L5 and L6 for information processing within vertical columns of the mouse brain, especially during specific behaviours.

3.3 Methods

3.3.1 Animal preparation

All Experimental procedures were conducted in accordance with the Ethical Principles and Guidelines for Experiments on Animals of the Veterinary Office of Switzerland and were approved by the Cantonal Veterinary Office in Zurich. Throughout viral injection, cranial window implantation and intrinsic imaging procedures, mice (six C57BL/6J and one Rbp4-KL100 BAC-cre mouse (Gong et al. 2007) (MMRRC no. 031125-UCD), male or female, 5-8 weeks old at the time of viral injection) were anesthetized with isoflurane (4% induction, 1% maintenance) and body temperature was maintained at around 37°C using a regulated heating blanket and rectal thermal probe. We stereotaxically injected AAV1-EFα1-R-CaMP1.07 (for C57BL/6J mice, approximately 1x1013 vg/ml) and AAV1-EFα1-DIO-RCaMP1.07 (for

Rbp4-KL100 BAC-cre mouse, approximately 1x1013 vg/ml) into whisker-related somatosensory cortex (S1) in experimental animals (1.1mm posterior to bregma, 3.3mm lateral, ~150 μl, approximately 800-1000 μm below the pial surface) (Lütcke et al. 2010).

3.3.2 Cranial window implantation and habituation

A circular craniotomy (4 mm in diameter) was made at the injection site, then we placed a round glass cover slip directly onto the dura mater and sealed it to the skull with dental cement as described in previous studies (Margolis et al. 2012; J. L. Chen et al. 2013). Head fixation habituation was carried out 7 days after the window implantation according to published procedures (J. L. Chen et al. 2013).

3.3.3 Intrinsic optical signal (IOS) imaging and selection of imaging sides

The barrel field for each mouse was identified using IOS imaging under anesthesia (approximately 1% isoflurane). Reference vasculature images were obtained using a 546 nm LED light. The reflectance images were collected by a x4 objective (UPlanFL N, 4x/0.13; Olympus) with a CCD camera (Toshiba TELI CS3960DCL; 12-bit; 3-pixel binning, 427 × 347 binned pixels, 8.6 μm pixel size, 10 Hz frame rate) when a 630 nm LED light illuminated the cortical surface. The multiple-whisker stimulation (2 to 4° rostro-caudal deflections at 10 Hz) was conducted by a piezo-stimulator. Intrinsic signal changes were calculated as the fractional changes in reflectance relative to the pre-stimulus average (50 frames; expressed as $\Delta R/R$) and were averaged over 15 trials. We selected the two-photon imaging sites based on IOS imaging results, density and discernment of neuronal labelling in L5 as well as the blood vessels patterns.

3.3.4 Two-photon calcium imaging

Two-photon imaging was performed earliest 14 days after the window implantation. We used a custom-built two-photon microscope controlled by HelioScan (Langer et al. 2013), equipped with a ytterbium-doped potassium gadolinium tungstate (Yb:KGW) laser (1040 nm; >2 W average power; 230 femtosecond pulses at 80 MHz; model Ybix; Tim-Bandwidth Products), a water immersion 16x objective (CFI LWD 16X/0.80; Nikon), a Pockels cell (model 350/80 with controller model 302RM, Conoptics) and galvanometric scan mirrors(model 6210; Cambridge Technology). We excited R-CaMP1.07 at 1040 nm and fluorescence was collected with a red (610/75 nm; AHF Analysetechnik) emission filters. Images were acquired with 100 x 100 pixels at 10Hz. 30s-movies were acquired continuously with an inter-trial-interval of 20s.

3.3.5 Whisker tracking and kinematic analysis

Free-air whisking videos were acquired at 200 Hz using a high-speed CMOS camera (CL600X2; Optronis), which was triggered by the shutter signal. We illuminated the whisker field with a 850-nm infrared LED light (IR-12/65LED; Monacor). The average whisker angle across all imaged whiskers was measure and calculated using automated whisker-tracking software (Knutsen et al. 2005). The resultant amplitude trace was down-sampled to match the two-photon image acquisition.

3.3.6 Electrophysiology

R-CaMP1.07 was expressed in L2/3 neurons of the barrel cortex by intracortical stereotaxic injection of AAV under the control of the unspecific promoter EF-1α. Intracortical injections were performed on 4-6 weeks old BL/C57 mice under isoflurane anaesthesia, and 200-300nl of virus were injected through glass micropipettes into the layer 2/3 of the somatosensory barrel cortex (300µm depth).

Acute *in vivo* Ca^{2+} imaging and electrophysiology experiment were performed on infected mice after at least two weeks from injection. Mice anaesthesia was induced and maintained by isoflurane vaporization, and temperature was controlled and kept steady at 35°C during the surgery by using a heating pad (Watlow). However, during imaging recordings, the temperature was increased up to 37°C and the anaesthesia level was lowered for increasing cortical activity. To perform experiments combining imaging and electrophysiology a stainless steel plate was implanted to the exposed skull by using dental acrylic cement; the dura was cleaned with normal rat ringer solution (NRR) and carefully removed after a craniotomy of 1x1 mm was performed over the virus injection spot. In order to reduce movement artefacts caused by heartbeat and breathing, the craniotomy was filled with low concentration agarose gel pressed with a glass coverslip.

Electrical activity was measured with juxtacellular recordings from expressing neurons in layer 2/3 of the barrel cortex with glass pipette (4-6 MΩ) containing NRR solution and coated with BSA Alexa-594 (Invitrogen) for pipette visualization (Sasaki et al. 2012). Action potentials occurrence was recorded in current clamp at 10Hz sampling rate using an Axoclamp 2-B amplifier (Axon Instruments, Molecular Devices) and digitized using the electrophysiology software Clampex 10.2. Peak amplitude of AP-evoked calcium transients were calculated as the average of three sampled points around the peak location. Signal to Noise ratio (SNR) is calculated as the peak amplitude divided by the standard deviation of 700 ms before the first AP. Half-decay time was estimated by fitting a decaying function to the average calcium transient evoked by spontaneous APs.

3.3.7 Histology.

After transcardial perfusion, mouse brains were fixed in PFA 4% over night at 4 C°. Within one week from tissue fixation, brains were cut into 50 µm coronal sections using a vibratome (VT 1000S; Leica

Instruments). Nuclear counterstaining was achieved with DAPI (0.5 µg/mL), Primary antibody used in the study was rabbit anti-GABA (1:500, Sigma-A2052) and the secondary was DyLight 488 (1:400, Jackson Immunoresearch). Images were acquired with a confocal microscope (Fluoview 1000; Olympus) with green (Anti-GABA), red (R-CaMP1.07), and ultraviolet (DAPI) excitation/emission filters.

3.3.8 Measure of tissue scattering length

For visualization of the vascular system we injected fluorescent dextran Texas Red (70K MW), a hydrophilic, red-emitting fluorophore that has spectra similar to R-CaMP1.07 (Titus et al., 1982), into the tail vein during anesthesia (Kleinfeld et al. 1998). Tail veins in anesthetized mice were dilated by heat application in warm water, and the end of the tail is softly clamped and a bolus of dye-containing solution (0.1 ml at 5%wt/vol, Invitrogen) is injected into a tail vein using a 29 gauge syringe needle.

We imaged the fluorescent stained blood plasma through a cranial craniotomy in the barrel cortex following the same surgical procedure for electrophysiology experiments. Fluorescence was excited in the range 740-930 nm wavelength by the Ti:Sapphire (Cameleon XR; Coherent) laser and at 1040-nm by the solid state Yb:KGW laser. The tissue scattering length ls is evaluated by fitting the analytical function to the in-depth signal decay. Stacks of images from 20 µm below the pia surface of the barrel cortex down to 800 µm were acquired. The average of fluorescence value is extracted from the identified blood vessel.

3.3.9 Analysis of calcium signals

ImageJ (National Institutes of Health) was used for online evaluation of data quality as well as for manual selection of regions of interest (ROIs) corresponding to individual neurons from the mean image of a single-trial time series. We used custom written MATLAB (MathWorks) routines

(OCIA; unpublished) for calcium data analysis. Background subtraction (bottom 1st percentile fluorescence signal across the entire frame) and frame-by-frame motion correction (TurboReg; http://bigwww.epfl.ch/thevenaz/turboreg/) were apply to red channel data before calculating the relative percentage fluorescence changes ($\Delta F/F_0$), where F is the fluorescence intensity at any time point and F_0 is the eight percentile of total fluorescence intensity for each trial.

3.4 Results

3.4.1 Efficient two-photon excitation of R-CaMP1.07 at 1040 nm

In order to verify the improved light penetration and reduced scattering effects at 1040 nm wavelength, we measured the scattering length by assessing the wavelength dependence of fluorescence attenuation in somatosensory barrel cortex by two-photon imaging of blood vasculature labelled with Texas Red (dextran conjugate) (Enk et al., 1998). *In vivo* stacks of images were acquired from the surface of the barrel cortex down to 800 µm at a constant excitation power. A plot of the fluorescence values against imaging depth displayed an approximately exponential decay, which was fitted to reveal the scattering length (l_{Scat}). The measurements were repeated for the range from 740 to 1040 nm, which are the most commonly used excitation wavelengths to excite GECIs (**Figure 3-1**). We observed a trend of gradual increase of attenuation length at longer wavelength with a mean scattering length of 141 ± 37 µm and 311 ± 42 µm at 740 nm and 1040 nm excitation wavelength, respectively (**Figure 3-1**). These results revealed a two-fold reduced scattering effect at 1040-nm as compared to 740-nm excitation and are comparable to other previous studies (Kobat et al., 2009; Smith et al., 2009). Thus we chose the 1040-nm

laser to excite R-CaMP1.07 and investigate neurons located in infragranular layers of the mouse barrel cortex.

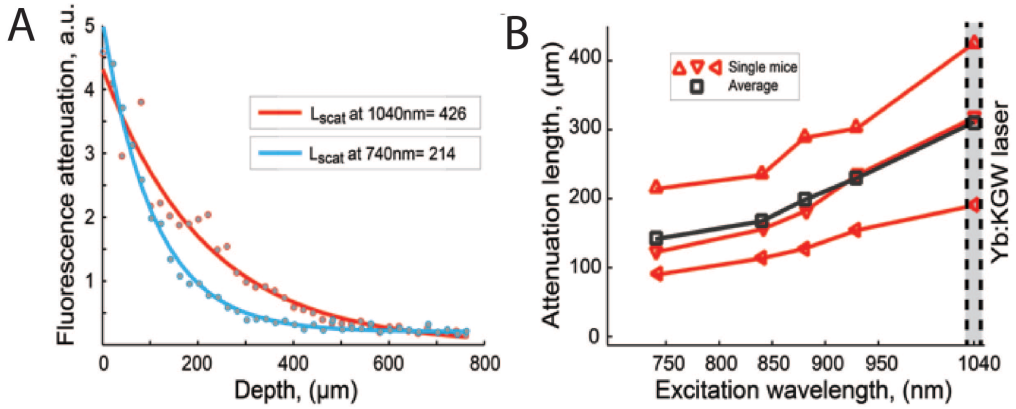

Figure 3-1: Wavelength-dependence of two-photon excited fluorescence attenuation with depth*. (A) Exponential function fitted to the attenuation of the two-photon fluorescence at 704 nm (blue trace) and 1040 nm with Yb:KGW laser (red trace). Data collected from one mouse. (B) Attenuation length as a function of the excitation wavelength at different depths.*

3.4.2 High sensitivity of R-CaMP1.07 as reporter of neuronal activity *in vivo*

We determined R-CaMP1.07 sensitivity for reporting AP firing *in vivo* by combination of targeted juxtacellular recordings of supragranular L2/3 pyramidal neurons in somatosensory cortex and two-photon laser imaging exciting the indicator at 1040 nm in anaesthetized mice. APs were recorded from layer 2/3 expressing neurons during spontaneous activity (Figure 3-2). Single APs yielded calcium transients with an average ΔF/F peak amplitude of 7.4 ± 0.7%, and signal to noise ratio was 4.5 ± 0.2 (mean ± s.e.m from 210 events from 9 cells). Under these conditions we could detect transients evoked by single APs in L2/3 neurons, but this might be more difficult in deeper layers because of higher noise level. However, in deeper layers we often observed large calcium transients indicative of bursts of APs, especially in awake

experiments. R-CaMP1.07 single APs evoked transients had fast in kinetics with an average decay time of 0.28 ± 0.03 seconds (Figure 3-2). We estimated also the maximum response at saturation ($\Delta F/F_{max}$) by injection of large current through recording pipette, $\Delta F/F_{max}$ of 208 ± 21% (12 cells).

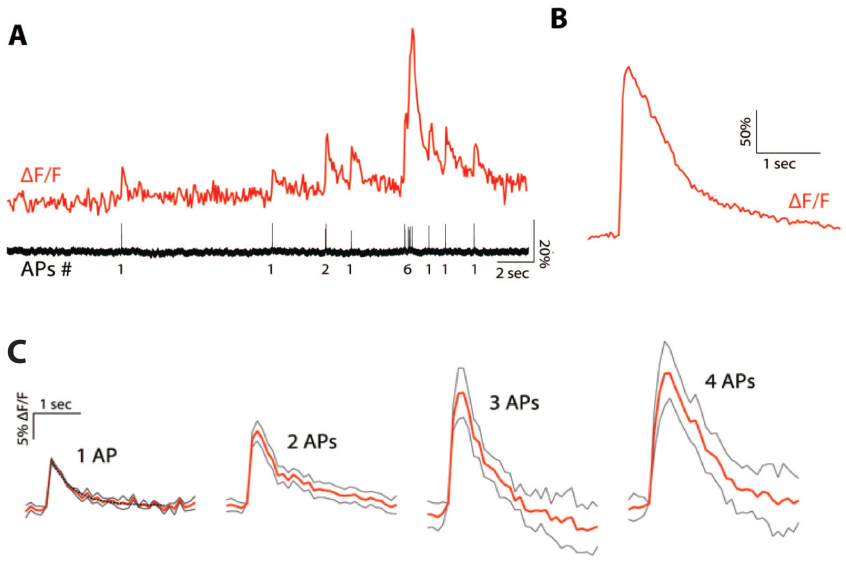

***Figure 3-2: Action potential-evoked R-CaMP1.07 signals**. (A) Example trace of R-CaMP1.07 calcium measurements combined with electrophysiological recording, in red and black respectively. The number of action potentials is shown at the bottom. (B) Estimate of maximum response at saturation ($\Delta F/F_{max}$) by injection of large current. (C) Mean fluorescence traces in response to 1, 2, 3 and 4 APs* in vivo.

3.4.3 *In vitro* confocal and *in vivo* two photon imaging of mouse barrel cortex using RCaMP1.07

Immunostaining performed post hoc on cortical slices showed that only cortical pyramidal neurons express the indicator, specificity is guaranteed by lack of overlap with anti-GABA staining (Figure 3-3 A). In all 6 mice, we could identify functional calcium signal imaging of R-CaMP1.07-expressing cells at least 700 μm below the pial surface. In one mouse, we could measure activity from sparse cells down to 830 μm deep, presumably upper L6 neurons (**Figure 3-3** B). We could distinguish supragranular from infragranular pyramidal neurons by the

density of labelled cells and by the lack of R-CaMP1.07 expression in L4, on average the most superficial L5 pyramidal neurons could be imaged at 540 ± 16 *µ*m deep *in vivo*. According to depth measurements on two Rbp4-cre mice, we estimate L5 expression to be confined between 530 ± 20 *µ*m and 720 ± 20 *µ*m deep. However, we could not distinguish between L5 and L6 cells in every mouse so we decided to consider our data only according to the imaging depth. We could demonstrate that R-CaMP1.07 calcium indicator excited at 1040 nm is suitable to study neuronal networks deep in the cortex also in awake, behaving mice.

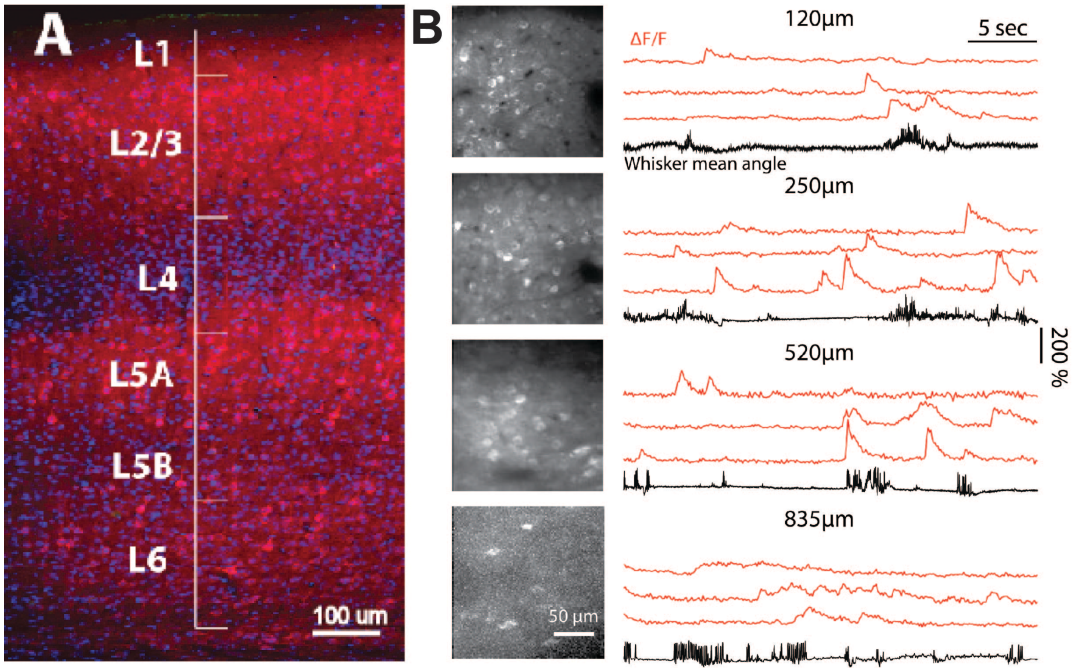

Figure 3-3: Calcium imaging across all cortical layers of barrel cortex during voluntary free-air whisking. *(A) Confocal image of fixed coronal slice, R-CaMP1.07 positive neurons in red and DAPI staining in blue. (B) left, In vivo two-photon images of R-CaMP1.07-expressing barrel cortex pyramidal cells in an awake freely-whisking mice; right, averaged whisker movement traces (black) acquired with high speed camera at 200Hz; in red, example R-CaMP1.07 two-photon calcium recordings at different pyramidal layers: 120 µm and 250 µm in L2/3, 520 µm in L5 and at 835 µm in L6.*

3.4.4 Vertical profile of mouse barrel cortex activity during free air exploratory whisking revealed by RCaMP1.07

Rodents sweep their whiskers rhythmically back and forth at high frequencies (typical exploratory whisking behaviours are at around 7-12 Hz) in order to explore their immediate environment (Fox, 2008). Here we analysed the calcium responses evoked by exploratory whisking behaviours. Any whisking behaviour that occurred at 7-12 Hz was defined as an exploratory whisking episode. Two neighbouring exploratory whisking episodes were joined if they were separated by less than 1.5 s, which indicates an on-going whisking bout.

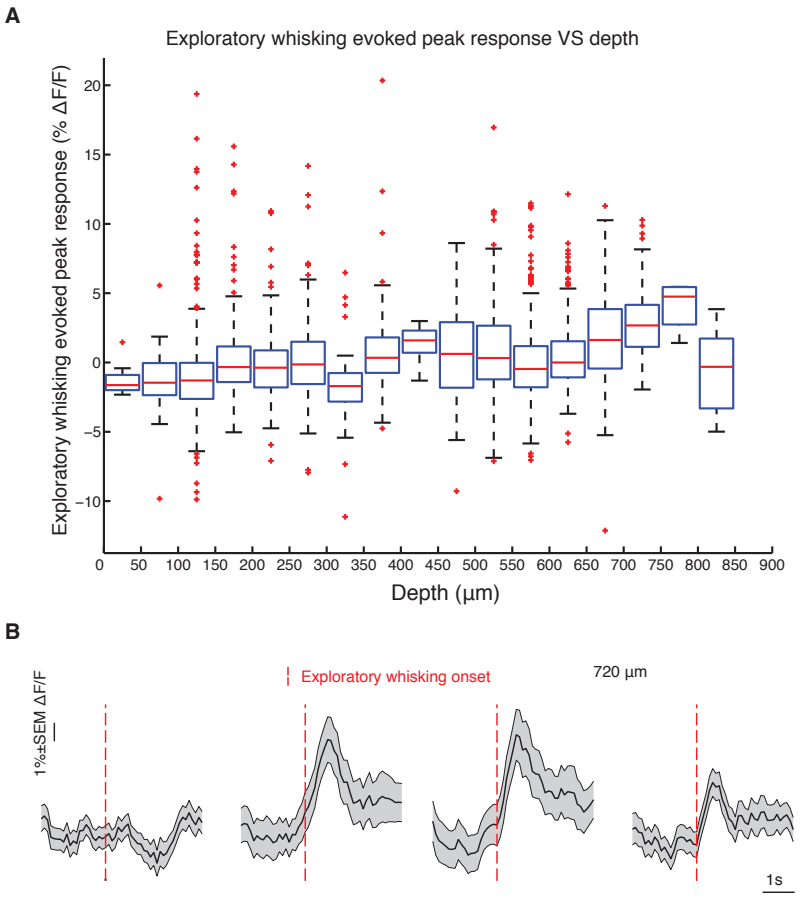

Figure 3-4: Vertical profile of mouse barrel cortex activity during free air exploratory whisking revealed by RCaMP1.07. *(A). Peak responsse evoked by the onset of exploratory whisking within 500 ms at all depths across mouse barrel cortex. (B). Examples of calcium traces that recorded from four neurons at 720 µm deep. Calcium traces were aligned to the exploratory whisking onset; averaged over 174 exploratory whisking episodes.*

The vertical profile of mouse barrel cortex activity during free air exploratory whisking was obtained by calculating the peak calcium responses within 500 ms after the exploratory whisking onset (**Figure 3-4** A). Neurons recorded at the depths between 600 – 800 µm showed a trend of increased peak response after the exploratory whisking onset. However, neuronal activity was heterogeneous in all investigated layers, with only few neurons showing strongly correlated activity with free-air whisking (**Figure 3-4** B).

3.5 Discussion

In this study we showed an approach based on two-photon microscopy using the red indicator R-CaMP1.07 that allows the *in vivo* functional imaging of nearly the entire cortical column *in vivo*. We sequentially recorded signals across all layers, sampling different neurons across imaging sessions. In total, we measured neuronal activity from 2353 cells while the animals were quiet or freely whisking in air.

As compared to other invasive methods for imaging deeper cortical tissue or subcortical structures, such as removing the covering tissues (Dombeck et al., 2010; Mizrahi et al., 2004), or inserting micro-endoscopes based on gradient refractive index (GRIN) lenses or optical fibers (Engelbrecht et al., 2008; Flusberg et al., 2005; Helmchen et al., 2013; Levene et al., 2004) as well as microprisms (Andermann et al., 2013), our method leaves the cortical tissue intact. This is particularly important when studying the functioning and contribution of certain cell group within an intact functional circuit.

As compared to other non-invasive methods for imaging deeper cortical tissue or subcortical structures, such as regenerative amplification multiphoton microscopy (Mittmann et al., 2011) or three-

photon fluorescence microscopy (Horton et al., 2013), our methods do not require special, expensive laser and can offer sufficient spatiotemporal resolution for functional imaging with an good SNR. Rather, a relatively inexpensive fixed-wavelength pulsed laser can be employed. Several companies nowadays sell suitable femtosecond lasers with wavelengths around 1050 nm and high average output power.

Moreover, in combination with the newly developed layer-specific labelling in transgenic mouse lines, image quality in deeper cortical layers can be improved by minimizing the fluorescence staining of upper layer neurons (GENSAT; S. Gong et al., 2007; Madisen et al., 2015; Taniguchi et al., 2011).

Our data revealed a high heterogeneity of activity across layers; in the future, we will attempt to identify different patterns of activity across layers and their correlation with whisking and non-whisking events. Another interesting direction is to investigate the anatomical and functional properties of specific subtype neurons within a neural circuit during specific behaviours. For example, by expressing red GECIs in specific type of interneurons in infragranular layers, we can have a better understanding of their function and contribution to sensory information processing.

4 General discussion and outlook

In order to have a deeper understanding of cortical structure-function relationship and information processing in neocortex, we need to investigate how neural activity spreads in both horizontal and vertical directions in the neocortex of awake, behaving animals over long periods of time. In the past, such investigations have been limited due to the lack of appropriate techniques and tools. With the rapid progress in calcium imaging techniques, new generations of sensitive genetically encoded calcium and voltage indicators as well as the expansion of the genetic toolbox, now it is possible to (1) image cortical activity over long time periods with high spatiotemporal precision in order to understand more about the spread of activity in horizontal (transverse) dimension throughout large areas of the mouse neocortex; (2) collecting sensory information processing data from neurons that are located in cortical infragranular layers in the intact brains of awake behaving animals.

In this thesis I contributed to two projects, which were aimed to advance *in vivo* calcium imaging for studying horizontal and vertical activity patterns in neocortex. In the first project, a method that enables chronic investigation of large-scale cortical activity with the temporal resolution necessary to capture signal onset kinetics and high-frequency responses has been established by combining wide-field calcium imaging with ratiometric GECI YC3.60. Sensory-evoked neuronal activity was imaged repeatedly in the same mouse over weeks, enabling new opportunities for the longitudinal study of cortical function and dysfunction (Minderer et al., 2012). This method can be flexibly applied across different cortical areas. In the second project, I present a method that allows two-photon calcium imaging data collection from all cortical layers in intact barrel cortex in head-fixed, awake mice by exciting the red GECI R-CaMP1.07 at 1040-nm wavelength with a compact, high-power, low-cost femtosecond laser. This method offers new

opportunities for chronic investigations of the functional role of deep neocortical L5 and L6 for information processing in the mouse brain during specific behaviours.

Here I would like to discuss how the methods I used in the projects and other emerging methods would contribute our further investigations of brain functioning, both the advantages and limitations.

4.1 Chronic large-scale imaging of mouse neocortex with high temporal resolution

How information is processed and exchanged between spatially distributed neural circuits is one of the fundamental questions in the field of neurosciences. Although the conventional electrophysiological techniques have been the most important tools for characterizing neuronal functional properties with high temporal resolution, yet it often cannot offer crucial information such as the recorded neurons types as well as their position within the studied neural circuit. Besides, it is not optimized for repeated long-term population recording of neuronal activity over large cortical areas. As compared to the conventional electrophysiological techniques, optical imaging techniques have enabled important advances in systems neuroscience by allowing investigation of spatiotemporal activity dynamics over large areas of cortex (Margolis et al., 2014).

For imaging large-scale neuronal activity, dye-free hemodynamic-based intrinsic optical signal imaging has been widely used over the last decades (Masino and Frostig, 1996; Polley et al., 1999). It allows longitudinal experiments in single animals over long periods of time. Other methods that measure NADH or flavoprotein autofluorescence changes from the oxidized to the deoxidized form can also be used to monitor large-scale cortical dynamics *in vivo* (Reinert et al., 2004; Vanni

and Murphy, 2014). However, in addition to the indirect relationship to neuronal activity, all these methods do not offer sufficient temporal resolution to capture signal onset kinetics and investigate the details of high-frequency responses. Although organic voltage- or calcium-sensitive dye imaging enables monitoring cortical activity with high temporal resolution on large-scale level, they have limitations such as phototoxicity, non-specific labelling and invasive dye loading procedures. Moreover, they are not optimized to perform experiments on the same animal over long periods of time, especially on awake behaving animals.

Wide-field imaging using genetically-encoded voltage indicators (GEVIs) or GECIs in combination with CCD/ CMOS-based cameras is an excellent method for measuring population signals from multiple areas simultaneously as well as chronically with a high spatiotemporal resolution. In Chapter 2 of this thesis, I presented a method using wide-field calcium imaging in combination with ratiometric GECI YC3.60 to repeatedly measure fast dynamics of sensory-evoked spatiotemporal activity across large areas of mouse somatosensory cortex over multiple weeks in the same animal. This method opens new possibilities for the longitudinal study of stability and plasticity of cortical sensory representations with high spatiotemporal resolution. For example, it can be used for investigating experience-dependent cortical map plasticity by introducing sensory deprivation (e.g., whisker trimming) or functional map stability in disease conditions (e.g., after stroke). As compared to GECIs, GEVIs offer a more direct observation on action potential waveforms and subthreshold transmembrane voltage dynamics. The first generation of GEVIs such as SPARC (Ataka and Pieribone, 2002) and VSFP1 (Sakai et al., 2001) are based on voltage-gated potassium channels and exhibit low SNR and slow kinetics. Like GECIs, the currently used GEVIs can be categorized into FRET-based GEVIs (Akemann et al., 2010) and a single FP-based family (Lundby et al., 2008; Perron et al., 2009). Ciona intestinalis (Ci-VSP), the voltage sensitive domain of a phosphatase (VSP) derived from the sea squirt, is

used in the most popular GEVIs (Akemann et al., 2010). For example, two-photon imaging using VSFP butterfly 1.2 successfully reported the membrane potential changes of L2/3 neurons in mouse barrel cortex with cellular resolution after extensive trial averaging (Akemann et al., 2013). The recent developed FRET-opsin sensors have improved brightness and fast kinetics (rise time about 5 ms), which enable them to report spikes in the dendritic arbors of Pukinje cells with single-trial precision (Gong et al., 2014). The state-of-the art GECIs such as GCaMP6 (T.-W. Chen et al., 2013), YC-Nanos (Horikawa et al., 2010), TN-XXL (Mank et al., 2008) and Twitch (Thestrup et al., 2014) have progressed in brightness and sensitivity. Additional efforts will be putting on achieving a sufficient fast binding kinetics for a more accurate read-out as well as increasing SNR by having bigger fluorescence change upon calcium binding.

Furthermore, in order to achieve non-invasive, stable, bright and cell-type specific expression of GECIs in target cells throughout the brain, scientists have been putting efforts into generating transgenic Cre-reporter lines and Cre-driver lines. For example, Cre-driver lines targeting different cell types and brain regions (Harris et al., 2014; Kuhlman and Huang, 2008). A recently developed novel transgenic Cre-driver line strategy (Madisen et al., 2015) allows a stronger and more consistent expression as compared to the previous methods that used the CAG promoter (Zariwala et al., 2012) or Thy1 promoter (Dana et al., 2014). In this new strategy, after the triggering of the transgene expression by tetracycline response in a Cre-dependent manner, a newly established locus called TIGRE will allow robust expression of the gene of interest when combined with tTA-based transcriptional amplification. Examples for Cre-reporter lines driving expression of activity indicators are GCaMP3 mice (Zariwala et al., 2012), GCaMP6 mice (Dana et al., 2014; Madisen et al., 2015), GCaMP7 mice (Sato et al., 2015), and YCX2.60 mice (Madisen et al., 2015). There are also new GEVI-expressing reporter lines available (Madisen et al., 2015). In a recent study, Carandini et al. expressed a GEVI, VSFP-Butterfly 1.2,

in L2/3 pyramidal cells of mouse visual cortex through in utero electroporation (Carandini et al., 2015). They recorded visual stimuli-evoked fluorescence changes using wide-field imaging in awake mice. Their results showed that GEVIs can serve as a powerful toll to study large-scale neural population dynamics in awake animals. In addition to many existed green GECI transgenic lines, transgenic lines express red GECIs will be available soon.

An recent example for using transgenic mice expressing GECI to investigate functional cortical connectivity chronically at the mesoscopic level was published the Murphy group in Vancouver (Vanni and Murphy, 2014). By crossing Emx1-cre and Rosa26-GCaMP3 lines, they achieved stable and homogenous GCaMP3 expression within cells of the entire cerebral cortex. In combination with a CCD camera they observed sensory stimulation evoked cortical responses in S1 and revealed the functional connections between S1, S2 and M1 with high temporal resolution and spatial accuracy through a large bilateral or unilateral cranial window covering multiple cortical areas. The further application of this method can be extended to chronic investigation of experience-dependent cortical plasticity or in disease models where specific functional connectivity may be affected. For example, in our group, Ariel Gilad is working on exploring the cortical circuit involved in accurate sensory perception in awake behaving animals over large cortical areas (Figure 4-1). Different transgenic lines can be used to explore and discriminate the specific contribution of different layers, cell types and neural pathways during behaviours (GENSAT; S. Gong et al., 2007; Madisen et al., 2015; Taniguchi et al., 2011). Moreover, fiber-optic based miniature head-mounted microscopes provide another excellent method for wide field-calcium imaging, especially for recording bulk dendritic activity in freely moving animals (Hamel et al., 2015; Helmchen et al., 2001).

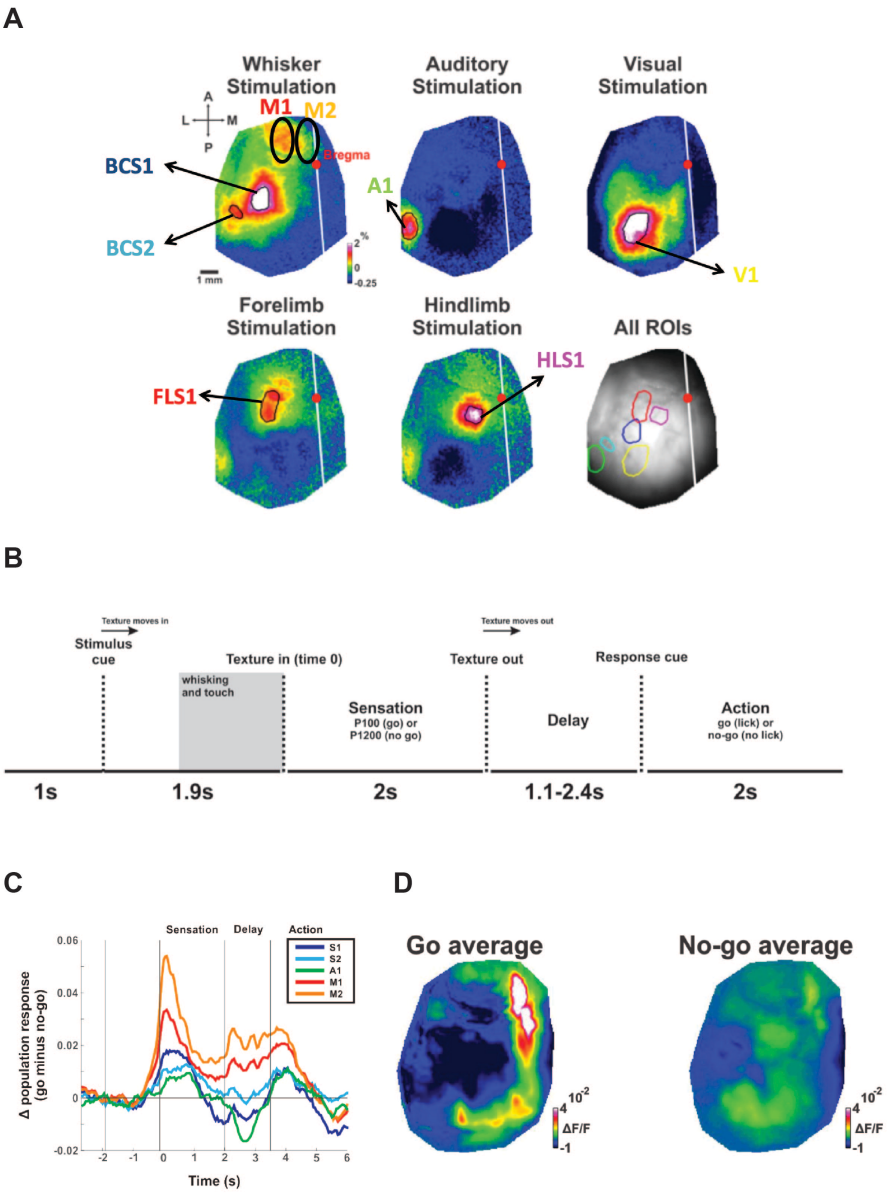

Figure 4-1: Wide-field functional cortical mapping using transgenic mice expressing GCaMP6 in cortical L2/3 pyramidal neurons. *(A). Functional cortical map obtained by stimulating different peripheral sensory organs in anesthetized mice (BCS1: whisker-related primary somatosensory cortex, BCS2: whisker-related secondary somatosensory cortex, M1: primary motor cortex, M2: secondary motor cortex, A1: primary auditory cortex, V1: primary visual cortex, FLS1: forelimb-related primary somatosensory cortex, HLS1: hindlimb-related somatosensory cortex). (B). Schematic illustration of the Go/No-go behavioural paradigm, a texture discrimination task with a delay period before reporting the decision by licking for reward. (C). The difference of population response between Go and No-go conditions. (D). Comparison of averaged functional cortical map between Go and No-go conditions. Unpublished data, Helmchen group. Image courtesy Dr. Ariel Gilad.*

In addition to single-photon imaging, many groups have been working on developing two-photon imaging techniques for monitoring neuronal activity across extended cortical networks with cellular resolution (Stirman et al., 2014; Tsai et al., 2015; Voigt et al., 2015). For example, a recent developed two-photon microscope can record neuronal activity in a ultra-large field of view (8 mm by 10 mm), however at the price of limited spatial resolution (Tsai et al., 2015). Another example is multi-area two-photon imaging system, utilizing two independent imaging beams for measuring neuronal activity in two spatially separated cortical areas simultaneously at cellular resolution within a wide field of view (1.8 mm with commercially available objective) (Stirman et al., 2014; Voigt et al., 2015). With such systems experimenters can now image multiple combinations of imaging regions at different depths within the field of view in a single imaging session.

In the future, chronic WF GECI imaging of defined neuronal networks will provide a bridge between systems and cellular neuroscience for the longitudinal study of cortical sensory processing and cortical plasticity in both health and disease conditions.

4.2 New possibilities to visualize the neural circuitry in deeper layers of the brain in behaving animals

Scientists have been trying to push the limits of imaging depth using different methods. A very direct but invasive way is to mechanically remove the covering tissue. For example, the removal of cortical tissue allows optical access to subcortical structure (Dombeck et al., 2010; Mizrahi et al., 2004). Other invasive methods include inserting micro-endoscopes based on gradient refractive index (GRIN) lenses or optical fibers (Engelbrecht et al., 2008; Flusberg et al., 2005; Helmchen et al., 2013; Levene et al., 2004) as well as microprisms (Andermann et al., 2013).

Non-invasively, optimizing specifications of the laser used for two-photon excitation can increase imaging depth. For example, to achieve higher pulse peak powers at lower repetition rates. The use of regenerative amplifiers for multi-photon microscopy can increase the efficiency of two-photon excitation by amplifying a selected subset of laser pulses (Mittmann et al., 2011). In addition, three-photon fluorescence microscopy has been successfully applied for structural imaging of RFP-labelled neurons within hippocampus (Horton et al., 2013). However, three-photon imaging requires long pixel dwell times due to the tiny cross-sections. Thus, applications of three-photon excitation microscopy in functional imaging are still limited currently. Besides, three-photon excitation requires very high peak intensities, which might lead to rapid photobleaching. Moreover, objectives that has low-magnification (20×) with high- numerical aperture (0.95) are beneficial for imaging deeper (Oheim et al., 2001).

In two-photon imaging, aberration and scattering are two main factors that limit *in vivo* imaging depth. Aberration could be reduced by using adaptive optics (AO) techniques (Ji et al., 2010; Rueckel et al., 2006) and by positioning the cranial window glass coverslip as perpendicular to the optical axis of the microscope objective as possible. AO techniques have a better performance of improving signal levels for small structures such as spines (on the order of or smaller than the two-photon excitation focal volume) as compared to large structures. Tissue scattering is weaker at longer wavelengths. Because red light has longer wavelength, a promising direction for deep imaging is developing red-shifted neuronal activity indicators. For example, a recently reported red fluorometric calcium sensitive dye, Cal-590, can be excited by infrared light at 1050 nm and successfully record neuronal activity in all six cortical layers in mouse cortex (Tischbirek et al., 2015). Moreover, RCaMP1a-h (Akerboom et al., 2013) and R-CaMP1.07 or R-CaMP2 (Inoue et al., 2014; Ohkura et al., 2012a) are two families of red GECIs that have started to be used more commonly. RCaMP1a-h are developed by replacing the GFP in GCaMP3 with a circularly permuted

version of mRuby. R-CaMP1.07 is developed by mutagenesis screening after replacing the GFP in GCaMP3 with mApple (Ohkura et al., 2012a; Zhao et al., 2011). R-CaMP2 is the improved version of R-CaMP1.07. It was reported in the paper that R-CaMP2 can have threefold faster rise and decay times of Ca^{2+} transients as compared to R-CaMP1.07 under certain experimental condition (Inoue et al., 2014). In addition to the efforts that have been invested in developing red GECIs, there are groups trying to screen for red GEVIs (Abdelfattah et al., 2015). Abdelfattah et. al. developed a family of red GEVIs, which consists of the voltage-sensing domain of the *Ciona intestinalis* voltage-sensitive phosphatase and a red fluorescent protein mApple. These GEVIs increase their fluorescence intensity in response to depolarization and allow reliable detection of spontaneous action potentials in cultured mammalian neurons in single trials with wide-field fluorescent light microscopy. Moreover, the newly developed layer-specific transgenic mouse lines can help to improve image quality in deeper cortical layers by minimizing the fluorescence staining of upper layer neurons (GENSAT; S. Gong et al., 2007; Madisen et al., 2015; Taniguchi et al., 2011). Combining the advantages of different methods can allow the investigation of the anatomical and functional properties of deeper cortical layer neurons within a neural circuit during specific behaviours.

References

Abdelfattah, A.S., Platisa, J., Zhao, Y., Pieribone, V.A., Campbell, R.E., 2015. Development of a Red Genetically-Encoded Voltage Indicator and its use with Channelrhodopsin for All-Optical Electrophysiology. Biophys. J. 106, 629a–630a.

Adesnik, H., Scanziani, M., 2010. Lateral competition for cortical space by layer-specific horizontal circuits. Nature 464, 1155–1160.

Akemann, W., Mutoh, H., Perron, A., Rossier, J., Knöpfel, T., 2010. Imaging brain electric signals with genetically targeted voltage-sensitive fluorescent proteins. Nat. Methods 7, 643–649.

Akemann, W., Sasaki, M., Mutoh, H., Imamura, T., Honkura, N., Knöpfel, T., 2013. Two-photon voltage imaging using a genetically encoded voltage indicator. Sci. Rep. 3, 2231.

Akerboom, J., Carreras Calderón, N., Tian, L., Wabnig, S., Prigge, M., Tolö, J., Gordus, A., Orger, M.B., Severi, K.E., Macklin, J.J., Patel, R., Pulver, S.R., Wardill, T.J., Fischer, E., Schüler, C., Chen, T.-W., Sarkisyan, K.S., Marvin, J.S., Bargmann, C.I., Kim, D.S., Kügler, S., Lagnado, L., Hegemann, P., Gottschalk, A., Schreiter, E.R., Looger, L.L., 2013. Genetically encoded calcium indicators for multi-color neural activity imaging and combination with optogenetics. Front. Mol. Neurosci. 6, 2.

Akerboom, J., Chen, T.-W., Wardill, T.J., Tian, L., Marvin, J.S., Mutlu, S., Calderon, N.C., Esposti, F., Borghuis, B.G., Sun, X.R., Gordus, A., Orger, M.B., Portugues, R., Engert, F., Macklin, J.J., Filosa, A., Aggarwal, A., Kerr, R.A., Takagi, R., Kracun, S., Shigetomi, E., Khakh, B.S., Baier, H., Lagnado, L., S.-H.Wang, S., Bargmann, C.I., Kimmel, B.E., Jayaraman, V., Svoboda, K., Kim, D.S., Eric R. Schreiter, Looger, L.L., 2012. Optimization of a GCaMP Calcium Indicator for Neural Activity Imaging. J. Neurosci. 32, 13819 – 13840.

Akerboom, J., Rivera, J.D.V., Rodríguez Guilbe, M.M., Malavé, E.C.A., Hernandez, H.H., Tian, L., Hires, S.A., Marvin, J.S., Looger, L.L., Schreiter, E.R., 2009. Crystal structures of the GCaMP calcium sensor reveal the mechanism of fluorescence signal change and aid rational design. J. Biol. Chem. 284, 6455–6464.

Alloway, K.D., 2008. Information Processing Streams in Rodent Barrel Cortex: The Differential Functions of Barrel and Septal Circuits. Cereb. Cortex 18, 979–989.

Andermann, M.L., Gilfoy, N.B., Goldey, G.J., Sachdev, R.N.S., Wölfel, M.,

McCormick, D. a., Reid, R.C., Levene, M.J., 2013. Chronic Cellular Imaging of Entire Cortical Columns in Awake Mice Using Microprisms. Neuron 80, 900–913.

Andermann, M.L., Kerlin, a M., Reid, R.C., 2010. Chronic cellular imaging of mouse visual cortex during operant behavior and passive viewing. Front. Cell. Neurosci. 4, 3.

Andermann, M.L., Moore, C.I., 2006. A somatotopic map of vibrissa motion direction within a barrel column. Nat. Neurosci. 9, 543–551.

Anderson, C.T., Sheets, P.L., Kiritani, T., Shepherd, G.M.G., 2010. Sublayer-specific microcircuits of corticospinal and corticostriatal neurons in motor cortex. Nat. Neurosci. 13, 739–744.

Aronoff, R., Matyas, F., Mateo, C., Ciron, C., Schneider, B., Petersen, C.C.H., 2010. Long-range connectivity of mouse primary somatosensory barrel cortex. Eur. J. Neurosci. 31, 2221–33.

Aschauer, D.F., Kreuz, S., Rumpel, S., 2013. Analysis of Transduction Efficiency, Tropism and Axonal Transport of AAV Serotypes 1, 2, 5, 6, 8 and 9 in the Mouse Brain. PLoS One 8, 1–16.

Ataka, K., Pieribone, V. a, 2002. A genetically targetable fluorescent probe of channel gating with rapid kinetics. Biophys. J. 82, 509–516.

Berger, T., Borgdorff, A., Crochet, S., Neubauer, F.B., Lefort, S., Fauvet, B., Ferezou, I., Carleton, A., Lüscher, H.-R., Petersen, C.C.H., 2007. Combined voltage and calcium epifluorescence imaging in vitro and in vivo reveals subthreshold and suprathreshold dynamics of mouse barrel cortex. J. Neurophysiol. 97, 3751–62.

Berridge, M., 1998. Neuronal calcium signaling. Neuron 21, 13–26.

Berridge, M.J., Bootman, M.D., Roderick, H.L., 2003. Calcium signalling: dynamics, homeostasis and remodelling. Nat. Rev. Mol. Cell Biol. 4, 517–529.

Berridge, M.J., Lipp, P., Bootman, M.D., 2000. The versatility and universality of calcium signalling. Nat. Rev. Mol. Cell Biol. 1, 11–21.

Betley, J.N., Sternson, S.M., 2011. Adeno-associated viral vectors for mapping, monitoring, and manipulating neural circuits. Hum. Gene Ther. 22, 669–677.

Bloodgood, B.L., Sabatini, B.L., 2007. Nonlinear Regulation of Unitary Synaptic Signals by CaV2.3 Voltage-Sensitive Calcium Channels Located in Dendritic Spines. Neuron 53, 249–260.

Bonnot, A., Mentis, G.Z., Skoch, J., O'Donovan, M.J., 2005. Electroporation loading of calcium-sensitive dyes into the CNS. J. Neurophysiol. 93, 1793–1808.

Borst, a, Egelhaaf, M., 1992. In vivo imaging of calcium accumulation in fly interneurons as elicited by visual motion stimulation. Proc. Natl. Acad. Sci. U. S. A. 89, 4139–4143.

Bozza, T., McGann, J.P., Mombaerts, P., Wachowiak, M., 2004. In vivo imaging of neuronal activity by targeted expression of a genetically encoded probe in the mouse. Neuron 42, 9–21.

Brecht, M., Grinevich, V., Jin, T.E., Margrie, T., Osten, P., 2006. Cellular mechanisms of motor control in the vibrissal system. Pflugers Arch. Eur. J. Physiol. 453, 269–281.

Brecht, M., Sakmann, B., 2002. Whisker maps of neuronal subclasses of the rat ventral posterior medial thalamus, identified by whole-cell voltage recording and morphological reconstruction. J. Physiol. 538, 495–515.

Briggman, K.L., Euler, T., 2011. Bulk electroporation and population calcium imaging in the adult mammalian retina. J. Neurophysiol. 105, 2601–2609.

Briggs, F., 2010. Organizing principles of cortical layer 6. Front. Neural Circuits 4, 3.

Bruno, R.M., Hahn, T.T.G., Wallace, D.J., de Kock, C.P.J., Sakmann, B., 2009. Sensory experience alters specific branches of individual corticocortical axons during development. J. Neurosci. 29, 3172–3181.

Bruno, R.M., Khatri, V., Land, P.W., Simons, D.J., 2003. Thalamocortical angular tuning domains within individual barrels of rat somatosensory cortex. J. Neurosci. 23, 9565–9574.

Bruno, R.M., Sakmann, B., 2006. Cortex is driven by weak but synchronously active thalamocortical synapses. Science 312, 1622–1627.

Buning, H., Perabo, L., Coutelle, O., Quadt-Humme, S., Hallek, M., 2008. Recent developments in adeno-associated virus vector technology. J Gene Med 10, 717–733.

Bureau, I., Von Paul, F. Saint, Svoboda, K., 2006. Interdigitated paralemniscal and lemniscal pathways in the mouse barrel cortex. PLoS Biol. 4, 2361–2371.

Burger, C., Gorbatyuk, O.S., Velardo, M.J., Peden, C.S., Williams, P., Zolotukhin, S., Reier, P.J., Mandel, R.J., Muzyczka, N., 2004. Recombinant AAV viral vectors pseudotyped with viral capsids from serotypes 1, 2, and 5 display differential efficiency and cell tropism after

delivery to different regions of the central nervous system. Mol. Ther. 10, 302–317.

Carafoli, E., 2003. The calcium-signalling saga: tap water and protein crystals. Nat. Rev. Mol. Cell Biol. 4, 326–332.

Carandini, M., Shimaoka, D., Rossi, L.F., Sato, T.K., Benucci, A., Knopfel, T., 2015. Imaging the Awake Visual Cortex with a Genetically Encoded Voltage Indicator. J. Neurosci. 35, 53–63.

Catterall, W.A., 2000. Structure and regulation of voltage-gated Ca2+ channels. Annu. Rev. Cell Dev. Biol. 16, 521–555.

Cetin, A., Komai, S., Eliava, M., Seeburg, P.H., Osten, P., 2006. Stereotaxic gene delivery in the rodent brain. Nat. Protoc. 1, 3166–73.

Chakrabarti, S., Alloway, K.D., 2006. Differential origin of projections from SI barrel cortex to the whisker representations in SII and MI. J. Comp. Neurol. 498, 624–636.

Chen, J.L., Carta, S., Soldado-Magraner, J., Schneider, B.L., Helmchen, F., 2013. Behaviour-dependent recruitment of long-range projection neurons in somatosensory cortex. Nature 499, 336–40. doi:10.1038/nature12236

Chen, Q., Cichon, J., Wang, W., Qiu, L., Lee, S.J.R., Campbell, N.R., DeStefino, N., Goard, M.J., Fu, Z., Yasuda, R., Looger, L.L., Arenkiel, B.R., Gan, W.B., Feng, G., 2012. Imaging Neural Activity Using Thy1-GCaMP Transgenic Mice. Neuron 76, 297–308.

Chen, T.-W., Wardill, T.J., Sun, Y., Pulver, S.R., Renninger, S.L., Baohan, A., Schreiter, E.R., Kerr, R. a, Orger, M.B., Jayaraman, V., Looger, L.L., Svoboda, K., Kim, D.S., 2013. Ultrasensitive fluorescent proteins for imaging neuronal activity. Nature 499, 295–300.

Clarke, W.B., Bowsher, D., 1962. Terminal distribution of primary afferent trigeminal fibers in the rat. Exp. Neurol. 6, 372–383.

Constantinople, C.M., Bruno, R.M., 2013. Deep Cortical Layers Are Activated Directly by Thalamus. Science (80-.). 340, 1591–1594.

Coulter, D.A., Huguenard, J.R., Prince, D.A., 1989. Calcium currents in rat thalamocortical relay neurones: kinetic properties of the transient, low-threshold current. J. Physiol. 414, 587–604.

Cruikshank, S.J., Urabe, H., Nurmikko, A. V, Connors, B.W., 2010. Pathway-Specific Feedforward Circuits between Thalamus and Neocortex Revealed by Selective Optical Stimulation of Axons. Neuron 65, 230–245.

Curtis, J.C., Kleinfeld, D., 2009. Phase-to-rate transformations encode touch in cortical neurons of a scanning sensorimotor system. Nat. Neurosci. 12, 492–501.

Dana, H., Chen, T.-W., Hu, A., Shields, B.C., Guo, C., Looger, L.L., Kim, D.S., Svoboda, K., 2014. Thy1-GCaMP6 Transgenic Mice for Neuronal Population Imaging In Vivo. PLoS One 9, e108697.

de Kock, C.P.J., Bruno, R.M., Spors, H., Sakmann, B., 2007. Layer- and cell-type-specific suprathreshold stimulus representation in rat primary somatosensory cortex. J. Physiol. 581, 139–154.

de Kock, C.P.J., Sakmann, B., 2009. Spiking in primary somatosensory cortex during natural whisking in awake head-restrained rats is cell-type specific. Proc. Natl. Acad. Sci. U. S. A. 106, 16446–50.

De Vry, J., Martínez-Martínez, P., Losen, M., Temel, Y., Steckler, T., Steinbusch, H.W.M., De Baets, M.H., Prickaerts, J., 2010. In vivo electroporation of the central nervous system: A non-viral approach for targeted gene delivery. Prog. Neurobiol. 92, 227–244.

Denk, W., Strickler, J.H., Webb, W.W., Series, N., Apr, N., 2008. Two-Photon Laser Scanning Fluorescence Microscopy. Science (80-.). 248, 73–76.

Diamond, M.E., von Heimendahl, M., Knutsen, P.M., Kleinfeld, D., Ahissar, E., 2008. “Where” and “what” in the whisker sensorimotor system. Nat. Rev. Neurosci. 9, 601–612.

Dombeck, D.A., Harvey, C.D., Tian, L., Looger, L.L., Tank, D.W., 2010. Functional imaging of hippocampal place cells at cellular resolution during virtual navigation. Nat. Neurosci. 13, 1433–1440.

Dong, J.Y., Fan, P.D., Frizzell, R.A., 1996. Quantitative analysis of the packaging capacity of recombinant adeno-associated virus. Hum. Gene Ther. 7, 2101–2112.

Dörfl, J., 1985. The innervation of the mystacial region of the white mouse. J. Anat. 142, 173–184.

Douglas, R.J., Koch, C., Martin, K.A.C., Suarezt, H.H., Mahowald, M., 1995. Recurrent Excitation in Neocortical Circuits. Science (80-.). 269, 981–985.

Douglas, R.J., Martin, K.A., 1991. A functional microcircuit for cat visual cortex. J. Physiol. 440, 735–769.

Douglas, R.J., Martin, K.A.C., 2004. Neuronal circuits of the neocortex. Annu. Rev. Neurosci. 27, 419–451.

Drew, P.J., Shih, A.Y., Driscoll, J.D., Knutsen, P.M., Blinder, P., Davalos, D., Akassoglou, K., Tsai, P.S., Kleinfeld, D., 2010. Chronic optical access through a polished and reinforced thinned skull. Nat. Methods 7, 981–984.

Duchen, M.R., 1999. Contributions of mitochondria to animal physiology: from homeostatic sensor to calcium signalling and cell death. J. Physiol. 516, 1–17.

Eilers, J., Konnerth, A., 2009. Dye loading with patch pipettes. Cold Spring Harb. Protoc. 2009.

Engelbrecht, C.J., Johnston, R.S., Seibel, E.J., Helmchen, F., 2008. Ultra-compact fiber-optic two-photon microscope for functional fluorescence imaging in vivo. Opt. Express 16, 5556–5564.

Enk, W.I.D., Kleinfeld, D., Mitra, P.P., Helmchen, F., Denk, W., 1998. Fluctuations and stimulus-induced changes in blood flow observed in individual capillaries in layers 2 through 4 of rat neocortex. Neurobiology 95, 15741–15746.

Erinjeri, J.P., Woolsey, T. a, 2002. Spatial integration of vascular changes with neural activity in mouse cortex. J Cereb Blood Flow Metab 22, 353–360.

Feldmeyer, D., Brecht, M., Helmchen, F., Petersen, C.C.H., Poulet, J.F.A., Staiger, J.F., Luhmann, H.J., Schwarz, C., 2013. Barrel cortex function. Prog. Neurobiol. 103, 3–27.

Feldmeyer, D., Egger, V., Lubke, J., Sakmann, B., 1999. Reliable synaptic connections between pairs of excitatory layer 4 neurones within a single “barrel” of developing rat somatosensory cortex. J. Physiol. 521 Pt 1, 169–190.

Feldmeyer, D., Lübke, J., Sakmann, B., 2006. Efficacy and connectivity of intracolumnar pairs of layer 2/3 pyramidal cells in the barrel cortex of juvenile rats. J. Physiol. 575, 583–602.

Feldmeyer, D., Lübke, J., Silver, R.A., Sakmann, B., 2002. Synaptic connections between layer 4 spiny neurone-layer 2/3 pyramidal cell pairs in juvenile rat barrel cortex: physiology and anatomy of interlaminar signalling within a cortical column. J. Physiol. 538, 803–822.

Flusberg, B.A., Cocker, E.D., Piyawattanametha, W., Jung, J.C., Cheung, E.L.M., Schnitzer, M.J., 2005. Fiber-optic fluorescence imaging. Nat. Methods 2, 941–950.

Fox, K.D., 2008. Barrel Cortex. Cambridge University Press.

Gee, J.M., Gibbons, M.B., Taheri, M., Palumbos, S., Morris, S.C., Smeal, R.M., Flynn, K.F., Economo, M.N., Cizek, C.G., Capecchi, M.R., Tvrdik, P., Wilcox, K.S., White, J. a, 2015. Imaging activity in astrocytes and neurons with genetically encoded calcium indicators following in utero electroporation. Front. Mol. Neurosci. 8, 10.

Gee, K.R., Brown, K.A., Chen, W.N., Bishop-Stewart, J., Gray, D., Johnson, I., 2000. Chemical and physiological characterization of fluo-4 Ca(2+)-indicator dyes. Cell Calcium 27, 97–106.

Gelperin, a., Flores, J., 1997. Vital staining from dye-coated microprobes identifies new olfactory interneurons for optical and electrical recording. J. Neurosci. Methods 72, 97–108.

Gong, S., Doughty, M., Harbaugh, C.R., Cummins, A., Hatten, M.E., Heintz, N., Gerfen, C.R., 2007. Targeting Cre recombinase to specific neuron populations with bacterial artificial chromosome constructs. J. Neurosci. 27, 9817–23.

Gong, Y., Wagner, M.J., Zhong Li, J., Schnitzer, M.J., 2014. Imaging neural spiking in brain tissue using FRET-opsin protein voltage sensors. Nat. Commun. 5, 3674.

Grewe, B.F., Helmchen, F., 2009. Optical probing of neuronal ensemble activity. Curr. Opin. Neurobiol. 19, 520–9.

Grienberger, C., Konnerth, A., 2012. Imaging calcium in neurons. Neuron 73, 862–85.

Grinvald, A., Hildesheim, R., 2004. VSDI: a new era in functional imaging of cortical dynamics. Nat. Rev. Neurosci. 5, 874–885.

Grynkiewicz, G., Poenie, M., Tsien, R.Y., 1985. A new generation of Ca2+ indicators with greatly improved fluorescence properties. J. Biol. Chem. 260, 3440–3450.

Hamel, E.J.O., Grewe, B.F., Parker, J.G., Schnitzer, M.J., 2015. Cellular Level Brain Imaging in Behaving Mammals: An Engineering Approach. Neuron 86, 140–159.

Harris, J. a., Hirokawa, K.E., Sorensen, S. a., Gu, H., Mills, M., Ng, L.L., Bohn, P., Mortrud, M., Ouellette, B., Kidney, J., Smith, K. a., Dang, C., Sunkin, S., Bernard, A., Oh, S.W., Madisen, L., Zeng, H., 2014. Anatomical characterization of Cre driver mice for neural circuit mapping and manipulation. Front. Neural Circuits 8, 1–16.

Hasan, M.T., Friedrich, R.W., Euler, T., Larkum, M.E., Giese, G., Both, M., Duebel, J., Waters, J., Bujard, H., Griesbeck, O., Tsien, R.Y., Nagai, T.,

Miyawaki, A., Denk, W., 2004. Functional fluorescent Ca2+ indicator proteins in transgenic mice under TET control. PLoS Biol. 2, 763–775.

Helmchen, F., Borst, J.G., Sakmann, B., 1997. Calcium dynamics associated with a single action potential in a CNS presynaptic terminal. Biophys. J. 72, 1458–1471.

Helmchen, F., Denk, W., 2005. Deep tissue two-photon microscopy. Nat. Methods 2, 932–940.

Helmchen, F., Denk, W., Kerr, J.N.D., 2013. Miniaturization of two-photon microscopy for imaging in freely moving animals. Cold Spring Harb. Protoc. 2013, 904–913.

Helmchen, F., Fee, M.S., Tank, D.W., Denk, W., 2001. A miniature head-mounted two-photon microscope: High-resolution brain imaging in freely moving animals. Neuron 31, 903–912.

Helmchen, F., Imoto, K., Sakmann, B., 1996. Ca2+ buffering and action potential-evoked Ca2+ signaling in dendrites of pyramidal neurons. Biophys. J. 70, 1069–1081.

Helmchen, F., Svoboda, K., Denk, W., Tank, D.W., 1999. In vivo dendritic calcium dynamics in deep-layer cortical pyramidal neurons. Nat. Neurosci. 2, 989–96.

Hendel, T., Mank, M., Schnell, B., Griesbeck, O., Borst, A., Reiff, D.F., 2008. Fluorescence changes of genetic calcium indicators and OGB-1 correlated with neural activity and calcium in vivo and in vitro. J. Neurosci. 28, 7399–7411.

Herculano-Houzel, S., 2014. The glia/neuron ratio: How it varies uniformly across brain structures and species and what that means for brain physiology and evolution. Glia 62, 1377–1391.

Herculano-Houzel, S., Mota, B., Lent, R., 2006. Cellular scaling rules for rodent brains. Proc. Natl. Acad. Sci. U. S. A. 103, 12138–43.

Hires, S.A., Tian, L., Looger, L.L., 2008. Reporting neural activity with genetically encoded calcium indicators. Brain Cell Biol. 36, 69–86.

Holmgren, C., Harkany, T., Svennenfors, B., Zilberter, Y., 2003. Pyramidal cell communication within local networks in layer 2/3 of rat neocortex. J. Physiol. 551, 139–153.

Holtmaat, A., Bonhoeffer, T., Chow, D.K., Chuckowree, J., De Paola, V., B, H.S., Hübener, M., Keck, T., Knott, G., Lee, W.-C.A., Mostany, R., Mrsic-Flogel, T.D., Nedivi, E., Portera-Cailliau, C., Svoboda, K., Trachtenberg, J.T., Wilbrecht, L., 2009. Long-term, high-resolution imaging in the

mouse neocortex through a chronic cranial window. Nat. Protoc. 4, 1128–44.

Homma, R., Baker, B.J., Jin, L., Garaschuk, O., Konnerth, A., Cohen, L.B., Zecevic, D., 2009. Wide-field and two-photon imaging of brain activity with voltage-and calcium-sensitive dyes. Philos. Trans. R. Soc. B Biol. Sci. 364, 2453.

Horikawa, K., Yamada, Y., Matsuda, T., Kobayashi, K., Hashimoto, M., Matsu-ura, T., Miyawaki, A., Michikawa, T., Mikoshiba, K., Nagai, T., 2010. Spontaneous network activity visualized by ultrasensitive Ca2+ indicators, yellow Cameleon-Nano. Nat. Methods 7, 729–732.

Horton, N.G., Wang, K., Kobat, D., Clark, C.G., Wise, F.W., Schaffer, C.B., Xu, C., 2013. In vivo three-photon microscopy of subcortical structures within an intact mouse brain. Nat. Photonics 7, 205–209.

Inoue, M., Takeuchi, A., Horigane, S., Ohkura, M., Gengyo-Ando, K., Fujii, H., Kamijo, S., Takemoto-Kimura, S., Kano, M., Nakai, J., Kitamura, K., Bito, H., 2014. Rational design of a high-affinity, fast, red calcium indicator R-CaMP2. Nat. Methods 12, 64–70.

Jacob, V., Petreanu, L., Wright, N.F.N., Svoboda, K., Fox, K.D., 2012. Regular Spiking and Intrinsic Bursting Pyramidal Cells Show Orthogonal Forms of Experience-Dependent Plasticity in Layer V of Barrel Cortex. Neuron 73, 391–404.

Jaffe, D.B., Johnston, D., Lasser-Ross, N., Lisman, J.E., Miyakawa, H., Ross, W.N., 1992. The spread of Na+ spikes determines the pattern of dendritic Ca2+ entry into hippocampal neurons. Nature 357, 244–246.

Jares-Erijman, E. a, Jovin, T.M., 2003. FRET imaging. Nat. Biotechnol. 21, 1387–1395.

Ji, N., Milkie, D.E., Betzig, E., 2010. Adaptive optics via pupil segmentation for high-resolution imaging in biological tissues. Nat. Methods 7, 141–147.

Kalatsky, V. a., Stryker, M.P., 2003. New paradigm for optical imaging: Temporally encoded maps of intrinsic signal. Neuron 38, 529–545.

Kano, M., Garaschuk, O., Verkhratsky, A., Konnerth, A., 1995. Ryanodine receptor-mediated intracellular calcium release in rat cerebellar Purkinje neurones. J. Physiol. 487, 1–16.

Kerr, J.N.D., Greenberg, D., Helmchen, F., 2005. Imaging input and output of neocortical networks in vivo. Proc. Natl. Acad. Sci. U. S. A. 102, 14063–8.

Kirkcaldie, M.T.K., 2012. The Mouse Nervous System, Chapter 4 Neocortex. Elsevier Inc.

Klein, R.L., Hamby, M.E., Gong, Y., Hirko, A.C., Wang, S., Hughes, J. a, King, M. a, Meyer, E.M., 2002. Dose and promoter effects of adeno-associated viral vector for green fluorescent protein expression in the rat brain. Exp. Neurol. 176, 66–74.

Klimczak, R.R., Koerber, J.T., Dalkara, D., Flannery, J.G., Schaffer, D. V, 2009. A novel adeno-associated viral variant for efficient and selective intravitreal transduction of rat Müller cells. PLoS One 4, e7467.

Kobat, D., Durst, M.E., Nishimura, N., Wong, A.W., Schaffer, C.B., Xu, C., 2009. Deep tissue multiphoton microscopy using longer wavelength excitation. Opt. Express 17, 13354–13364.

Kozloski, J., Hamzei-Sichani, F., Yuste, R., 2001. Stereotyped position of local synaptic targets in neocortex. Science 293, 868–872.

Kügler, S., Kilic, E., Bähr, M., 2003. Human synapsin 1 gene promoter confers highly neuron-specific long-term transgene expression from an adenoviral vector in the adult rat brain depending on the transduced area. Gene Ther. 10, 337–47.

Kuhlman, S.J., Huang, Z.J., 2008. High-resolution labeling and functional manipulation of specific neuron types in mouse brain by Cre-activated viral gene expression. PLoS One 3, e2005.

Kumar, M., Keller, B., Makalou, N., Sutton, R.E., 2001. Systematic determination of the packaging limit of lentiviral vectors. Hum. Gene Ther. 12, 1893–1905.

Kumar, P., Ohana, O., 2008. Inter- and intralaminar subcircuits of excitatory and inhibitory neurons in layer 6a of the rat barrel cortex. J. Neurophysiol. 100, 1909–1922.

Larkum, M.E., Zhu, J.J., Sakmann, B., 1999. A new cellular mechanism for coupling inputs arriving at different cortical layers. Nature 398, 338–341.

Larsen, D.D., Callaway, E.M., 2006. Development of layer-specific axonal arborizations in mouse primary somatosensory cortex. J. Comp. Neurol. 494, 398–414.

Larsen, D.D., Wickersham, I.R., Callaway, E.M., 2007. Retrograde tracing with recombinant rabies virus reveals correlations between projection targets and dendritic architecture in layer 5 of mouse barrel cortex. Front. Neural Circuits 1, 5.

Ledergerber, D., Larkum, M.E., 2010. Properties of layer 6 pyramidal neuron

apical dendrites. J. Neurosci. 30, 13031–13044.

Lefort, S., Tomm, C., Floyd Sarria, J.C., Petersen, C.C.H., 2009. The Excitatory Neuronal Network of the C2 Barrel Column in Mouse Primary Somatosensory Cortex. Neuron 61, 301–316.

Lein, E.S., Hawrylycz, M.J., Ao, N., Ayres, M., Bensinger, A., Bernard, A., Boe, A.F., Boguski, M.S., Brockway, K.S., Byrnes, E.J., Chen, L., Chen, L., Chen, T., Chin, M.C., Chong, J., Crook, B.E., Czaplinska, A., Dang, C.N., Datta, S., Dee, N.R., Desaki, A.L., Desta, T., Diep, E., Dolbeare, T.A., Donelan, M.J., Dong, H., Dougherty, J.G., Duncan, B.J., Ebbert, A.J., Eichele, G., Estin, L.K., Faber, C., Facer, B.A., Fields, R., Fischer, S.R., Fliss, T.P., Frensley, C., Gates, S.N., Glattfelder, K.J., Halverson, K.R., Hart, M.R., Hohmann, J.G., Howell, M.P., Jeung, D.P., Johnson, R.A., Karr, P.T., Kawal, R., Kidney, J.M., Knapik, R.H., Kuan, C.L., Lake, J.H., Laramee, A.R., Larsen, K.D., Lau, C., Lemon, T.A., Liang, A.J., Liu, Y., Luong, L.T., Michaels, J., Morgan, J.J., Morgan, R.J., Mortrud, M.T., Mosqueda, N.F., Ng, L.L., Ng, R., Orta, G.J., Overly, C.C., Pak, T.H., Parry, S.E., Pathak, S.D., Pearson, O.C., Puchalski, R.B., Riley, Z.L., Rockett, H.R., Rowland, S.A., Royall, J.J., Ruiz, M.J., Sarno, N.R., Schaffnit, K., Shapovalova, N. V, Sivisay, T., Slaughterbeck, C.R., Smith, S.C., Smith, K. a, Smith, B.I., Sodt, A.J., Stewart, N.N., Stumpf, K., Sunkin, S.M., Sutram, M., Tam, A., Teemer, C.D., Thaller, C., Thompson, C.L., Varnam, L.R., Visel, A., Whitlock, R.M., Wohnoutka, P.E., Wolkey, C.K., Wong, V.Y., Wood, M., Yaylaoglu, M.B., Young, R.C., Youngstrom, B.L., Yuan, X.F., Zhang, B., Zwingman, T.A., Jones, A.R., 2007. Genome-wide atlas of gene expression in the adult mouse brain. Nature 445, 168–176.

Levene, M.J., Dombeck, D.A., Kasischke, K.A., Molloy, R.P., Webb, W.W., 2004. In vivo multiphoton microscopy of deep brain tissue. J. Neurophysiol. 91, 1908–1912.

Lowenstein, P.R., Mandel, R.J., Xiong, W.-D., Kroeger, K., Castro, M.G., 2007. Immune responses to adenovirus and adeno-associated vectors used for gene therapy of brain diseases: the role of immunological synapses in understanding the cell biology of neuroimmune interactions. Curr. Gene Ther. 7, 347–360.

Lübke, J., Feldmeyer, D., 2007. Excitatory signal flow and connectivity in a cortical column: Focus on barrel cortex. Brain Struct. Funct.

Lundby, A., Mutoh, H., Dimitrov, D., Akemann, W., Knöpfel, T., 2008. Engineering of a genetically encodable fluorescent voltage sensor exploiting fast Ci-VSP voltage-sensing movements. PLoS One 3, 1–5.

Lütcke, H., Murayama, M., Hahn, T., Margolis, D.J., Astori, S., Zum Alten Borgloh, S.M., Göbel, W., Yang, Y., Tang, W., Kügler, S., Sprengel, R., Nagai, T., Miyawaki, A., Larkum, M.E., Helmchen, F., Hasan, M.T., 2010. Optical recording of neuronal activity with a genetically-encoded calcium indicator in anesthetized and freely moving mice. Front. Neural Circuits 4, 9.

Ma, P.M., 1991. Vibrissal Representations in the Brainstem Trigeminal Complex of the Mouse. I. Normal Structural Organization. J. Comp. Neurol. 199, 161–199.

Madisen, L., Garner, A.R., Shimaoka, D., Chuong, A.S., Klapoetke, N.C., Li, L., van der Bourg, A., Niino, Y., Egolf, L., Monetti, C., Gu, H., Mills, M., Cheng, A., Tasic, B., Nguyen, T.N., Sunkin, S.M., Benucci, A., Nagy, A., Miyawaki, A., Helmchen, F., Empson, R.M., Knöpfel, T., Boyden, E.S., Reid, R.C., Carandini, M., Zeng, H., 2015. Transgenic Mice for Intersectional Targeting of Neural Sensors and Effectors with High Specificity and Performance. Neuron 85, 942–958.

Malonek, D., Grinvald, A., 1996. Interactions between electrical activity and cortical microcirculation revealed by imaging spectroscopy: implications for functional brain mapping. Science 272, 551–554.

Mank, M., Reiff, D.F., Heim, N., Friedrich, M.W., Borst, A., Griesbeck, O., 2006. A FRET-based calcium biosensor with fast signal kinetics and high fluorescence change. Biophys. J. 90, 1790–1796.

Mank, M., Santos, A.F.F., Direnberger, S., Mrsic-flogel, T.D., Hofer, S.B., Stein, V., Hendel, T., Reiff, D.F., Levelt, C., Borst, A., Bonhoeffer, T., Mark, H., Griesbeck, O., Hübener, M., Griesbeck, O., 2008. A genetically encoded calcium indicator for chronic in vivo two-photon imaging. Nat. Methods 5, 805–811.

Manns, I.D., Sakmann, B., Brecht, M., 2004. Sub- and suprathreshold receptive field properties of pyramidal neurones in layers 5A and 5B of rat somatosensory barrel cortex. J. Physiol. 556, 601–622.

Mao, T., Kusefoglu, D., Hooks, B.M., Huber, D., Petreanu, L., Svoboda, K., 2011. Long-Range Neuronal Circuits Underlying the Interaction between Sensory and Motor Cortex. Neuron 72, 111–123.

Margolis, D.J., Al., E., 2010. Chronic two-photon calcium imaging of stability and plasticity of sensory representations in mouse barrel cortex. Soc. Neurosci. Abstr.

Margolis, D.J., Lütcke, H., Helmchen, F., 2014. Microcircuit dynamics of map plasticity in barrel cortex. Curr. Opin. Neurobiol. 24, 76–81.

Marx, M., Feldmeyer, D., 2013. Morphology and physiology of excitatory neurons in layer 6b of the somatosensory rat barrel cortex. Cereb. Cortex 23, 2803–17.

Masino, S.A., Frostig, R.D., 1996. Quantitative long-term imaging of the functional representation of a whisker in rat barrel cortex. Proc. Natl. Acad. Sci. U. S. A. 93, 4942–4947.

Mastakov, M.Y., Baer, K., Xu, R., Fitzsimons, H., During, M.J., 2001. Combined injection of rAAV with mannitol enhances gene expression in the rat brain. Mol. Ther. 3, 225–32.

Minderer, M., Liu, W., Sumanovski, L.T., Kügler, S., Helmchen, F., Margolis, D.J., 2012. Chronic imaging of cortical sensory map dynamics using a genetically encoded calcium indicator. J. Physiol. 590, 99–107.

Mitchinson, B., Martin, C.J., Grant, R. a, Prescott, T.J., 2007. Feedback control in active sensing: rat exploratory whisking is modulated by environmental contact. Proc. Biol. Sci. 274, 1035–1041.

Mittmann, W., Wallace, D.J., Czubayko, U., Herb, J.T., Schaefer, A.T., Looger, L.L., Denk, W., Kerr, J.N.D., 2011. Two-photon calcium imaging of evoked activity from L5 somatosensory neurons in vivo. Nat. Neurosci. 14, 1089–93.

Miyawaki, A., Llopis, J., Heim, R., McCaffery, J.M., Adams, J. a, Ikura, M., Tsien, R.Y., 1997. Fluorescent indicators for Ca2+ based on green fluorescent proteins and calmodulin. Nature 388, 882–887.

Mizrahi, A., Crowley, J.C., Shtoyerman, E., Katz, L.C., 2004. High-resolution in vivo imaging of hippocampal dendrites and spines. J. Neurosci. 24, 3147–3151.

Molyneaux, B.J., Arlotta, P., Menezes, J.R.L., Macklis, J.D., 2007. Neuronal subtype specification in the cerebral cortex. Nat. Rev. Neurosci. 8, 427–437.

Mountcastle, V.B., 1957. Modality and topographic properties of single neurons of cat's somatic sensory cortex. J. Neurophysiol. 20, 408–434.

Müller, W., Connor, J.A., 1991. Dendritic spines as individual neuronal compartments for synaptic Ca2+ responses. Nature 354, 73–76.

Muto, A., Ohkura, M., Abe, G., Nakai, J., Kawakami, K., 2013. Real-time visualization of neuronal activity during perception. Curr. Biol. 23, 307–311.

Nagai, T., Yamada, S., Tominaga, T., Ichikawa, M., Miyawaki, A., 2004. Expanded dynamic range of fluorescent indicators for Ca2+ by circularly

permuted yellow fluorescent proteins. Proc. Natl. Acad. Sci. U. S. A. 101, 10554–9.

Nakai, J., Ohkura, M., Imoto, K., 2001. A high signal-to-noise Ca2+ probe composed of a single green fluorescent protein. Nat. Biotechnol. 19, 137–141.

Narayanan, R.T., Egger, R., Johnson, A.S., Mansvelder, H.D., Sakmann, B., de Kock, C.P.J., Oberlaender, M., 2015. Beyond Columnar Organization: Cell Type- and Target Layer-Specific Principles of Horizontal Axon Projection Patterns in Rat Vibrissal Cortex. Cereb. Cortex 1–19.

Nathanson, J.L., Jappelli, R., Scheeff, E.D., Manning, G., Obata, K., Brenner, S., Callaway, E.M., 2009. Short Promoters in Viral Vectors Drive Selective Expression in Mammalian Inhibitory Neurons, but do not Restrict Activity to Specific Inhibitory Cell-Types. Front. Neural Circuits 3, 19.

Nevian, T., Helmchen, F., 2007. Calcium indicator loading of neurons using single-cell electroporation. Pflugers Arch. Eur. J. Physiol. 454, 675–688.

Niswender, C.M., Conn, P.J., 2010. Metabotropic glutamate receptors: physiology, pharmacology, and disease. Annu Rev Pharmacol Toxicol 50, 295–322.

O'Donovan, M.J., Ho, S., Sholomenko, G., Yee, W., 1993. Real-time imaging of neurons retrogradely and anterogradely labelled with calcium-sensitive dyes. J. Neurosci. Methods 46, 91–106.

Oberlaender, M., Boudewijns, Z.S.R.M., Kleele, T., Mansvelder, H.D., Sakmann, B., de Kock, C.P.J., 2011. Three-dimensional axon morphologies of individual layer 5 neurons indicate cell type-specific intracortical pathways for whisker motion and touch. Proc. Natl. Acad. Sci. U. S. A. 108, 4188–4193.

Oberlaender, M., De Kock, C.P.J., Bruno, R.M., Ramirez, A., Meyer, H.S., Dercksen, V.J., Helmstaedter, M., Sakmann, B., 2012. Cell type-specific three-dimensional structure of thalamocortical circuits in a column of rat vibrissal cortex. Cereb. Cortex 22, 2375–2391.

Oheim, M., Beaurepaire, E., Chaigneau, E., Mertz, J., Charpak, S., 2001. Two-photon microscopy in brain tissue: parameters influencing the imaging depth. J. Neurosci. Methods 111, 29–37.

Ohkura, M., Matsuzaki, M., Kasai, H., Imoto, K., Nakai, J., 2005. Genetically encoded bright Ca2+ probe applicable for dynamic Ca2+ imaging of dendritic spines. Anal. Chem. 77, 5861–5869.

Ohkura, M., Sasaki, T., Kobayashi, C., Ikegaya, Y., Nakai, J., 2012a. An improved genetically encoded red fluorescent Ca2+ indicator for detecting optically evoked action potentials. PLoS One 7, e39933.

Ohkura, M., Sasaki, T., Sadakari, J., Gengyo-Ando, K., Kagawa-Nagamura, Y., Kobayashi, C., Ikegaya, Y., Nakai, J., 2012b. Genetically encoded green fluorescent Ca2+ indicators with improved detectability for neuronal Ca2+ signals. PLoS One 7, e51286.

Oliver, A.E., Baker, G.A., Fugate, R.D., Tablin, F., Crowe, J.H., 2000. Effects of temperature on calcium-sensitive fluorescent probes. Biophys. J. 78, 2116–2126.

Perron, A., Mutoh, H., Launey, T., Knöpfel, T., 2009. Red-Shifted Voltage-Sensitive Fluorescent Proteins. Chem. Biol. 16, 1268–1277.

Petreanu, L., Huber, D., Sobczyk, A., Svoboda, K., 2007. Channelrhodopsin-2-assisted circuit mapping of long-range callosal projections. Nat. Neurosci. 10, 663–8.

Petreanu, L., Mao, T., Sternson, S.M., Svoboda, K., 2009. The subcellular organization of neocortical excitatory connections. Nature 457, 1142–5.

Pierret, T., Lavallée, P., Deschênes, M., 2000. Parallel streams for the relay of vibrissal information through thalamic barreloids. J. Neurosci. 20, 7455–7462.

Polley, D.B., Chen-bee, C.H., Frostig, R.D., 1999. Two Directions of Plasticity in the Sensory-Deprived Adult Cortex 24, 623–637.

Polley, D.B., Kvasnák, E., Frostig, R.D., 2004. Naturalistic experience transforms sensory maps in the adult cortex of caged animals. Nature 429, 67–71.

Purves D, Augustine GJ, Fitzpatrick D, et al., E., 2001. Neuroscience, Sunderland (MA): Sinauer Associates.

Reep, R.L., 2000. Cortical layer VII and persistent subplate cells in mammalian brains. Brain. Behav. Evol. 56, 212–234.

Reid, C.A., Fabian-Fine, R., Fine, A., 2001. Postsynaptic calcium transients evoked by activation of individual hippocampal mossy fiber synapses. J. Neurosci. 21, 2206–2214.

Reinert, K.C., Dunbar, R.L., Gao, W., Chen, G., Ebner, T.J., 2004. Flavoprotein autofluorescence imaging of neuronal activation in the cerebellar cortex in vivo. J. Neurophysiol. 92, 199–211.

Rueckel, M., Mack-Bucher, J.A., Denk, W., 2006. Adaptive wavefront

correction in two-photon microscopy using coherence-gated wavefront sensing. Proc. Natl. Acad. Sci. U. S. A. 103, 17137–17142.

Sachdev, R.N.S., Sato, T., Ebner, F.F., 2002. Divergent movement of adjacent whiskers. J. Neurophysiol. 87, 1440–1448.

Sakai, R., Repunte-Canonigo, V., Raj, C.D., Knöpfel, T., 2001. Design and characterization of a DNA-encoded, voltage-sensitive fluorescent protein. Eur. J. Neurosci. 13, 2314–2318.

Sasaki, T., 2015. Optogenetics. Chapter 10 Probing Neuronal Activity Using Genetically Encoded Red Fluorescent Calcium Indicators.

Sato, M., Kawano, M., Ohkura, M., Gengyo-Ando, K., Nakai, J., Hayashi, Y., 2015. Generation and Imaging of Transgenic Mice that Express G-CaMP7 under a Tetracycline Response Element. PLoS One 10, e0125354.

Sato, T.R., Svoboda, K., 2010. The functional properties of barrel cortex neurons projecting to the primary motor cortex. J. Neurosci. 30, 4256–4260.

Schubert, D., Ko, R., Luhmann, H.J., Staiger, J.F., Kötter, R., Luhmann, H.J., Staiger, J.F., 2006. Morphology, electrophysiology and functional input connectivity of pyramidal neurons characterizes a genuine layer va in the primary somatosensory cortex. Cereb. Cortex 16, 223–36.

Schwaller, B., 2010. Cytosolic Ca2+ Buffers. Cold Spring Harb. Perspect. Biol. 2, a004051.

Sehara, K., Toda, T., Iwai, L., Wakimoto, M., Tanno, K., Matsubayashi, Y., Kawasaki, H., 2010. Whisker-related axonal patterns and plasticity of layer 2/3 neurons in the mouse barrel cortex. J. Neurosci. 30, 3082–92.

Shepherd, G.M.G., Stepanyants, A., Bureau, I., Chklovskii, D., Svoboda, K., 2005. Geometric and functional organization of cortical circuits. Nat. Neurosci. 8, 782–90.

Shepherd, G.M.G., Svoboda, K., 2005. Laminar and columnar organization of ascending excitatory projections to layer 2/3 pyramidal neurons in rat barrel cortex. J. Neurosci. 25, 5670–5679.

Shibuki, K., Hishida, R., Murakami, H., Kudoh, M., Kawaguchi, T., Watanabe, M., Watanabe, S., Kouuchi, T., Tanaka, R., 2003. Dynamic imaging of somatosensory cortical activity in the rat visualized by flavoprotein autofluorescence. J. Physiol. 549, 919–927.

Shimomura, O., Johnson, F.H., Saiga, Y., 1962. Extraction, purification and properties of aequorin, a bioluminescent protein from the luminous

hydromedusan, Aequorea. J. Cell. Comp. Physiol. 59, 223–239.

Shoham, D., Glaser, D.E., Arieli, A., Kenet, T., Wijnbergen, C., Toledo, Y., Hildesheim, R., Grinvald, A., 1999. Imaging cortical dynamics at high spatial and temporal resolution with novel blue voltage-sensitive dyes. Neuron 24, 791–802.

Silver, R.A., Lubke, J., Sakmann, B., Feldmeyer, D., 2003. High-probability uniquantal transmission at excitatory synapses in barrel cortex. Science 302, 1981–1984.

Simonato, M., Manservigi, R., Marconi, P., Glorioso, J., 2000. Gene transfer into neurones for the molecular analysis of behaviour: Focus on herpes simplex vectors. Trends Neurosci. 23, 183–190.

Simons, D.J., 1978. Response properties of vibrissa units in rat SI somatosensory neocortex. J. Neurophysiol. 41, 798–820.

Slovin, H., Arieli, A., Hildesheim, R., Grinvald, A., 2002. Long-term voltage-sensitive dye imaging reveals cortical dynamics in behaving monkeys. J. Neurophysiol. 88, 3421–3438.

Smith, A.M., Mancini, M.C., Nie, S., 2009. Bioimaging: second window for in vivo imaging. Nat. Nanotechnol. 4, 710–711.

Soudais, C., Skander, N., Kremer, E.J., 2004. Long-term in vivo transduction of neurons throughout the rat CNS using novel helper-dependent CAV-2 vectors. FASEB J. 18, 391–393.

Spruston, N., Schiller, Y., Stuart, G., Sakmann, B., 1995. Activity-dependent action potential invasion and calcium influx into hippocampal CA1 dendrites. Science 268, 297–300.

Stirman, J.N., Smith, I.T., Kudenov, M.W., Smith, S.L., 2014. Wide field-of-view, twin-region two-photon imaging across extended cortical networks. bioRxiv 11320.

Stosiek, C., Garaschuk, O., Holthoff, K., Konnerth, A., 2003. In vivo two-photon calcium imaging of neuronal networks. Proc. Natl. Acad. Sci. U. S. A. 100, 7319–7324.

Tanaka, Y.R., Tanaka, Y.H., Konno, M., Fujiyama, F., Sonomura, T., Okamoto-Furuta, K., Kameda, H., Hioki, H., Furuta, T., Nakamura, K.C., Kaneko, T., 2011. Local connections of excitatory neurons to corticothalamic neurons in the rat barrel cortex. J. Neurosci. 31, 18223–36.

Taniguchi, H., He, M., Wu, P., Kim, S., Paik, R., Sugino, K., Kvitsani, D., Fu, Y., Lu, J., Lin, Y., Miyoshi, G., Shima, Y., Fishell, G., Nelson, S.B.,

Huang, Z.J., 2011. A Resource of Cre Driver Lines for Genetic Targeting of GABAergic Neurons in Cerebral Cortex. Neuron 71, 995–1013.

Theer, P., Hasan, M.T., Denk, W., 2003. Two-photon imaging to a depth of 1000 microm in living brains by use of a Ti:Al2O3 regenerative amplifier. Opt. Lett. 28, 1022–1024.

Thestrup, T., Litzlbauer, J., Bartholomäus, I., Mues, M., Russo, L., Dana, H., Kovalchuk, Y., Liang, Y., Kalamakis, G., Laukat, Y., Becker, S., Witte, G., Geiger, A., Allen, T., Rome, L.C., Chen, T.-W., Kim, D.S., Garaschuk, O., Griesinger, C., Griesbeck, O., 2014. Optimized ratiometric calcium sensors for functional in vivo imaging of neurons and T lymphocytes. Nat. Methods 11, 175–82.

Tian, L., Andrew Hires, S., Looger, L.L., 2012. Imaging neuronal activity with genetically encoded calcium indicators. Cold Spring Harb. Protoc. 7, 647–656.

Tian, L., Hires, S.A., Mao, T., Huber, D., Chiappe, M.E., Chalasani, S.H., Petreanu, L., Akerboom, J., McKinney, S.A., Schreiter, E.R., Bargmann, C.I., Jayaraman, V., Svoboda, K., Looger, L.L., 2009. Imaging neural activity in worms, flies and mice with improved GCaMP calcium indicators. Nat. Methods 6, 875–881.

Tischbirek, C., Birkner, A., Jia, H., Sakmann, B., Konnerth, A., 2015. Deep two-photon brain imaging with a red-shifted fluorometric Ca 2+indicator. Proc. Natl. Acad. Sci. 112, 11377–11382.

Titus, J.A., Haugland, R., Sharrow, S.O., Segal, D.M., 1982. Texas Red, a hydrophilic, red-emitting fluorophore for use with fluorescein in dual parameter flow microfluorometric and fluorescence microscopic studies. J. Immunol. Methods 50, 193–204.

Tsai, P.S., Mateo, C., Field, J.J., Schaffer, C.B., Anderson, M.E., Kleinfeld, D., 2015. Ultra-large field-of-view two-photon microscopy. Opt. Express 23, 13833–13847.

Tsien, R.Y., 1981. A non-disruptive technique for loading calcium buffers and indicators into cells. Nature 290, 527–528.

Tsien, R.Y., 1980. New calcium indicators and buffers with high selectivity against magnesium and protons: design, synthesis, and properties of prototype structures. Biochemistry 19, 2396–2404.

Tsuchiya, R., Yoshiki, F., Kudo, Y., Morita, M., 2002. Cell type-selective expression of green fluorescent protein and the calcium indicating protein, yellow cameleon, in rat cortical primary cultures. Brain Res. 956, 221–229.

Ustione, a., Piston, D.W., 2011. A simple introduction to multiphoton microscopy. J. Microsc. 243, 221–226.

Van Der Loos, H., 1976. Barreloids in mouse somatosensory thalamus. Neurosci. Lett. 2, 1–6.

Vanderhaeghen, P., Polleux, F., 2004. Developmental mechanisms patterning thalamocortical projections: Intrinsic, extrinsic and in between. Trends Neurosci. 27, 384–391.

Vanni, M.P., Murphy, T.H., 2014. Mesoscale transcranial spontaneous activity mapping in GCaMP3 transgenic mice reveals extensive reciprocal connections between areas of somatomotor cortex. J. Neurosci. 34, 15931–46.

Veinante, P., Deschênes, M., 2003. Single-cell study of motor cortex projections to the barrel field in rats. J. Comp. Neurol. 464, 98–103.

Veinante, P., Jacquin, M.F., Deschênes, M., 2000a. Thalamic projections from the whisker-sensitive regions of the spinal trigeminal complex in the rat. J. Comp. Neurol. 420, 233–243.

Veinante, P., Lavallée, P., Deschênes, M., 2000b. Corticothalamic projections from layer 5 of the vibrissal barrel cortex in the rat. J. Comp. Neurol. 424, 197–204.

Voigt, F.F., Chen, J.L., Krueppel, R., Helmchen, F., 2015. A modular two-photon microscope for simultaneous imaging of distant cortical areas in vivo. SPIE Proc. 9329, 93292C–93292C–7.

Waters, J., Schaefer, A., Sakmann, B., 2005. Backpropagating action potentials in neurones: measurement, mechanisms and potential functions. Prog. Biophys. Mol. Biol. 87, 145–70.

Weitz, A.C., Behrend, M.R., Lee, N.S., Klein, R.L., Chiodo, V. a., Hauswirth, W.W., Humayun, M.S., Weiland, J.D., Chow, R.H., 2013. Imaging the Response of the Retina to Electrical Stimulation with Genetically Encoded Calcium Indicators. J. Neurophysiol. 109, 1979–1988.

Wimmer, V.C., Bruno, R.M., De Kock, C.P.J., Kuner, T., Sakmann, B., 2010. Dimensions of a projection column and architecture of VPM and POm axons in rat vibrissal cortex. Cereb. Cortex 20, 2265–2276.

Witten, I.B., Steinberg, E.E., Lee, S.Y., Davidson, T.J., Zalocusky, K.A., Brodsky, M., Yizhar, O., Cho, S.L., Gong, S., Ramakrishnan, C., Stuber, G.D., Tye, K.M., Janak, P.H., Deisseroth, K., 2011. Recombinase-driver rat lines: Tools, techniques, and optogenetic application to dopamine-mediated reinforcement. Neuron 72, 721–733.

Woolsey, T. a, van der Loos, H., 1970. About the Physiological Organization of the Cerebral Cortex of the Mouse and the Rat . in Which the Shape , Size , Organization and Number of the Barrels Is Particularly. Brain Res. 17, 205–242.

Xu, N., Harnett, M.T., Williams, S.R., Huber, D., O'Connor, D.H., Svoboda, K., Magee, J.C., 2012. Nonlinear dendritic integration of sensory and motor input during an active sensing task. Nature 492, 247–51.

Xu, X., Callaway, E.M., 2009. Laminar specificity of functional input to distinct types of inhibitory cortical neurons. J. Neurosci. 29, 70–85.

Yizhar, O., Fenno, L.E., Davidson, T.J., Mogri, M., Deisseroth, K., 2011. Optogenetics in Neural Systems. Neuron 71, 9–34.

Yu, C., Derdikman, D., Haidarliu, S., Ahissar, E., 2006. Parallel thalamic pathways for whisking and touch signals in the rat. PLoS Biol. 4, e124.

Zariwala, H.A., Borghuis, B.G., Hoogland, T.M., Madisen, L., Tian, L., De Zeeuw, C.I., Zeng, H., Looger, L.L., Svoboda, K., Chen, T.-W., 2012. A Cre-Dependent GCaMP3 Reporter Mouse for Neuronal Imaging In Vivo. J. Neurosci. 32, 3131–3141.

Zhao, Y., Araki, S., Wu, J., Teramoto, T., Chang, Y.-F., Nakano, M., Abdelfattah, A.S., Fujiwara, M., Ishihara, T., Nagai, T., Campbell, R.E., 2011. An expanded palette of genetically encoded Ca^{2+} indicators. Science 333, 1888–91.

Zucker, R.S., 1999. Calcium- and activity-dependent synaptic plasticity. Curr. Opin. Neurobiol. 9, 305–313.

List of Abbreviations

AAV: adeno-associated virus

AM: acetoxymethyl

AO: adaptive optics

AP: action potential

ATP: adenosine triphosphate

CaM: calmodulin

CaMKIIα: calmodulin-dependent protein kinase IIα

CCD: charged coupled detector

CFP: cyan fluorescent protein

ChR2: Channelrhodopsin-2

CMOS: complementary metal-oxide semiconductor

COX: cytochrome oxidase staining

cpEGFP: circularly permuted enhanced green fluorescent protein

CSD: calcium-sensitive dye

DAPI: 4',6-diamidino-2-phenylindole

ECFP: enanched cyan fluorescent protein

ER: endoplasmatic reticulum

EF-1α: human elongation factor-1α

ECG: electrocardiogram

FLEX: flip-excision

FP: fluorescent protein

FRET: Förster resonance energy transfer

GABA: γ-aminobutyric acid

GEVI: genetically-encoded voltage indicator

GECI: genetically encoded calcium indicator

GFP: green fluorescent protein

GFAP: glial fibrillary acidic protein

GRIN: gradient refractive index

HL: hindlimb

HSV: Herpes Simplex Virus

hSyn1: human synapsin

HVA: high-voltage-activated

ICMS: intracortical microstimulation

IOS: intrinsic optical signal

IP_3R: inositol trisphosphate receptor

IR: infrared

K_d: dissociation constant

LED: light-emitting diode

LFP: local field potential

LVA: low-voltage-activated

mGluR: metabotropic glutamate receptor

NMDA: N-methyl-D-aspartic acid

nAChR : nicotinic acetylcholine receptor

NA: numerical aperture

OGB: oregon green bapta

PFA: paraformaldehyde

PMT: photomultiplier tube

POm: posteromedial nucleus

PrV: principal trigeminal nucleus

Rbp4: retinol binding protein 4

RyR: ryanodine receptor

ROI: region of interest

S1: primary somatosensory cortex

S2: secondary somatosensory cortex

SD: standard deviation

SNR: signal to noise ratio

SpV: spinal trigeminal nucleus

TG: trigeminal ganglion

TN: trigeminal nuclei

VPM: ventral posteromedial nucleus

VGCC: voltage-gated calcium channel

VSD: voltage-sensitive dye

WF: wide-field

wM1: primary whisker motor cortex

Yb:KGW: ytterbium-doped potassium gadolinium tungstate

YC: yellow cameleon

YFP: yellow fluorescent protein

Acknowledgements

The completion of my PhD projects and dissertation has been a long journey. I could not have finished without the invaluable support of a several. Without them, especially the selected few I'm about to mention, I could not have gotten to where I am today.

First and foremost I want to thank my supervisor Prof. Fritjof Helmchen. I appreciate all his time, ideas and patience to support my PhD work. His help and advice during the past five years are essential for me to finish my dissertation. In addition, his enthusiasm towards scientific research and his positive attitude are infectious. I would also like to thank my committee members, Prof. Sebastian Jessberger and Prof. Bruno Weber for joining my steering committee and for their valuable supports.

I am grateful to Dr. David Margolis for his supervision, his scientific advice and many insightful suggestions. He was my primary resource for getting my scientific and technical questions answered. Special mention also goes to Matthias Minderer and Lazar Sumanovski for their collaboration on the wide-field chronic imaging project. And I have appreciated Dr. Stefano Carta, Dr. Yaroslav Sych, Balazs Laurenczy and Dr. Asli Ayaz for their contribution on the RCaMP deep imaging project.

I would like to thank Dr. Shankar Sachidhanandam, Dr. Ariel Gilad, Dr. I-Wen Chen, Andreas Stäuble, Alexander van der Bourg, and Minhao Yang for their friendship and kind supports.

In addition, I want to express my gratitude to Dr. Ladan Egolf and Dr. Asli Ayaz, especially for being supportive and for helping me in everything and everyway that possible. I think of them as big sisters.

Last but not least, I would like to thank my mom and dad for their love and almost unbelievable support under any circumstance.

Curriculum Vitae

Wenrui LIU

Date of Birth: 03.01.1985

Place of Birth: Kunming

Citizenship: Chinese

■ EDUCATION

2010 - 2015	University of Zürich, Brain Research Institute, Zurich, Switzerland PhD, Neurosciences
2008 - 2010	University of Regensburg, Regensburg, Germany Master of Science, Neurosciences
2003 - 2007	Sichuan University, Chengdu, China Bachelor of Science, Biotechnology
2000 - 2003	Yunnan Normal University Secondary High School
1997 - 2000	Yunnan University Secondary Middle School
1992 - 1997	Yunnan Normal University Secondary Primary School

■ RESEARCH AND PROFESSIONAL EXPERIENCE

06.2010- 10.2015	Laboratory of Neural Circuit Dynamics, Prof. Fritjof Helmchen Brain Research Institute, University of Zurich, Switzerland
07.2009- 09.2009	"Syntactic complexity". Dr. Jens Brauer, Max-Planck-Institute for Human Cognitive and Brain Sciences, Leipzig.
05.2009- 07.2009	"Decisions about ambiguous stimuli: electrophysiological correlates". Prof. Dr. Mark W. Greenlee, Dr. Gyula, Kovacs, University of Regensburg.
03.2009-05.2009	"The neural representation of multiple-face stimuli: an fMRI study". Prof. Dr. Mark W. Greenlee, Dr. Gyula, Kovacs, University of Regensburg.

■ PUBLICATIONS

Thesis

Wenrui Liu, 2010

"Electrophysiological correlates of priming and adaptation".

Master thesis in Neuroscience, supervisors: Prof. Dr. Mark W. Greenlee, Dr. Gyula Kovacs, University of Regensburg, Germany.

Articles

Chronic imaging of cortical sensory map dynamics using a genetically encoded calcium indicator. Minderer, Matthias.*, Liu, Wenrui.* et al. The Journal of physiology (2011).

The sensitivity of face specific ERP components to the nature of stimulus noise. Krisztina Nagy*, Marta Zimmer, Wenrui Liu, Gyula Kovacs. Learning & Perception (2009).